TECHNISCHE UNIVERSITÄT MÜNCHEN

Lehrstuhl für Technische Chemie II

New Insights on Fe-Zeolite Catalysts for the Reduction of NO_x with NH_3

Sarah Maria Maier

Vollständiger Abdruck der von der Fakultät für Chemie der Technischen Universität München zur Erlangung des akademischen Grades eines

Doktors der Naturwissenschaften (Dr.rer.-nat.)

genehmigten Dissertation.

Vorsitzender:	Univ. Prof. Dr. K.-O. Hinrichsen
Prüfer der Dissertation:	1. Univ. Prof. Dr. J.A. Lercher
	2. Univ. Prof. Dr. K. Köhler

Die Dissertation wurde am 06.06.2011 bei der Technischen Universität München eingereicht und durch die Fakultät für Chemie am 14.07.2011 angenommen.

„Tu erst das Notwendige, dann das Mögliche,
und plötzlich schaffst du das Unmögliche.“

Franz von Assisi
(1181-1226)

Acknowledgements

There are a number of people who supported me during the work on this thesis and whom I want to express my gratefulness. Your support and motivation were a major contribution to this work.

First of all I want to thank Professor Johannes A. Lercher for taking me into his group and giving me the chance to work on such an interesting and challenging topic. While leaving me on a long line and allowing me to progress according to my own plans and judgement, our thought-provoking discussions always offered fresh ideas, insights and new approaches to solve upcoming problems.

I am also grateful to Prof. Köhler for his role as a secondary reviewer, for evaluating this thesis and for the many fruitful discussions we had during the last three years.

Prof. Andreas Jentys played a major role during the studies on this topic. Thank you for your support, the numerous discussions and for proof-reading this thesis.

From the side of my project partner Süd Chemie AG I want to thank Dr. Wanninger, Dr. Maletz and Dr. Reichinger for the very good collaboration and for giving me free-hand on my research.

During the work on my thesis I had the opportunity to employ several complex characterziazion techniques and I want to thank all the people who supported me with these techniques. Thanks to Gabriele Raudaschl-Sieber, Gerhard Althoff-Ospelt and Jiří Dědeček for their help with MAS NMR spectroscopy and to Ezzeldin Metwalli, Prof. Peter Müller-Buschbaum and Prof. Wagner for the excellent collaboration during the studies concerning Mößbauer spectroscopy. Special thanks go also to Adam Webb, Michael Murphy and Matthias Hermann from HASYLAB, DESY in Hamburg for supporting me during the X-ray absorption measurements and for your uncomplicated help.

In this context I want to thank all my colleagues who went with me to Hamburg to measure X-ray absorption spectroscopy: Tobias, Daniela, Jennifer, Ana, Richard, Anna, Iulius, Stefanie, Michael, Linus and Yanzhe. Thank you for spending your nights on measuring my catalysts!

Jeroen van Bokhoven and Markus Janousch from the Paul-Scherrer-Institue in Villigen, Switzerland are also thanked for the measurements of the Al XANES and the subsequent enlightening discussions.

The work in our institute would not be as productive without the never-ending technical support from Xaver Hecht, Andreas Marx, Martin Neukamm and all the members of the workshop. You always found a way to keep my system running, although I had sometimes already given up!

Steffi Maier, Helen Brenner, Katharina Thies, Bettina Federmann and Karen Schulz were a great support on all the administrative work. Thank you also very much for your motivation and for sharing a good mood during the last three years!

I want to thank the students Edith Ball, Carolin Grotz, Elisabeth Hahnrieder, Dominik Jarde, Andreas Räder and Daniela Rascher who prepared their theses on this topic and who were of great help. Special thanks go to Andreas Räder who additionally worked as a student assistant for one year.

Now it is time to thank all my colleagues! Frederik, Oliver, Sabine, Florian, Anna, Eva, Robin, John, Tobi, Michi, Stefan, Steffi and Jennifer: I had a wonderful time with you and I am thankful for your motivation, for the fun we always had and for having the opportunity to work with you! Special thanks also go to the members of our terrific “girls” office! Daniela, Sonja, Pamina, Claudia (and all the best for our institute baby Jonathan), Despina, Linus, Christian and “the sheep”, thank you for being good friends and sticking together all the time. I will really miss you!

Ein ganz besonderer Dank geht an Andi, dafür dass Du mich während meiner Arbeit mit so viel Liebe unterstützt hast und meine schlechte Laune und meinen Stress ohne Wiederspruch ertragen hast!

Und natürlich möchte ich mich bei meinen Eltern Elisabeth und Josef bedanken! Ohne euch hätte ich diese Arbeit nie angefertigt und hätte nicht den Weg gehen können den ich gegangen bin. Danke auch für die Hilfe bei der Anfertigung der Arbeit und dem Layout!

Sarah

Nomenclature

Å	Angström
B_0	Magnetic Field
bar	Bar
cm^{-1}	Wavenumber
δ	Chemical Shift (NMR)
δ	Isomeric Shift (Mößbauer Spectroscopy)
Δ	Quadrupole Splitting Constant
eV	Electron Volt
h	Hour
Hz	Hertz
K	Kelvin
kg	Kilogramm
l	Litre
m	Metre
mA	Milliampere
min	Minute
mol	mol
p	Pressure
ppm	Parts per million
s	Second
T	Tesla
V	Volts
vol. %	Volume per cent
wt. %	Weight per cent

Abbreviations

AAS	Atomic Absorption Spectroscopy
BEA	Beta zeolite
BET	Brunnauer, Emmet, Teller
DOC	Diesel Oxidation Catalyst
DPF	Diesel Particulate Filter
DFT	Density Functional Theory
DR	Diffuse Reflectance
EFAL	Extraframework Aluminium
EPR	Electron Paramagnetic Resonance
EXAFS	Extendend X-ray Absorption Fine Structure
FeBEA	Fe-exchanged BEA zeolite
FTC	Framework Type Code
FTIR	Fourrier Transformation Infrared
GHSV	Gas Hourly Space Velocity
HC	Hydrocarbons
HPLC	High Pressure Liquid Chromatography
IR	Infrared
IZA	International Zeolite Association
MAS	Magic Angle Spinning
MFI	Mobile Five
MQ	Multiple Quantum
NMR	Nuclear Magnetic Resonance
NO_x	Nitrogen Oxides
PM	Particulate Matter
R	Reflectance
SEM	Scanning Electron Microscopy
SBU	Secondary Building Unit
SCR	Selective Catalytic Reduction
T atom	Tetrahedrally coordinated Al or Si atom
TEM	Transmission Electron Microscopy

TOF	Turnover Frequency
TPD	Temperature Programmed Desorption
TPR	Temperature Programmed Reduction
USY	Ultra stable Y-type Faujasite zeolite
VOC	Volatile Organic Compounds
XAS	X-ray Absorption Spectroscopy
XANES	X-ray Absorption Near Edge Structure
XRD	X-ray Diffraction
ZSM-5	Zeolite Socony Mobile 5

Table of Contents

Chapter 1

Introduction

During the last two centuries the environmental awareness has significantly risen, leading to a higher demand for the protection of the earth and the increase of the air quality. Nitrogen oxides are one of the substances which add to the pollution of the air and are responsible e.g. for the formation of ozone and acid rain and lead to respiratory ailments. The main source for nitrogen oxides formation is the transportation sector, especially the emissions of diesel engines have to be named. To reduce emissions from mobile sources, the exhaust gases can be treated by catalytic systems, including the reduction of nitrogen oxides by the selective catalytic reduction with ammonia (NH_3-SCR). Regarding this technology, the current focus lies on the optimization of the catalytic activity by the application of zeolite based Fe catalysts. Zeolites are acidic aluminosilicates with a high specific surface area, outstanding adsorption properties and good temperature stability under hydrothermal conditions, which makes them an ideal choice as support materials for exhaust gas treatment.

The following chapter introduces the topics of the thesis, gives an overview on the reduction of nitrogen oxides by the NH_3-SCR technology and presents the main characteristics of Fe-zeolite catalysts.

1.1. Application of heterogenous catalysts for emission reduction reactions

1.1.1. Heterogeneous Catalysis

"A catalyst is a substance which affects the rate of a chemical reaction without being part of its end products." (Ein Katalysator ist jeder Stoff, der, ohne im Endprodukt einer chemischen Reaktion zu erscheinen, ihre Geschwindigkeit verändert.) This definition for catalysts was already given more than 100 years ago in the year 1901 by *Wilhelm Ostwald* and is still valid in its main statement today.[1] The number of materials being active as homo- and heterogeneous catalysts is unaccountable and especially heterogeneous catalysts have found their way towards essential components in environmental friendly processes and exhaust gas treatment. One main, highly relevant topic regarding the environmental protection is the control of air pollutants among which ozone, carbon dioxide, sulfur dioxide, hydrocarbons (HC), particulate matters (PM) and nitrogen oxides (NO_x) should be named. This chapter will give an overview of the reduction of nitrogen oxides in the exhaust gas of diesel engines in a heterogeneous catalytic process.

1.1.2. NO_x Reduction

Nitrogen oxides are mostly formed during combustion processes by oxidation of nitrogen containing components in the fuel or by the oxidation of nitrogen from air. The negative influence of NO_x emissions to the environment is caused by their contributions to acid rain, smog, the greenhouse effect (especially N_2O) and to the depletion of the earth protective ozone layer. In addition, nitrogen oxides produce several negative health effects through NO_x intrusion in the respiratory system.

The majority of the environmentally harmful nitrogen oxides stems from the transportation sector (70 %), while industrial installations contribute about 19 % and private heating 11 % to the annual emission of nitrogen oxides.[2] The main producers of nitrogen oxides in Bavaria are shown in Figure 1.1.

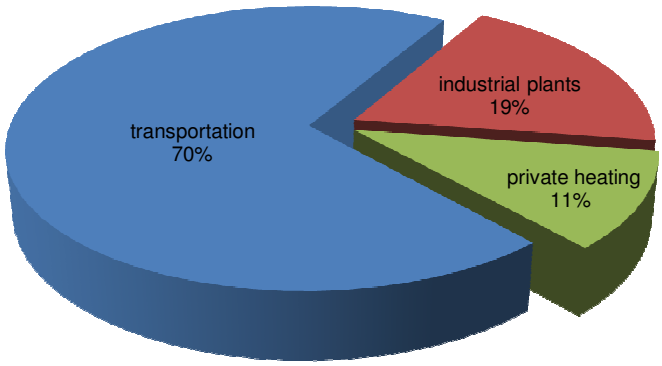

Figure 1.1: Origins of NO_x emissions in Bavaria 2004.

As the demand for transportation will further increase in the future – especially developing countries will increase their number of vehicles – means have to be found to reduce the NO_x emissions resulting from the transportation sector.

At the same time, the increasing concentration of CO_2 in the atmosphere and its contribution to the greenhouse effect is of general concern and techniques with low CO_2 emissions have good chances to be implemented as future technologies. Among the existing technologies for transportation, diesel engines are among those with the lowest fuel consumption and therefore low CO_2 emission. Especially for vehicles with a demand for high power density, diesel engines with lean-burn abilities are already the state-of-the-art for low fuel consumption. The diesel engines suffer, however, from relatively higher NO_x emissions and production of particulate matters compared with competing technologies such as gasoline engines equipped with three way catalysts.[3] Diesel engines are operated under lean conditions, which prevent the operation of three way catalysts, as it is the standard for petrol engines. Therefore, the emission of nitrogen oxides has to be regulated by the optimization of the engine operation conditions and by the selective catalytic reduction.[4]

The European Union regulates the emission limits for passenger cars since 1992 and over the following years increasingly stricter limits were implemented for new cars (see Table 1.1).[5] Similar restrictions are also valid in the United States of America and Japan.

Table 1.1: Emission limit values for passenger cars with diesel engine.[5]

	Emission limit values in mg/km					
	Euro I 1992	Euro II 1196	Euro III 2000	Euro IV 2005	Euro V 2006	Euro VI 2014
CO	3160	1000	640	500	500	500
(HC + NOx)	1130	700/900*	560	300	230	170
Nox	-	-	500	250	180	80
PM	180	80/100*	50	25	5	5

*vehicles with direct fuel injection

1.1.3. SCR technology

In order to achieve the goals set by the Euro VI norm, the exhaust gas of passenger cars has to be treated by a complex catalytic system, as the optimization of the combustion processes in diesel engines is not sufficient to fulfill these limits. The exhaust gas treatment unit consists of a diesel oxidation catalyst (DOC), diesel particulate filter (DPF) and a selective catalytic reduction (SCR) catalyst to reach the emission limits (see Figure 1.2).

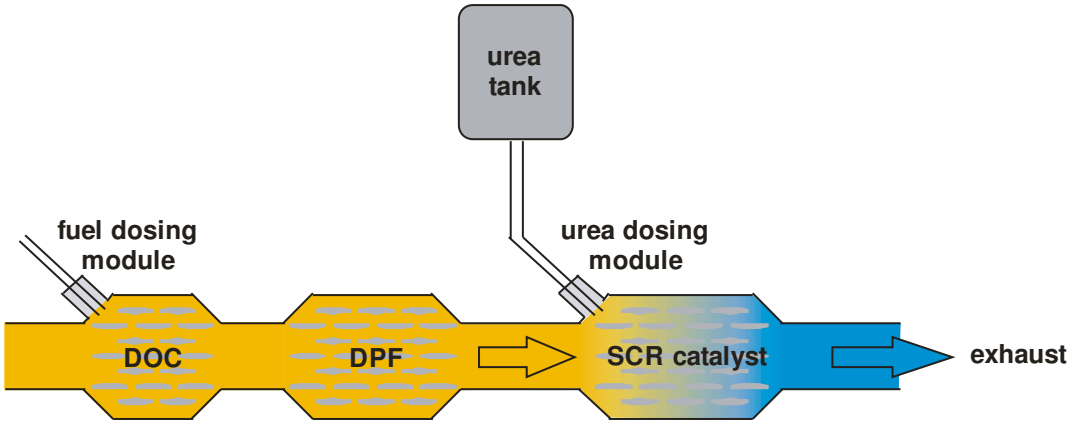

Figure 1.2: Scheme of a SCR exhaust gas treatment unit.[6]

The function of the DOC is to oxidize the unconverted hydrocarbons, to convert CO to CO_2 and to adjust the ratio of NO to NO_2 in order to enhance the conversion rate on the downstream positioned SCR catalyst. For this purpose, supported noble metal

catalysts are usually used. The role of the DPF is to remove sooty particles in the exhaust gas. In the last years, new noble metal coated DPFs, which combine the function of the DOC and the DPF were developed.[7] The last part of the exhaust gas treatment unit is the SCR catalyst, which reduces the environmentally harmful nitrogen oxides in a continuous mode. Although NO is thermodynamically unstable and would decompose to N_2 and O_2, no catalyst has been found today to overcome the kinetic energy barrier to enable the direct decomposition at reasonable rates.[8,9] The situation changes if reducing agents such as hydrocarbons or ammonia are added into the exhaust gas stream. In the first case, additional fuel has to be injected leading to a higher overall fuel consumption. For the second case, ammonia can be obtained from the thermal/catalytic decomposition of urea in an aqueous solution – merchandised under the name AdBlue – preventing the increase of the fuel consumption.[10,11]

$$NH_2\text{-}CO\text{-}NH_2 + H_2O \rightarrow CO_2 + 2\ NH_3 \quad (1)$$

Hereby, ammonia acts as reducing agent in the stoichiometric conversion of nitrogen oxide in the presence of oxygen. This reaction leads to the formation of the environmentally friendly products nitrogen and water.[10,12,13]

$$4\ NO + 4\ NH_3 + O_2 \rightarrow 6\ H_2O + 4\ N_2 \quad (2)$$

The rate of the NO_x reduction is enhanced in the presence of NO_2 as the reduction can then take place via the so-called fast SCR.[10,12,14]

$$NO + NO_2 + 2\ NH_3 \rightarrow 3\ H_2O + 2\ N_2 \quad (3)$$

Today, V_2O_5/WO_3 based systems supported on TiO_2 are the state of the art catalysts for the SCR reaction.[15,16] As V_2O_5 is volatile, classified as toxic and dangerous for the environment, has a high activity for oxidizing SO_2 to SO_3 and shows a rapid decrease in activity and selectivity above 823 K, several attempts are made to find alternative catalysts such as Fe based systems.[17] Zeolites have proven to be promising supports for Fe based catalysts as they can stabilize Fe cations and store NH_3 due to their acid properties.[18]

A different approach for reduction of NO_x, which should be mentioned here, is the NO_x storage reduction (NSR) being operated in a non-continuous mode. The NSR catalyst consists of a noble metal (e.g. Pt) site and an alkali or alkaline earth metal site (e.g. Ba) as storage function supported on a high surface area material.[19] During the lean

operation of the motor (storage phase), NO_x (mainly NO) are oxidized to NO_2 on the noble metal site and react further with the storage component (Ba) to form nitrates. When the available storage component is saturated, the engine is briefly operated under fuel-rich conditions to reduce the stored NO_x with the excess exhaust components H_2, CO and HC on the noble metal to nitrogen.[20]

1.2. Zeolites

Zeolites are often used as support materials for Fe-based SCR catalysts and are characterized by promising adsorption properties. In the following chapter, a general overview of their properties and typical applications is given.

1.2.1. Historical overview

The term “zeolite” was first used by the Swedish mineralogist Baron Axel Fredrick von Cronstedt back in 1756 after heating the mineral stilbite and observing the release of water.[21] The term is derived from the Greek words ζέω (zeo) meaning to boil and λίθος (lithos) meaning stone. The background for this observation is the fact that zeolites can adsorb large amounts of water in the micro- and mesopores, which is desorbed during the heating process. Today, the term zeolite is referred to crystalline microporous (alumino-) silicates of natural or synthetic origin with highly ordered structures and micropores of molecular dimensions (pore diameter < 20 Å). The Subcommittee on Zeolites of the International Mineralogical Association specifies the term zeolite as follows:[22]

“A zeolite mineral is a crystalline substance with a structure characterized by a framework of linked tetrahedra, each consisting of four O atoms surrounding a cation. This framework contains open cavities in the form of channels and cages. These are usually occupied by H_2O molecules and extra-framework cations that are commonly exchangeable. The channels are large enough to allow the passage of guest species. In the hydrated phases, dehydration occurs at temperatures mostly below about 400°C and is largely reversible.
The framework may be interrupted by (OH, F) groups; these occupy a tetrahedron apex that is not shared with adjacent tetrahedra.”

In the 1930s R. M. Barrer was the first to note the potential of zeolites for industrial application and started studies towards the synthesis of these materials under high pressure and temperature.[23] These works were further deepened by R. Milton working at the research laboratory of Union Carbide where he successfully developed a reproducible synthesis of zeolite A and zeolite B by 1949.[24] R. M. Barrer and R. Milton

share together the title of the "*Founding Fathers*" of synthetic zeolites and their studies, undoubtedly, led to the development of these materials as cheap, perfectly defined, highly reproducible molecular sieve adsorbents and shape-selective catalysts. Today, nearly 200 synthetic zeolite frameworks have been identified, and over 40 naturally occurring zeolite frameworks are known.[25]

The interest in synthesis and the understanding of zeolite properties has not waned since the 1950s; in contrast, a high increase in literature concerning zeolites can be observed since the 1990s. In 2010, 2985 papers containing the word "*zeolite**" could be identified by "Web of Knowledge" (see Figure 1.3).

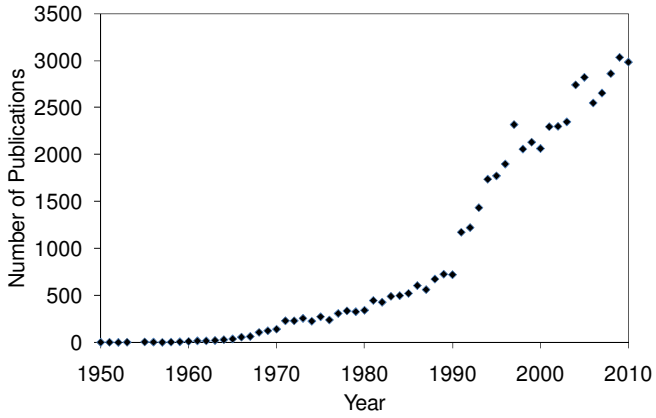

Figure 1.3: Number of literature contributions concerning zeolites from 1950 to 2010.

1.2.2. Structure and Application

The general empirical formula for a zeolite composition is:

$$M_{x/m}Al_xSi_{2-x}O_4 \cdot nH_2O$$

where *m* is the valence of the cation M, *n* is the water content and x the Al content ($0 \leq x \leq 1$). The structure of a zeolite is composed of a three-dimensional supporting network filled with loosely bound exchangeable cations and adsorbed phase. The building blocks of the underlying network are TO_4 tetrahedra, where the central T atom is typically silicon or aluminum, or more rarely a phosphorus, titanium, gallium or iron. Thus, the framework of a zeolite is made of aluminium and silicon tetrahedra with the restriction that, according to Loewenstein' rule, two AlO_4 tetrahedra will never lie side by side.[26]

The backbone structure of a zeolite is constructed of TO_4 tetrahedral units linked by shared oxygen corners, yielding a network-like pattern. This pattern replicates periodically, giving rise to well-organized arrays of channels that comprise topological characteristics specific to the zeolites.[27] The resulting framework does not depend on specific cations, adsorbent phase, chemical composition, or physical and mechanical properties of the zeolite crystals. Following the rules set up by the Commission on Zeolite Nomenclature of the International Union of Pure and Applied Chemistry, a distinct framework type is labeled by a framework type code (FTC) denoted by three capital letters.[28,29] FTCs are assigned and curated by the Structure Commission of the International Zeolite Association (IZA).[29]

By replacing a silicon atom with a net +4 charge in the framework by an aluminium (or other trivalent) atom, which carries a +3 charge, a net negative charge is introduced in the framework. To compensate this charge, a wide variety of cations, such as H^+, Na^+, K^+, Ca^{2+}, etc. are held in the pores and cages of a zeolite.[30] These cations do not only allow zeolite crystals to be used in ion-exchange processes, but they also create a strong Brønsted acid site if a proton is used as counter ion (see Figure 1.4).

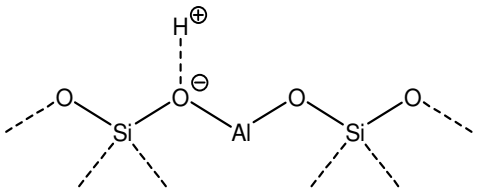

Figure 1.4: Brønsted acid site generated by substitution of Si with Al.

Concerning Brønsted acidity, both the density and actual strength of the acid sites are important in catalysis. Sites of different strength are able to catalyze different reactions e.g. only very strong Brønsted acid sites are active in fluid catalytic cracking.[31] Brønsted acidity is influenced by both the chemical composition and by the lattice structure of the zeolite (topography). The density of acid sites is related to the Si/Al ratio: The lower the ratio of Si/Al, the higher the concentration of acid sites. On the other hand, as the density of aluminum atoms in the framework increases, the strength of the Brønsted acid sites decreases. Quantum chemical calculations indicate that this

effect has its origin in the lower electronegativity of aluminum *versus* silicon atoms in the vicinity of a given Al-OH group.[32]

Zeolites have a highly ordered crystal structure with regular pores. These micropores (3 - 20 Å for most zeolites) are of similar size as common reactant molecules, allowing them to act as molecular sieves with a special property known as shape selectivity. This refers to the selectivity achieved in heterogeneous catalysis reactions, which depends specifically on the pore diameter, the framework architecture of the microporous material and the size of the reactants. One distinguishes between three types of shape selectivity:[33]

- *Reactant selectivity*: Only reactants below a certain molecular size can enter into the zeolite pore system and can undergo a catalytic reaction at the active sites in the micropores.
- *Product selectivity*: Only products of a certain size and/or shape can exit from the pore system. Larger products are retained and converted again until a smaller product, which is then able to exit the pore system, is formed.
- *Restricted transition state selectivity*: Only those reaction intermediates that geometrically fit into the zeolite cavities can be formed during catalysis, exit the pore system and turn into the desired product.

1.2.3. Synthesis routes

A large variety of synthesis routes have been developed for the synthesis of zeolites, among which, the hydrothermal route is the most convenient and most commonly used one.[30,34] This method was established in the 1950s by Barrer and coworkers who developed the basics of zeolite synthesis by systematic studies.[35] In contrast to the first attempts to synthesize zeolites, dated back to 1862, where geologic conditions were mimicked ($T > 673$ K and $p > 100$ bar),[36] now low temperatures (~373 K) and autogenous pressures were used for the hydrothermal synthesis. The crystallization of the zeolites from the precursors takes place via a sol-gel process (see Figure 1.5). For zeolite synthesis, the following five groups of reactants are necessary: source for T atoms, templates, mineralizer, solvent and (possibly) seed crystals.

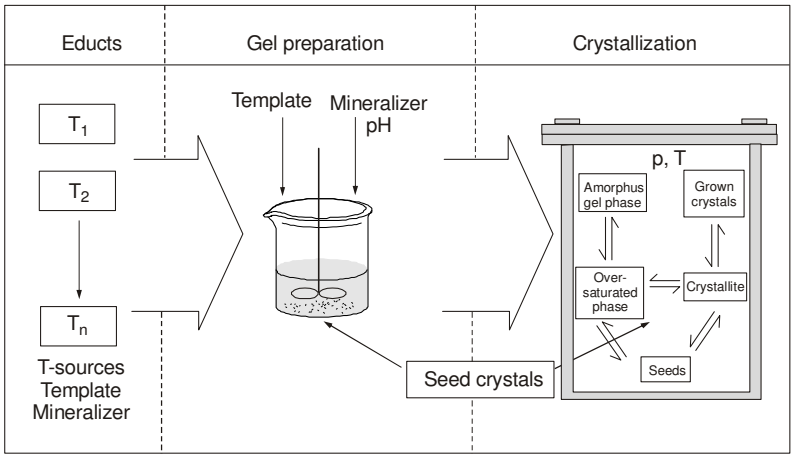

Figure 1.5: Synthesis of zeolites after the sol-gel process under hydrothermal conditions.

The most common T atoms are silicon and aluminium. However, also other cations such as titania, germanium or iron can be used if they fulfil certain conditions:[35]

- $R(T^{n+})/R(O^{2-})$ is between 0.225 and 0.414 (Pauling law)
- electronegativity allows a balanced ion-covalent bonding with oxygen
- the oxidation state is +3/+4
- the resulting framework has a mean charge per tetrahedron between -1 and 0

The precursors for the T atoms are generally present in the reaction mixture as amorphous hydroxides, hydrous oxides or related solids (e.g. precipitated gels). Silica can be present as soluble glass, volcanic ashes, colloidal suspensions or fumed silicas, while aluminium can be present as salts of mineralic acids, aluminium oxides or hydroxides.

For templates, inorganic cations (Sr^{2+}, K^{+}) are often applied but also organic cations can be used (tetramethylammonium cation). Templates possess structure directing properties and stabilize the zeolite structure during the synthesis procedure. The choice of the template is essential for receiving the desired crystal structure of the zeolite material.[37]

The most common mineraliser for silica- and aluminosilica-based zeolites is OH^{-}, which is often present in the source of the T atoms. According to the pH required for the reaction, fluoride salts or acids are added as sources of the F^{-} mineraliser. The most

important task of mineralisers is the decomposition of the amorphous aluminosilicates during the synthesis. An additional function is to increase the solubility of T atom containing species in the reaction mixture.

The most commonly used solvent is water, as it is suited for dissolution of all educts and can be easily applied for large-scale synthesis processes.

The mechanisms of zeolite formation during the sol-gel process are very complex due to the variety of chemical reactions, euqilibria and solubility variations that occur throughout the heterogeneous synthesis mixture during the crystallization process. In addition, zeolites are thermodynamically metastable phases. According to Ostwald's law of successive reactions, the first phase produced, is consumed and replaced by a thermodynamically more stable second phase and so on, until the most stable phase, which is usually quartz is formed. Therefore, the formation of the zeolite phase has to be kinetically controlled and an exact choice of the reaction parameters is essential for synthesizing the desired crystal structure.[37]

The as-synthesized zeolite product can be further modified by e.g. calcination, ion-exchange, dealumination or desilication to alter zeolite properties like acidity and porosity.

1.2.4. Zeolite BEA

Zeolite BEA is a large pore, high-silica zeolite and was first synthesized by Waldinger et al. working for Mobile Oil Corporation in 1967.[38] Today, it can be synthesized with Si/Al ratios between 10 and 100 and is used as catalyst in a large variety of industrial applications ranging from acid catalyzed hydrocarbon conversions to the selective synthesis of organic compounds.[39-48]

Zeolite BEA crystallizes in a tetragonal structure with 12-membered ring channels (0.66 × 0.67 nm) in the 100 direction, which are crossed with a second type of 12-membered ring channels (0.56 × 0.5 nm) in the 001 direction. Figure 1.6 shows a model of zeolite BEA, viewed along the 100 plane. One set of 12-membered pores is oriented perpendicular to the projection plane, while the second type of 12-membered pores is oriented from left to right within the projection plane. As these two pore systems are interconnected, they form cavities with a diameter of 1.2 nm. The unit cell

of zeolite BEA consists of nine structurally different T atom positions (Al and Si in tetrahedral coordination), which can be identified by high-resolution ^{29}Si MAS NMR.[49,50]

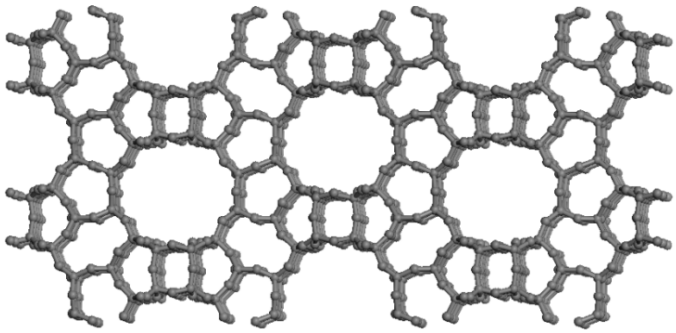

Figure 1.6: Scheme of zeolite BEA.

The material consists of an intergrowth of two structures, polymorph A and B, being characterized by a different arrangement of the periodical building unit (see Figure 1.7). For polymorph A, the translation of the building unit is alternating 1/3 a and -1/3 a, while it is periodically 1/3 a for polymorph B.[51] Both Polymorphs exist to equal fractions in the material and therefore, the stacking disorder in the region connecting the two polymorphs induces internal defects resulting from distorted and partially incomplete T-O-T bonds. Therefore, zeolite BEA is characterized by a high concentration of internal SiOH groups (silanol nests) which is expected to be important during healing processes or the insertion of external metal atoms.

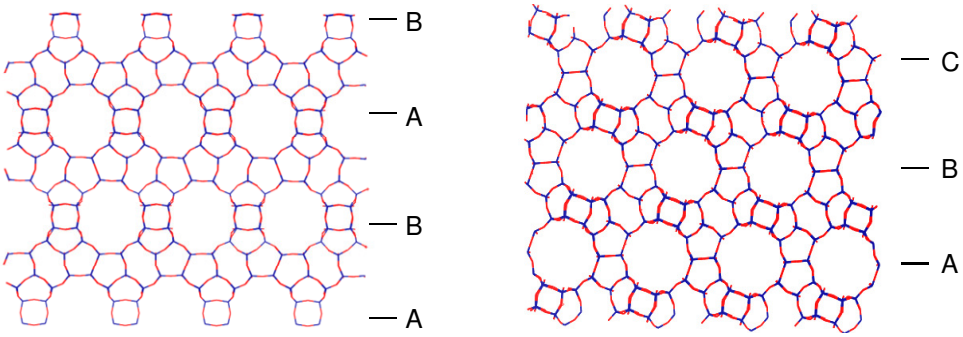

Figure 1.7: Framework structure of polymorph A (left) and polymorph B (right).[52]

1.2.5. Hydrothermal stability of zeolites

The application of zeolites in several industrial processes requires the knowledge about the hydrothermal stability of zeolites in the presence of water, as it is commonly present in industrial processes. This is also important for the application of zeolites in exhaust gas treatment, where water is produced during the combustion process and a high hydrothermal stability is essential.

Therefore, the processes occurring in zeolites during steaming treatments have been subject to a large number of studies, but they are not fully understood yet. It is generally accepted, however, that steaming leads to the hydrolysis of the Si-O-Al bonds and to the subsequent formation of slianol nests and extraframework aluminum oxide or hydroxide species as it is shown in Scheme 1.1.[53]

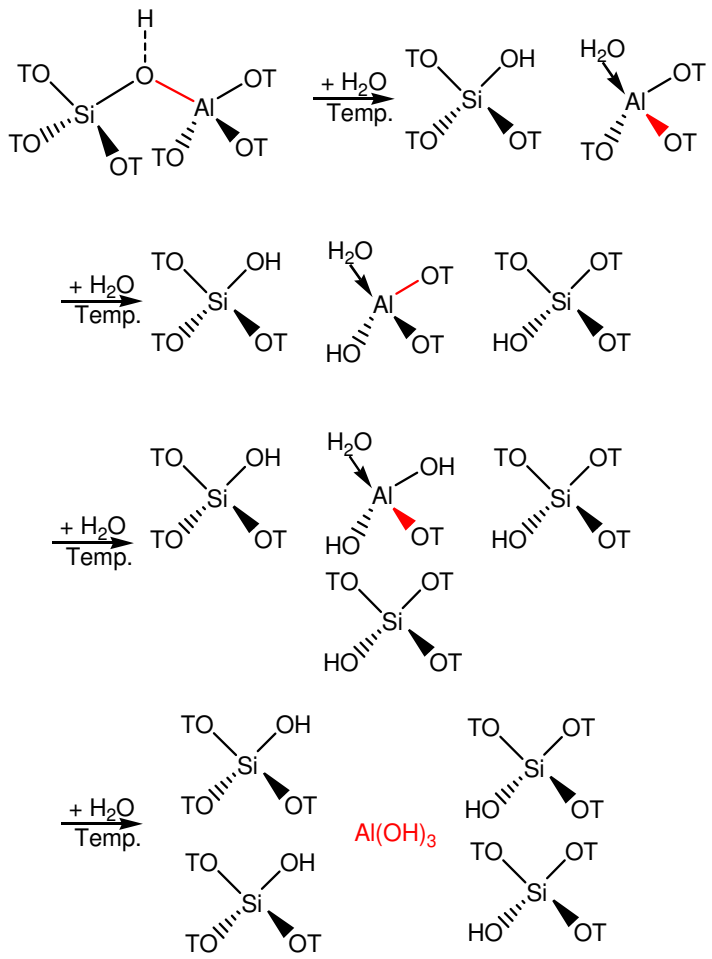

Scheme 1.1: Dealumination of zeolites by hydrolysis of the SiO-Al Bond.

The dealumination has a high impact on the acidity of the zeolite material, which is the reason why steaming of zeolites is often applied to specifically influence the acid properties of the as-synthesized materials.[54] As structure for the formed extraframework Al oxide/hydroxide species, cationic moieties (Al^{3+}, AlO^{+}, $Al(OH)^{2+}$, $Al(OH)_2^{+}$) and neutral or polymerized species (AlO(OH), $Al(OH)_3$, Al_2O_3) in four- and sixfold coordination have been proposed based on experimental techniques (NMR, XAS) as well as on DFT calculations.[55-57] It was also reported that a steaming treatment and subsequent formation of extraframework Al species leads to the stabilization of the zeolites. This is utilized to create ultra stable zeolite type Y (USY) which is steamed in large-scale for the use as catalysts in cracking reactions.[58]

The reverse process of the dealumination was first examined by van Bokhoven et al., who were able to reinsert Al in the presence of NH_3 at low temperatures (373 K) from octahedral coordinated extraframework positions into tetrahedral coordinated framework T atom positions.[53,59] Due to the basic properties of the reactant, the condensation of the OH groups is accelerated and the insertion of Al atoms into silanol nests is favored at lower temperatures.

The presence of both water and ammonia under NH_3-SCR conditions is expected to have oppositional effects on the hydrothermal stability of the zeolite, which will be dependent on the exact reaction conditions and the reaction temperature.

1.3. Fe-zeolites

In the last two decades, the modification of zeolites by incorporation of transition metals, especially with Fe has received much attention because Fe-zeolites are active as catalysts in some important reactions as the N_2O decomposition,[60] the selective catalytic reduction of NO by hydrocarbons or ammonia,[61-64] the direct (single step) oxidation of benzene to phenol,[65] the oxidative dehydrogenation of propane [66] and the oxidation of volatile organic compounds (VOCs).[67] Their application in the NH_3-SCR reaction is of great importance for exhaust gas aftertreatment and will be the main focus of this work.

1.3.1. Synthesis

The many possible applications for Fe-zeolites have led to the development and optimization of several synthesis procedures, from which the most common are presented in the following:

Wet-Ion Exchange

This exchange method is mostly used for preparation of ion-exchanged zeolites. The respective metal salt precursor (e.g. $FeSO_4$) is added to a suspension of the parent zeolite material and stirred. This can be also done at elevated temperature. To prevent the formation of geleous Fe-hydroxo species, the pH has to be controlled during the ion-exchange by acids and bases. Afterwards, the samples are washed, filtrated and dried.[60,68,69]

Chemical Vapour Deposition

Chemical vapour deposition is an efficient method to obtain high metal loadings.[70,71] A metal salt with high vapor pressure (e.g. $FeCl_3$) is hereby sublimated under high temperature into the pores of the parent zeolite material. To remove the formed anions, the catalyst has to be thoroughly washed and calcined.[72]

Solid-State Ion-Exchange

Solid-state ion-exchange is another easily applied and industrially used method.[60,69] A mixture of the parent zeolite material and the respective metal salt precursor is prepared in a ball mill. To obtain a more homogeneous distribution of the metal

precursor soluble compounds can be impregnated additionally. The obtained mixture is calcined for several hours to allow the ion-exchange inside the zeolite pores.

Calcination of Fe-Silicalite

A method to obtain highly dispersed Fe is to treat Fe-zeolites containing Fe in T atom positions at elevated temperatures. Fe has to be added to the precursor mixture during the synthesis step of the parent zeolite material to insert it into T atom positions. Due to a following high temperature treatment, Fe cations can be extracted from the T atom positions and are stabilized in ion-exchange positions.[73]

1.3.2. Structure and Nuclearity of Fe sites

The first studies concerning Fe-exchanged zeolites date back to the late 1960's and since then a very controversial debate about the structure and nuclearity of the Fe sites in Fe-zeolites was carried out in the scientific literature.[74,75] It was debated whether the above mentioned synthesis routes lead to the formation of isolated Fe ions, binuclear Fe-O-Fe species, Fe_xO_y-clusters of varying nuclearity or to larger particles of Fe_2O_3 present at the external surface of the zeolite crystals (see Figure 1.8).[76-81]

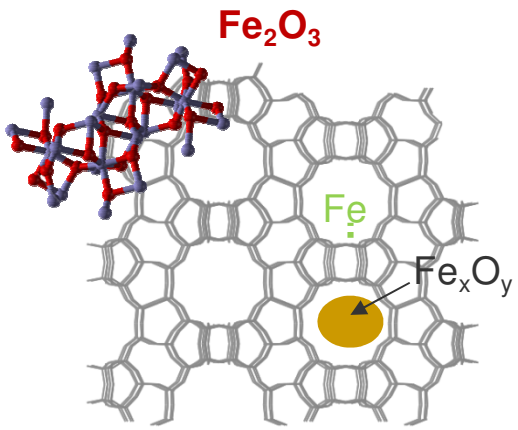

Figure 1.8: Overview of the different Fe species which can be present in Fe-zeolites.

For the characterization of the Fe species a broad variety of techniques is generally used. Among them are e.g. UV/Vis-, Mößbauer-, X-ray absorption (XANES and EXAFS)-, Electron Paramagnetic Resonance (EPR)-, Infrared (IR)- spectroscopy, temperature programmed reduction and desorption (H_2-TPR, NH_3-TPD), Electronmicroscopy (TEM, SEM) and X-ray diffraction (XRD).[18]

Although, a thorough characterization was carried out on Fe-zeolites and a series of structures was proposed, the question about the actual structure of the catalytic species in the NH_3-SCR reaction could not be solved until today. Different authors have proposed numerous active species and structures of the Fe species based on their observations from characterization, but interestingly the reported activities in the NH_3-SCR reaction were mostly similar. During the last years, all groups of Fe species have been proposed to be the active species, but among the reported species the binuclear Fe-O-Fe species were favored as the active species in the reduction of nitrogen oxides.[79,82] The structure of the binuclear Fe-species was proposed to be similar to that of the Fe cluster in methane monooxygenase serving as oxygen source in the selective oxidation of methane to methanol.[74,83-86] Dubkov et al. proposed a similar binuclear Fe structure, the so called alpha-oxygen species, to be active in the reduction of N_2O by aromatics and reported the uptake of one oxygen atom per alpha oxygen site.[87] They claim that these sites are generated by the oxidation of Fe with N_2O.

In general, the main reason for the uncertainty about the active Fe species in the NH_3-SCR reaction is the coexistence of Fe species with different nuclearity from monomeric Fe ions to big Fe_2O_3 clusters. In addition, the Fe species can be present as Fe^{2+} and Fe^{3+} species, as the oxidation state of Fe can be changed easily. From the above mentioned characterization techniques, some are specific for only one oxidation state (e.g. EPR, UV/Vis) and therefore, the chance exists that certain Fe centres can escape detection.[88] In addition, for a quantitative estimation of the respective species by IR or UV/Vis spectroscopy, the extinction coefficients, which are often not known, would be necessary. Other techniques exhibit similar problems: e.g. in EXAFS, the relationship between the average Fe-Fe coordination number and the average nuclearity is often ambiguous due to the heterogeneity of iron species. An average Fe-Fe coordination number of 1 could be interpreted as 100 % dimers or as 50 % isolated monomers and 50 % trimers.[89]

Therefore, the determination of the active Fe species in the NH_3-SCR reaction is still an ongoing debate and cannot be solved by conventional characterization. Brandenberger et al. proposed a statistical method to estimate the distribution of the different species dependant on the Fe loading of the catalyst.[90] But this method lacks experimental

prove and is not relevant for *in situ* studies. The only way to solve the question of the active species seems to be the combination of several characterization techniques to profit from the respective advantages of the different techniques. Especially the combination of different *in situ* techniques seems to be relevant in the future to get a picture about the coordination of the Fe species under reaction conditions. The knowledge of the active Fe species is essential to clear the way to the understanding of the whole mechanism of the NH_3-SCR reaction over Fe-zeolites and to the subsequent optimization of the catalytic systems.

1.3.3. Mechanistic aspects of NO_x reduction over Fe zeolites

A variety of parallel and side reactions could be identified for the mechanism of the NH_3-SCR reaction and the debate on the overall reaction mechanism over Fe-zeolites is still going on. One reason for this lack of clarity is the uncertainty about the structure of the Fe centres making it difficult to postulate a reaction mechanism. Therefore, only a short overview should be given at this point in order to get a general idea about the reaction network of the NH_3-SCR reaction. The overall reaction equations of the "normal" and "fast" SCR reaction are the following:[12]

"normal" $4\ NO + 4\ NH_3 + O_2 \rightarrow 6\ H_2O + 4\ N_2$ (2)

"fast" $NO + NO_2 + 2\ NH_3 \rightarrow 3\ H_2O + 2\ N_2$ (3)

Experiments with isotopically labeled nitrogen oxides and ammonia have shown that the generated nitrogen consists of one nitrogen atom from NO and one nitrogen atom from NH_3 proving the 1:1 stoichiometry between the educts.[91,92] However, it has been proposed that NO has to be first oxidized to NO_2 and that the reaction proceeds mainly via the fast SCR route over zeolites.[12,17,93,94] This is based on the fact that H-ZSM-5 shows only negligible SCR activity if only NO is present and a high SCR activity in the presence of 50 % NO_2. The role of the Fe centre in the zeolite catalyst is, therefore, to oxidize NO to NO_2 and adjust the right ratio between these oxides. As NO_2 is consumed immediately after its production as adsorbed species and does not show up as gas-phase NO_2, this thesis could not be unequivocally proven until now.[18] Devadas et al. found that the Fe sites also enhance the further reaction steps as the SCR activity on Fe-ZSM-5 was higher than the activity on H-ZSM-5 when a 1:1 mixture of NO and NO_2 was added as educts.[12]

They suggested the following mechanism of the oxidation of NO over Fe-zeolites, which is based on a redox cycle in which Fe is reversibly oxidized and reduced.[95]

$$NO + Fe^{3+}\text{-}O \rightarrow Fe^{3+}\text{-}O\text{-}NO \quad (4)$$

$$Fe^{3+}\text{-}O\text{-}NO \rightarrow Fe^{2+} + NO_{2,ads} \quad (5)$$

$$NO_{2,ads} \rightarrow NO_2\uparrow \quad (6)$$

$$Fe^{2+} + 0.5\ O_2 \rightarrow Fe^{3+}\text{-}O \quad (7)$$

It was concluded that the rate of the NO oxidation is controlled by the desorption of $NO_{2,ads}$ and this reaction step was postulated as the overall rate determining step for the NH_3-SCR reaction.

The formed NO_2 can react further either to N_2O_3 or by disproportionation of the intermediate N_2O_4 to NO^+ which can form nitrous acid in the presence of water:[96,97]

$$NO + NO_2 \rightarrow N_2O_3 \quad (8)$$

$$NO^+ + H_2O \rightarrow HNO_2 + H^+ \quad (9)$$

In addition, NO^+ can be produced from NO on metal sites and Brønsted acid sites. These two intermediates are important for the formation of NH_4NO_2, which decomposes even at room temperature to the environmentally friendly products N_2 and H_2O.[92]

$$HNO_2 + NH_3 \rightarrow NH_4NO_2 \quad (10)$$

$$N_2O_3 + 2NH_3 + H_2O \rightarrow 2NH_4NO_2 \quad (11)$$

$$NH_4NO_2 \rightarrow N_2 + 2\ H_2O \quad (12)$$

1.4. Scope of the thesis

Global warming and increasing environmental pollution have focused public concern on environmental protection and the development of more environmental friendly processes in industry as well as in every-day life. Among the main sources for environmental pollution are the exhausts from the transportation sector, including CO_2, hydrocarbons, particulate matters and nitrogen oxides. The emission of nitrogen oxides from diesel engines can be reduced by a catalytic treatment of the exhaust gases by the selective catalytic reduction using ammonia as reducing agent. Promising catalysts for the conversion of nitrogen oxides are Fe containing zeolites, whose characterization will be the main topic of this thesis. Understanding the ageing processes of these systems, especially in the presence of steam, is crucial for the application of these catalysts in the transportation sector. Therefore, this thesis will also deal with the examination of the processes going on under reaction conditions and the consequences of this treatment on the structure of the catalytic systems. To reach these targets, the studies were structured into three parts:

Steaming of the parent zeolite material

In the first part of the studies, it is our aim to understand the properties of the parent material zeolite HBEA. The concentration of the acid sites, the distribution of aluminum and the porous structure will be characterized by means of IR and MAS NMR spectroscopy as well as adsorption of probe molecules. These properties will also be determined for steam treated HBEA samples in order to understand the dealumination processes and their influence on the concentration of acid sites. This work will lay the basis for further ageing studies of the Fe-zeolite SCR catalysts.

Characterization of the redox properties of Fe under reaction conditions

Once the properties of the parent material HBEA are understood, the characterization will focus on the Fe-exchanged catalysts and the determination of their activity in the NH_3-SCR reaction. The most crucial point for the further study and understanding of the catalytic system is to identify the active Fe species and its structure, which is subject to controversial discussion in literature. In order to achieve this, a combination of X-ray absorption, UV/Vis and Mößbauer spectroscopy will be applied. Another

important issue will be the *in situ* characterization of the Fe species especially in respect to the oxidation-/reduction cycle. Therefore a combined XANES and Mößbauer spectroscopic study will be necessary to determine the oxidation state of the active Fe species *in situ*.

Ageing of the Fe containing zeolites under NH_3-SCR conditions

In the third and concluding part of this work, the results of the first two chapters will be combined with studies about the changes in the FeBEA catalysts under reaction conditions and in the presence of steam. Here, it should be compiled to what extent the Fe structure of the Fe species is changed and how the dealumination of the zeolite matrix takes place in Fe-exchanged samples under reaction conditions. Therefore, again, a combination of several characterization techniques such as IR, UV/Vis and X-ray absorption spectroscopy will be applied. The influence of these structural changes on the activity of the Fe-zeolite catalysts in the NH_3-SCR reaction will also be examined.

1.5. References

(1) Ostwald, W. *Z. Phys.* **1902**, *3*, 313.

(2) *Emissionskataster Bayern 2004***, 2009**.

(3) Walker, A. P. *Top. Catal.* **2004**, *28*, 165.

(4) Jobson, E. *Top. Catal.* **2004**, *28*, 191.

(5) *Verordnung (EG) Nr. 715/2007 des Europäischen Parlaments und des Rates, Amtsblatt der Europäischen Union* **2007**.

(6) Haeberer, R. *IAV MinNOx Conference, Berlin,* **2007**.

(7) Liu, Z. G.; Wall, J. C.; Barge, P.; Dettmann, M. E.; Ottinger, N. A. *Environ. Sci. Technol.* **2011**, *45*, 2965.

(8) Jacob, E.; Müller, R.; Schneeder, A.; Cartus, T.; Dreisbach, R.; Mai, H.; Paulus, M. *Motortechnische Zeitschrift* **2006**, 67.

(9) Martinez-Arias, A.; Conesa, J. C.; Fernandez-Garcia, M.; Anderson, J. A. *Supported Metals in Catalysis*, Imperial College Press: London **2005**, Vol. 5.

(10) Koebel, M.; Elsener, M.; Madia, G. *SAE Technical Paper* **2001**, 3625.

(11) Held, W.; Koenig, A.; Richter, T. *SAE Technical Paper* **1990**, 900496.

(12) Devadas, M.; Kröcher, O.; Elsener, M.; Wokaun, A.; Söger, N.; Pfeifer, M.; Demel, Y.; Mussmann, L. *Appl. Catal. B* **2006**, *67*, 187–196.

(13) Koebel, M.; Elsener, M.; Kleemann, M. *Catal. Today* **2000**, *59*, 335.

(14) Tuenter, G.; Vanleeuwen, W. F.; Snepvangers, L. J. M. *Ind. Eng. Chem. Prod.Res. Dev.* **1986**, *25*, 633.

(15) Wood, S. C. *Chem. Eng. Prog.* **1994**, *90*, 32.

(16) Forzatti, P.; Lietti, L. *Heterogen. Chem. Rev.* **1996**, *3*, 33.

(17) Rahkamaa-Tolonen, K.; Maunula, T.; Lomma, M.; Huuhtanen, M.; Keiski, R. L. *Catal. Today* **2005**, *100*, 217.

(18) Brandenberger, S.; Krocher, O.; Tissler, A.; Althoff, R. *Catal. Rev. - Sci. Eng.* **2008**, *50*, 492.

(19) Miyoshi, N.; Tanizawa, T.; Kasahara, K.; Tateishi, S. *Eur. Pat. Appl.* **1995**.

(20) Fridell, E.; Skoglundh, M.; Westerberg, B.; Johansson, S.; Smedler, G. *Journal of Catalysis* **1999**, *183*, 196.

(21) Cronstedt, A. F. *Akad. Handl. Stockholm* **1756**, *18*, 120.

(22) Coombs, D. S.; Alberti, A.; Armbruster, T.; Artioli, G.; Colella, C.; Galli, E.; Grice, J. D.; Liebau, F.; Mandarino, J. A.; Minato, H.; Nickel, E. H.; Passaglia, P., E., D. R.; Quartieri, S.; Rinaldi, R.; Ross, M.; Sheppard, R. A.; Tillmanns, E.; Vezzalini, G. *Can. Mineral.* **1997**, *35*, 1571.

(23) Barrer, R. M. *Proc. R. Soc. Lond. A-Math. Phys. Sci.* **1938**, *167*, 0392.

(24) Flanigen, E. M.; Rabo, J. A. *Microporous Mesoporous Mater.* **2001**, *47*, 120.

(25) http://izasc-mirror.la.asu.edu/fmi/xsl/IZA-SC/ft.xsl.

(26) Loewenstein, W. *Am. Miner.* **1954**, *39*, 92.

(27) McCusker, L. B.; Liebau, F.; Engelhardt, G. *Pure Appl. Chem.* **2001**, *73*, 381.

(28) Barrer, R. M. *Pure Appl. Chem.* **1979**, *51*, 1091–1100.

(29) Baerlocher, C.; McCusker, L. B. *Database of Zeolite Structures: http://www.izastructure.org/databases/*

(30) Weitkamp, J.; Puppe, L. *Catalysis and zeolites: Fundamentals and Applications* **1999**.

(31) Corma, A.; Gonzalez-Alfaro, V.; Orchilles, A. *Appl. Catal. A* **1995**, *129*, 203.

(32) Bartholomew, C. H.; Farrauto, R. J. *Fundamentals of Industrial Catalytic Processes*; John Wiley & Sons, 1997.

(33) Hagen, J. *Industrial Catalysis*; Wiley: Weinheim, **2006.**

(34) Barrer, R. M. *Zeolites* **1981**, *1*, 130.

(35) Kühl, G. *Catalysis and Zeolites (Fundamentals and Applications)*; Springer: Berlin, **1999.**

(36) de St. Claire Deville, H. *Compt. Rend.* **1862**, *54*, 324.

(37) Davis, M. E.; Lobo, R. F. *Chem. Mater.* **1992**, 756.

(38) Waldinger, R. L.; Kerr, G. T.; Rossinski, E. J. *US Patent* **1967**, 3308069.

(39) Newsam, J. M.; Treacy, M. M. J.; Koetsier, W. T.; Gruyter, C. B. D. *Proc. R. Soc. London, A* **1988**, *420*, 375.

(40) Higgins, J. B.; LaPierre, R. B.; Schlenker, J. L.; Rohrman, A. C.; Wood, J. D.; Kerr, G. T.; Rohrbaugh, W. J. *Zeolites* **1988**, *8*, 446.

(41) Dartt, C. B.; Davis, M. E. *Catal. Today* **1994**, *19*, 151.

(42) Tanabe, K.; Hölderich, W. F. *Appl. Catal., A* **1999**, *181*, 399.

(43) Nivarthy, G. S.; He, Y. J.; Seshan, K.; Lercher, J. A. *J. Catal.* **1998**, *176*, 192.

(44) Feller, A.; Guzman, A.; Zuazo, I.; Lercher, J. A. *Science And Technology In Catalysis 2002* **2003**, *145*, 67.

(45) Bellussi, G.; Pazzuconi, G.; Perego, C.; Girotti, G.; Terzoni, G. *J. Catal.* **1995**, *157*, 227.

(46) Degnan, T. F.; Smith, C. M.; Venkat, C. R. *Appl. Catal., A* **2001**, *221*, 283.

(47) Jansen, J. C.; Creyghton, E. J.; Njo, S. L.; van Koningsveld, H.; van Bekkum, H. *Catal. Today* **1997**, *38*, 205.

(48) Creyghton, E. J.; Ganeshie, S. D.; Downing, R. S.; vanBekkum, H. *J. Mol. Catal. A: Chem.* **1997**, *115*, 457.

(49) Fyfe, C. A.; Feng, Y.; Grondey, H.; Kokotailo, G. T.; Gies, H. *Chem. Rev.* **1991**, *91*, 1525.

(50) Stelzer, J.; Paulus, M.; Hunger, M.; Weitkamp, J. *Microporous Mesoporous Mater.* **1998**, *22*, 1.

(51) http://www.iza-structure.org/databases/Catalog/Beta.pdf.

(52) Corma, A.; Moliner, M.; Cantin, A.; Diaz-Cabanas, M. J.; Jorda, J. L.; Zhang, D.; Sun, J.; Jansson, K.; Hovmöller, S.; Zou, X. *Chem. Mater.* **2008**, *20*, 3218.

(53) van Bokhoven, J. A.; Koningsberger, D. C.; Kunkeler, P.; van Bekkum, H.; Kentgens, A. P. M. *J. Am. Chem. Soc.* **2000**, *122*, 12842.

(54) de Lucas, A.; Canizares, P.; Durán, A.; Carrero, A. *Applied Catalysis A: General* **1997**, *154*, 221.

(55) Benco, L.; Demuth, T.; Hafner, J.; Hutschka, F.; Toulhoat, H. *J. Catal.* **2002**, *209*, 480.

(56) Bhering, D. L.; Ramirez-Solis, A.; Mota, C. J. A. *J. Phys. Chem. B* **2003**, *107*, 4342.

(57) Lisboa, O.; Sánchez, M.; Ruette, F. *J. Mol. Catal. A: Chem.* **2008**, *294*, 93.

(58) Beyerlein, R. A.; Choi-Feng, C.; Hall, J. B.; Huggins, B. J.; Ray, G. J. *Fluid Catalytic Cracking III*, 1994.

(59) Omegna, A.; Vasic, M.; van Bokhoven, J. A.; Pirngruber, G.; Prins, R. *Phys. Chem. Chem. Phys.* **2004**, *6*, 447.

(60) Pieterse, J. A. Z.; Boonevold, S.; Brink, R. W. v. d. *Appl.Catal., B* **2004**, *51*, 215.

(61) Guzman-Vargas, A.; Delahay, G.; Coq, B.; P., L.; Bosh, P.; Jumas, J. C. *Catal. Today* **2005**, *107*, 94.

(62) Schwidder, M.; Kumar, M. S.; Bentrup, U.; Perez-Ramirez, J.; Brückner, A.; Grünert, W. *Microporous Mesoporous Mater.* **2008**, *111*, 124.
(63) Qi, G. S.; Yang, R. T. *Appl. Catal. B* **2005**, *60*, 13.
(64) Schwidder, M.; Heikens, S.; De Toni, A.; Geisler, S.; Berndt, M.; Brückner, A.; Grünert, W. *J. Catal.* **2008**, *259*, 96.
(65) Panov, G. I.; Sheveleva, G. A.; Kharitonov, A. S.; Romannikov, V. N.; Vostrikova, L. A. *Appl. Catal., A* **1992**, *82*, 31.
(66) Perez-Ramirez, J.; Gallardo-Llamas, A. *Appl. Catal. A* **2005**, *279*, 117.
(67) Halazs, J.; Hodos, I.; Hannus, G.; Held, I.; Kiricsi, I. *Coloids Surf. A* **2005**, *265*, 171.
(68) Long, R. Q.; Yang, R. T. *J. Catal.* **1999**, *188*, 332.
(69) Long, R. Q.; Yang, R. T. *Catalysis Letters* **2001**, *74*, 201.
(70) Lobree, L. J.; Hwang, I. C.; Reimer, J. A.; Bell, A. T. *J. Catal.* **1999**, *186*, 242.
(71) Chen, H. Y.; Sachtler, W. M. H. *Catal. Today* **1998**, *42*, 73.
(72) Lee, H. T.; Rhee, H. K. *Catal. Lett.* **1999**, *61*, 71.
(73) Bordiga, S.; Buzzoni, R.; Geobaldo, F.; Lamberti, C.; Giamello, E.; Zecchina, A.; Leofanti, G.; Petrini, G.; Tozzola, G.; Vlaic, G. *J. Catal.* **1996**, *158*, 486.
(74) Garten, R. L.; Delgass, W. N.; Boudart, M. *J. Catal.* **1970**, *18*, 90.
(75) Morice, J. A.; Rees, L. V. C. *Trans. Faraday Soc.* **1968**, *64*, 1388.
(76) Brandenberger, S.; Kröcher, O.; Tissler, A.; Althoff, R. *Appl. Catal., B* **2010**, *95*, 348.
(77) Long, R. Q.; Yang, R. T. *Catal. Lett.* **2001**, *74*, 201.
(78) Kumar, M. S.; Schwidder, M.; Grünert, W.; Bentrup, U.; Brückner, A. *J. Catal.* **2006**, *239*, 173.
(79) Schwidder, M.; Kumar, M. S.; Brückner, A.; Grünert, W. *Chem. Commun.* **2005**, 805.
(80) Sklenak, S.; Andrikopoulos, P. C.; Boekfa, B.; Jansang, B.; Nováková, J.; Benco, L.; Bucko, T.; Hafner, J.; Dedecek, J.; Sobalík, Z. *J. Catal.* **2010**, *272*, 262.
(81) Sobalik, Z.; Vondrová, A.; Tvaruzková, Z.; Wichterlová, B. *Catal. Today* **2002**, *75*, 347.
(83) Joyner, R.; Stockenhuber, M. *J. Phys. Chem. B* **1999**, *103*, 5963.

(84) Battiston, A. A.; Bitter, J. H.; de Groot, F. M. F.; Overweg, A. R.; Stephan, O.; van Bokhoven, J. A.; Kooyman, P. J.; van der Spek, C.; Vankó, G.; Koningsberger, D. C. *J. Catal.* **2003**, *213*, 251.

(85) Battiston, A. A.; Bitter, J. H.; Heijboer, W. M.; de Groot, F. M. F.; Koningsberger, D. C. *J. Catal.* **2003**, *215*, 279.

(86) Chen, H. Y.; El-Malki, E.-M.; Wang, X.; van Santen, R. A.; Sachtler, W. M. H. *J. Mol. Catal. A: Chem.* **2000**, *162*, 159.

(87) Chen, H. Y.; Sachtler, W. M. H. *Cataly. Today* **1998**, *42*, 73.

(88) Marturano, P.; Drozdová, L.; Kogelbauer, A.; Prins, R. *J. Catal.* **2000**, *192*, 236.

(89) Dubkov, K. A.; Ovanesyan, N. S.; Shteinman, A. A.; Starokon, E. V.; Panov, G. I. *J. Catal.* **2002**, *207*, 341.

(90) Brandenberger, S.; Kröcher, O.; Tissler, A.; Althoff, R. *Appl. Catal., A*, *373*, 168.

(91) Zecchina, A.; Rivallan, M.; Berlier, G.; Lamberti, C.; Ricchiardi, G. *Phys. Chem. Chem. Phys.* **2007**, *9*, 3483.

(92) Otto, K.; Shelef, M.; Kummer, J. T. *J. Phys. Chem.* **1970**, *74*, 2690.

(93) Sun, Q.; Gao, Z. X.; Chen, H. Y.; Sachtler, W. M. H. *J. Catal.* **2001**, *201*, 89.

(94) Delahay, G.; Valade, D.; Guzman-Vargas, A.; Coq, B. *Appl. Catal. B* **2005**, *55*, 149.

(95) Huang, H. Y.; Long, R. Q.; Yang, R. T. *Appl. Catal. A* **2002**, *235*, 241.

(96) Schmidt, R.; Amiridis, M. D.; Dumesic, J. A.; Zelewski, L. M.; Millman, W. S. *J. Phys. Chem. B* **1992**, *96*, 8142.

(97) Centi, G.; Perathoner, S. *Catal. Today* **1996**, *1-4*, 117.

Chapter 2

Steaming of Zeolite BEA and its Effect on Acidity: A comparative NMR and IR Spectroscopic Study

The kinetics and impact of steaming on the acid site concentration of zeolite BEA was studied by ^{1}H, ^{27}Al and ^{29}Si MAS NMR spectroscopy as well as IR spectroscopy of adsorbed pyridine and temperature programmed desorption of NH_3. The main effects of steaming were the dealumination of the T3 – T9 sites, the formation and migration of extraframework Al species and the healing of defect sites by condensation of silanol groups. These effects took place mainly in the first five hours of steaming, while after 14 hours of steaming the system appeared to be stabilized. The concentration of framework Al atoms detected by ^{27}Al MAS NMR spectroscopy is significantly higher than the concentration of Brønsted acid sites determined by ^{1}H MAS NMR spectroscopy as well as by the sorption of basic probe molecules such as NH_3 and pyridine. This shows conclusively that extraframework Al oxide/hydroxide species act as cations balancing the framework charge. The concentration of extraframework Al atoms matches the discrepancy between the concentration of framework Al atoms and the concentration of Brønsted acid sites indicating that each charge balancing entity contains only one aluminum.

2.1. Introduction

Zeolite BEA, which can be synthesized with Si/Al ratios between 10 and 100, is used in a large variety of industrial applications as catalyst for acid catalyzed hydrocarbon conversions and the selective synthesis of organic compounds.[1-10] Due to the numerous industrial applications, information about its stability in the presence of water is of high importance. Water-free conditions cannot be always guaranteed in practice and it is also established that pre-steaming of zeolites enhances the activity and the resistance against water vapor for selective reactions.[11-13] Examples of large-scale pre-steaming in industrial applications are zeolite Y to create ultra-stable Y (USY)[14] and mordenite catalysts used in paraffin hydroisomerization.[15]

The processes occurring in zeolites during steaming have been subject to a large number of studies, but are still not fully understood in their specificity for a particular structure. It is generally accepted, however, that steaming leads to dealumination of the framework via hydrolysis of the Si-O-Al bonds and to the formation of extraframework aluminum oxide or hydroxide species.[16] The rates and efficiency of these processes depend on the geometry of the aluminum coordination and the conditions of hydrolysis.

Zeolite BEA has a three-dimensional pore system with intersecting channels formed by 12-membered rings with a diameter of 0.67 nm. The material consists of an intergrowth of two structures, i.e., polymorph A and B.[2,17] The stacking disorder in the region connecting the two polymorphs induces internal defects resulting from distorted and partially incomplete T-O-T bonds.

In the unit cell of zeolite BEA nine structurally different T atom positions (Al and Si in tetrahedral coordination) can be identified by high-resolution ^{29}Si MAS NMR.[18,19] Van Bokhoven et al. reported that Al atoms occupying the T1 and T2 positions remain stable during steaming and that dealumination occurs only for Al atoms at the T3 – T9 positions. For the extraframework Al species, generally associated with Lewis acid sites,[20] four and six fold coordinations of aluminum to oxygen have been observed by ^{27}Al MAS NMR and ^{27}Al MQ MAS NMR.[16, 21] Bourgeat-Lami studied the relation of the coordination of extraframework aluminum and the nature of the charge compensation cation and described the possibility of a transformation between four and six fold coordinated Al during ion-exchange of alkali metals.[22] Van Bokhoven et al. observed a

similar behavior in the presence of water, where Al in the tetrahedral framework sites is transformed into extraframework octahedral aluminum species.[16] DFT calculations proposed two types of extraframework cationic moieties (Al^{3+}, AlO^{+}, $Al(OH)^{2+}$, $Al(OH)_2^{+}$) and neutral or polymerized species (AlO(OH), $Al(OH)_3$, Al_2O_3).[23-25]

The formation of extraframework Al species can affect the pore structure and porosity of the zeolite. Removal of a large fraction of Al from the lattice leads to rearrangements of Si T atoms and hence to the generation of large voids in the structure. The presence of such micro- and mesopores can be crucial to obtain a high catalytic activity, when diffusion processes affect the overall rate. On the other hand, Marques et al. [26] reported the blockage of micropores due to condensation of extraframework Al species and suggested that polymerization of extraframework Al species mainly takes place in the first three hours of steaming, while polymerization occurring after longer steaming times only takes place when polymeric species were already formed earlier.[27,28]

Six types of hydroxyl groups can be observed by IR spectroscopy of zeolite BEA: internal and external silanol groups (3740 and 3725 cm^{-1}), bridging Si-OH-Al groups (3606 cm^{-1}), two kinds of Al-OH groups (3670 cm^{-1} and 3784 cm^{-1}) and hydrogen bonded hydroxyl groups (3500 cm^{-1}-3200 cm^{-1}).[29-33] Brønsted acidity results from the bridging Si-OH-Al groups and, thus, should be proportional to the concentration of Al atoms in the framework, while Lewis acidity is mainly related to the presence of extraframework Al species. A significant number of papers have been dedicated to the effect of steaming on the acidity. In general, it was found that steaming decreases both, Brønsted and Lewis acid sites, the former by removal of Al from the lattice by hydrolysis, the latter by condensation of alumina moieties.[33, 34]

The aim of this work is to explain the effects of steaming treatment on zeolite BEA with respect to the acidity and framework stability. ^{29}Si, ^{27}Al and ^{1}H MAS NMR, IR spectroscopy as well as temperature programmed desorption of NH_3 were used to characterize the material. We will show that the framework of zeolite BEA is highly stable against dealumination and that several processes influence its acidity in this course. Steaming leads to the formation, conversion and migration of extraframework Al species, which may block acid sites and, therefore, reduce the acid site concentration of the material.

2.2. Experimental

2.2.1. Materials

The parent material was an acidic H-BEA zeolite with a Si/Al ratio of 18 provided by Süd-Chemie AG. The steaming treatment was carried out at 753 K in 100 % steam inside a horizontal quartz tube oven. Water was fed into the system with a *Gilson 307* HPLC pump at a constant flow rate of 1.2 g (H_2O)/h·g (zeolite). The steaming procedure was carried out for four different durations (1 h, 5 h, 14 h and 24 h). Afterwards the samples were dried in nitrogen flow (100 ml/min) for 2 h at 353 K. The samples were named HBEA35-parent, HBEA35-s1, HBEA35-s5, HBEA35-s14 and HBEA35-s24.

2.2.2. Specific surface area and porosity

The surface area and pore diameters were calculated from nitrogen sorption measurements performed on an automated BET system (PMI automated Sorptomatic 1990) at liquid nitrogen temperature (77 K) after outgassing in vacuum ($p = 10^{-3}$ mbar) at 473 K for 2 h. The apparent surface area was calculated by applying the Brunauer-Emmett-Teller (BET) theory to the adsorption isotherms over a relative pressure range from $p/p_0 = 0.03$ - 0.30. The pore volumes were evaluated using the t-plot method [35] according to Harkins and Jura.[36] Because of the limitations of the PMI instrument, the isotherms were measured at relative partial pressures higher than $p/p_0 > 10^{-5}$.

2.2.3. Scanning electron microscopy

Scanning electron microscopy (SEM) images of the samples HBEA35-parent and HBEA35-s24 were recorded on a JEOL JSM 5900 LV microscope operating at 25 kV with a resolution of 5 nm and a nominal magnification of 3.0×10^6.

2.2.4. X-ray diffraction

The crystal structure of all samples was analyzed by X-ray powder diffraction. Measurements were done using a *"Philips X'Pert Pro System"* using Cu-Kα-radiation of 0.154056 nm (45 kV and 40 mA). The experiments were carried out on a rotating powder sample holder in a 2θ range of 5° to 70° with a step size of 0.019°/s.

2.2.5. Nuclear magnetic resonance spectroscopy

All solid-state magic-angle-spinning NMR (MAS-NMR) measurements were performed on a Bruker AV500 spectrometer ($B_0 = 11.7$ T) at a rotating frequency of 12 kHz and at 298 K.

^{27}Al MAS NMR For ^{27}Al-MAS NMR the samples were fully hydrated in a desiccator at 338 K for 5 days and packed into a 4 mm ZrO_2 rotor. The spectra were recorded at a resonance frequency of 130.3 MHz. The excitation pulse length was 0.46 µs; the recycle time was 0.25 s. The chemical shifts were referenced to an external standard of $Al(NO)_3$ ($\delta = -0.54$ ppm). The spectra were normalized to the sample mass for quantitative comparison.

^{29}Si MAS NMR For ^{29}Si-MAS NMR the samples were packed into a 4 mm ZrO_2 rotor. The spectra were recorded at a resonance frequency of 99.3 MHz. The pulse length was 1.5 µs; the recycle time was 50 s. The chemical shifts were referenced to an external standard of tetrakis-trimethylsilylsilane ($\delta = 9.84$ ppm). The spectra were normalized to the sample mass for quantitative comparison.

^{1}H MAS NMR For ^{1}H-MAS NMR spectra, the samples were activated in vacuum at 723 K for 1 h to eliminate adsorbed water. Then, they were transferred to a glove box and packed into a 4 mm ZrO_2 rotor in a water and oxygen free atmosphere. For recording the spectra, an excitation pulse ($\pi/2$) with a power level of 6.00 dB and a length of 3.80 µs was applied. The recycle time was 40 s. The chemical shifts were referenced to an external standard of adamantane ($\delta = 1.78$ ppm). The spectra were normalized to the sample mass for quantitative comparison. The concentration of the Brønsted acid sites was determined from the integral areas using an external standard of a standard zeolite material with known acid site concentration (H-ZSM-5, Si/Al = 45 from Süd-Chemie AG, 0.360 mmol acid sites g^{-1}, determined by microgravimetric adsorption of NH_3) as reference.

All NMR spectra were fitted with Gaussian functions for quantitative deconvolution of overlapping peaks.

2.2.6. Infrared spectroscopy

The infrared spectra were measured on a Perkin-Elmer 2000 spectrometer at a resolution of 4 cm^{-1}. The samples were prepared as self-supporting wafers (density approximately 10 mg/cm^{-2}) and activated in vacuum ($p = 10^{-6}$ mbar) for 1 h at 723 K (heating rate = 10 K/min). After cooling to 423 K the samples were exposed to pyridine ($p = 10^{-1}$ mbar) for 1 h and then outgassed ($p = 10^{-6}$ mbar) at 423 K for 1 h. Subsequently, the sample was heated to 723 K at a rate of 10 K/min, outgassed for 1 h at this temperature and again cooled to 423 K. All spectra were collected at 423 K. To directly compare the surface coverage of the adsorbed species all spectra were normalized using the overtone and combination vibrations of zeolite BEA between 2095 and 1755 cm^{-1} after activation. For quantification, molar integral extinction coefficients of 0.73 cm/µmol and 0.96 cm/µmol were used for Brønsted and Lewis acid sites, respectively. These were determined for a reference material (H-ZSM-5, $SiO_2/Al_2O_3 = 90$ from Süd-Chemie AG; 0.360 mmol acid sites g^{-1}) using a combination of IR spectroscopy of adsorbed pyridine and microgravimetric measurements of the thermal stability of adsorbed pyridine.

2.2.7. Temperature-programmed desorption of ammonia

Temperature programmed desorption of ammonia was carried out in a six-fold TPD set-up. About 50 mg of the samples were granulated to a particle size between 500 and 710 µm and activated in vacuum ($p = 10^{-3}$ mbar) at 723 K (heating rate = 10 K/min) for 1 h. After cooling to 373 K, 1 mbar of NH_3 was adsorbed for 1 h followed by outgassing of the samples for 2 h. The temperature was increased to 1043 K at a rate of 7 K/min while desorption of NH_3 was monitored by mass spectroscopy using the $m/z^+ = 16$ signal. The acid site concentration was determined by normalization to the sample weight and comparison of the resulting integral area of the desorption peaks with that of a standard zeolite material with known acid site concentration (H-ZSM-5, $SiO_2/Al_2O_3 = 90$ from Süd-Chemie AG, 0.360 mmol acid sites g^{-1}).

2.3. Results

2.3.1. Physicochemical Characterization

The sample HBEA35-parent consists of cubic particles with an uneven size distribution ranging from 100 nm to 500 nm as determined by SEM images. After 24 h of steaming significant changes in particle size and shape were not observed (see Figure 2.1).

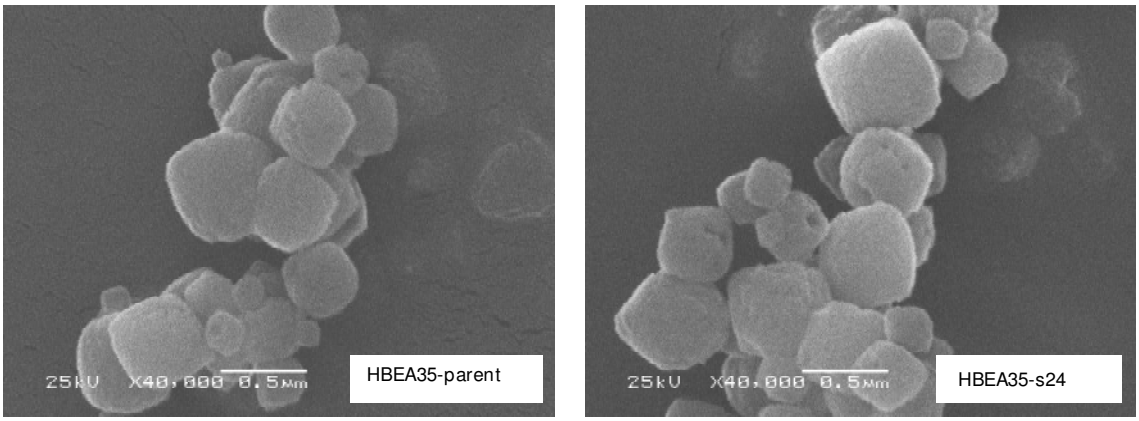

Figure 2.1: SEM images of the samples HBEA35-parent and HBEA35-24 h.

The sample HBEA35-parent shows an apparent BET surface area of 675 m^2/g and a micropore volume of 206 mm^3/g. Steaming for 24 h leads to a decrease of the micropore volume to 167 mm^3/g, which is equal to a loss of 19 % as well as a decrease of the apparent BET surface area to 613 m^2/g. Pore volumes and apparent specific surface areas of all investigated samples are summarized in Table 2.1.

Table 2.1: Surface areas and pore volumes obtained from N_2-physisorption.

sample	spec. surface area [m^2/g]	micropore volume [cm^3/g]
HBEA35-parent	675	0.206
HBEA35-s1	672	0.213
HBEA35-s5	644	0.193
HBEA35-s14	618	0.180
HBEA35-s24	613	0.167

X-ray diffraction of the samples confirmed that all samples are highly crystalline and that an amorphous phase was not formed during the steaming treatment to an appreciable extent (see A.1).

2.3.2. Changes in the Environment of Si and Al Species during Dealumination

The changes in the local structure of the Al T atoms and the Si atoms during the steaming treatment were characterized by ^{29}Si MAS NMR and ^{27}Al MAS NMR spectroscopy. In the ^{29}Si MAS NMR spectra, which are shown in Figure 2.2, four peaks assigned to Q^4 (-115 ppm and -111 ppm), Q^3 (-104 ppm) and Q^2 (-95 ppm) sites were detected (see A.2).[37] The two peaks for Q^4 sites originate from the two different stacking orders polymorph A and polymorph B known for zeolite BEA. The Q^3 peak at -104 ppm is a superposition of two peaks at -103 ppm and -107 ppm originating from $Si(OSi)_3(OH)_1$ and $Si(OSi)_3(OAl)_1$ tetrahedrons, respectively.

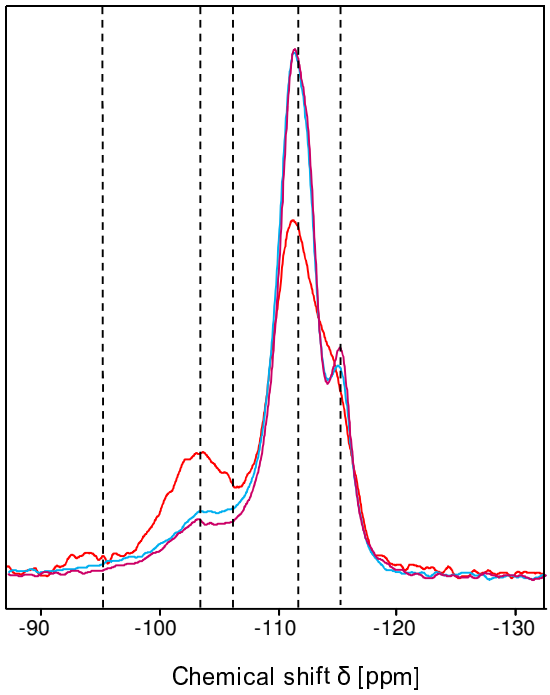

Figure 2.2: ^{29}Si MAS NMR spectra of HBEA35-parent (red), HBEA35-s5 (light blue), HBEA35-s24 (purple).

All peaks were fitted with Gaussian functions and the resulting relative peak areas are shown in Table 2.2.

The main effect of the steaming treatment observed by ^{29}Si MAS NMR spectroscopy was the decrease of the signal at -107 ppm originating from $Si(OSi)_3(OH)_1$ defect sites and silanol groups. This was accompanied by an increase of the signal at -111 ppm originating from Q^4 sites. The transformation of Q^3 defect sites to Q^4 sites occurred in the first five hours of steaming, while a longer steaming treatment had no further influence on the Si-coordination. In addition, the dealumination of the Q^3 and Q^2 sites assigned to $Si(OSi)_3(OAl)_1$- and $Si(OSi)_2(OAl)_2$-tetrahedrons was observed. About 25 % of the Q^2 sites were lost in the first five hours of steaming, while another 25 % were lost in the next 19 h. The dealumination of the Q^3 sites occurred in the first five hours of steaming, during which the intensity decreased by about 20 %, while a further decrease of 10 % occurred in the following 19 h of steaming.

Table 2.2: Percentage of the peak areas determined by deconvolution of the ^{29}Si MAS NMR spectra.

sample	-115 ppm [%]	-111 ppm [%]	-107 ppm [%]	-103 ppm [%]	-97 ppm [%]
HBEA35-parent	16	53	10	16	4
HBEA35-s5	15	64	8	9	3
HBEA35-s24	17	64	7	9	2

In the ^{27}Al MAS NMR spectra (see Figure 2.3 and A.3) several signals assigned to overlapping tetrahedral species in the region between 40 and 65 ppm as well as resonances of extraframework octahedral Al species around 0 ppm were observed. The peak at around 0 ppm is a superposition of a sharp peak assigned to well-ordered octahedral Al species and a broad peak assigned to distorted octahedral Al species. The intensity of the sharp peak decreases during the steaming treatment, while the total concentration of octahedral Al species increases from 16 % to 18 %. The signal of the tetrahedral Al species is assigned to extraframework Al species in a distorted environment (44 ppm), framework Al atoms occupying T1 and T2 sites (54 ppm), framework Al species occupying T3 – T9 sites (57 ppm) and extraframework

tetrahedral Al species (63 ppm).[16,38] The relative areas of the different peaks are shown in Table 2.3.

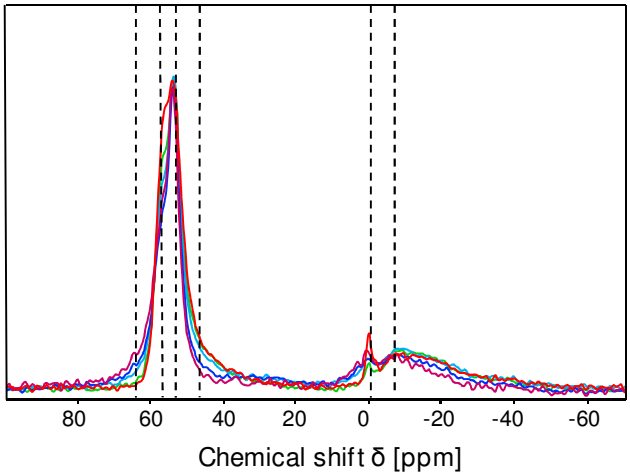

Figure 2.3: ^{27}Al MAS NMR spectra of HBEA35-parent (red), HBEA35-s1 (green), HBEA35-s5 (light blue), HBEA35 s14 (dark blue), HBEA35-s24 (purple).

In the untreated sample HBEA35-parent 69 % of the Al was tetrahedrally incorporated into the framework, while after 1 h of steaming treatment this fraction decreased to 64 %. Further steaming for 5 h and 14 h led to a decrease to 62 and 59 %, respectively, while after 24 h of steaming no further decrease was observed. The deconvolution of the spectra showed that the steaming treatment led to a decrease of the signal at 57 ppm (T3 - T9 sites), while the signal at 54 ppm (T1 and T2 sites) was not affected by the steaming treatment at all. The dealumination process of Al in T3 – T9 sites occurred mainly in the first hour of steaming, during which 18 % of the Al atoms in T3 – T9 sites were removed, while only further 14 % were removed from these lattice sites during the following 14 h (of steaming).

The integral of the signal at 44 ppm decreased during steaming from initially 15 % for the parent sample to 2 % relative integral area after 24 h of steaming. At the same time the formation of extraframework Al in tetrahedral coordination (signal at 63 ppm) was observed. The relative integral area of this peak increased to 7 % after 24 h of treatment. The total concentration of Al detected in ^{27}Al MAS NMR spectroscopy decreased by about 14 % after 24 h of steaming time, which indicates the formation of “NMR-invisible Al” in highly distorted extraframework coordination. Due to the high

quadrupolar coupling constant of Al with a spin of 5/2, Al atoms located in this highly distorted and strained coordinations, it cannot be observed in ^{27}Al MAS NMR due to a severe line broadening of the signal under the experimental conditions used.[22, 39]

Table 2.3 Relative peak areas determined from the ^{27}Al MAS NMR spectra. The percentages of the peak areas were referred to the total integral area of the sample HBEA35-parent.

sample	44 ppm [%]	54 ppm [%]	57 ppm [%]	63 ppm [%]	~0 ppm [%]	missing Al [%]
HBEA35-parent	15	41	28	0	16	0
HBEA35-s1	15	41	23	2	17	3
HBEA35-s5	13	40	20	4	18	4
HBEA35-s14	8	40	19	4	18	11
HBEA35-s24	2	40	19	7	18	14

2.3.3. Influence of Steaming on Zeolite Acidity

The characterization of the steamed zeolite BEA samples by ^{1}H MAS NMR spectroscopy allows a quantitative analysis of the different hydroxyl groups. The ^{1}H MAS NMR spectra of the five samples showed characteristic signals at 0.6 ppm, 1.7 ppm, 1.9 ppm, 2.7 ppm, 4.0 ppm and 5.0 ppm (see Figure 2.4 and A.4). The signals at 0.6 ppm and 2.7 ppm are assigned to extraframework Al species, while the signals at 1.7 ppm, 1.9 ppm can be assigned to silanol groups and defect sites located at the Q^3 Si sites.[40] The signal at 1.9 ppm decreased with increasing steaming time, which reflects the condensation of Q^3 SiOH sites, also detected by ^{29}Si MAS NMR spectroscopy. The relative peak areas of the silanol groups decreased from 65 % relative area to 45 %, which is mainly due to the condensation of internal defect sites (1.9 ppm), while the concentration of terminal silanol sites (1.7 ppm) stayed nearly constant. In addition, one can observe, the migration of extraframework Al species, as the intensity of the signal at 2.7 ppm decreased and in parallel the signal at 0.6 ppm increased during the steaming process.

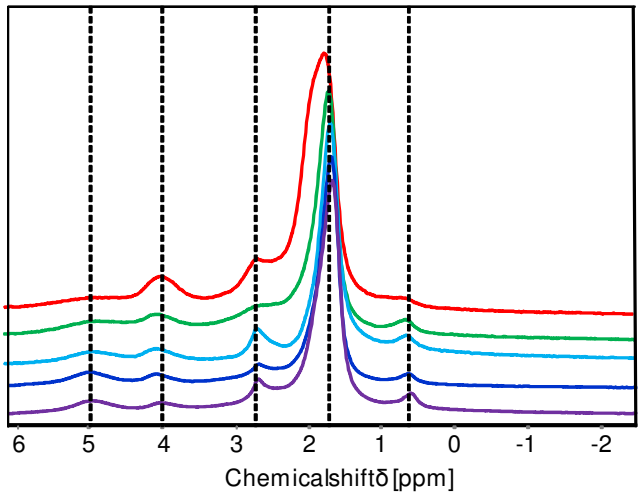

Figure 2.4: ^{1}H MAS NMR spectra of HBEA35-parent (red), HBEA35-s1 (green), HBEA35-s5 (light blue), HBEA35 s14 (dark blue), HBEA35-s24 (purple).

In addition to the signals of the silanol groups and extraframework Al species, the ^{1}H MAS NMR spectra showed signals at 4.0 ppm and 5.0 ppm resulting from the bridging SiOHAl groups (Brønsted acid sites). Their concentration decreased very fast in the first hour of steaming from 341 µmol/g to 167 µmol/g and reached a constant value of 118 µmol/g after 14 h of steaming time (see Table 2.4 and Table 2.5).

Table 2.4: Relative peak areas determined from the ^{1}H MAS NMR spectra. The percentage of the peak areas were referred to the total integral area of the sample HBEA35-parent.

sample	0.6 ppm [%]	1.7 ppm + 1.9 ppm [%]	2.7 ppm [%]	4.0 ppm [%]	5.0 ppm [%]
HBEA35-parent	2.2	65.0	13.3	12.1	7.3
HBEA35-s1	3.6	49.6	13.5	6.9	9.9
HBEA35-s5	5.5	46.3	5.7	5.6	6.2
HBEA35-s14	6.8	44.6	6.5	5.0	5.3
HBEA35-s24	6.9	45.1	6.3	5.2	6.4

Further information on the concentration of hydroxyl groups in the zeolite samples was obtained by infrared spectroscopy and temperature programmed desorption of NH_3. As already observed by NMR spectroscopy, zeolite BEA shows a high concentration of

internal and terminal SiOH groups. The region of the OH stretching vibrations as well as the difference spectra of the decrease of the hydroxyl groups are shown in Figure 2.5. The bands observed in the IR spectra can be assigned to OH groups at extra-framework Al (3784 cm^{-1}), terminal (3740 cm^{-1}) and internal (3724 cm^{-1}) SiOH groups, hydrogen bonded hydroxyl groups (3700 cm^{-1} – 3200 cm^{-1}, broad peak) and SiOHAl groups (3606 cm^{-1}).[41]

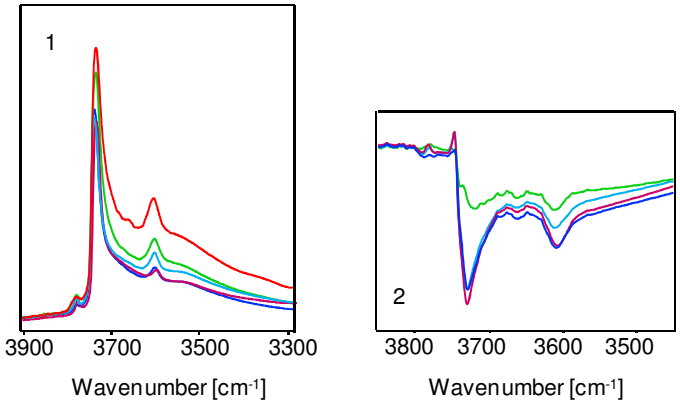

Figure 2.5: IR-spectra (1) and difference spectra [HBEA35-parent – HBEA35sn] (2) of the stretching vibrations of HBEA35-parent (red), HBEA35-s1 (green), HBEA35-s5 (light blue), HBEA35 s14 (dark blue), HBEA35-s24 (purple).

Steaming leads to a decrease of all bands originating from hydroxyl groups except for the ones originating from extraframework Al species (3784 cm^{-1}), whose intensity stayed approximately constant. In analogy to the ^{1}H MAS NMR experiments, the concentration of internal SiOH groups decreased stronger than the concentration of terminal SiOH groups, illustrating the healing of defect sites during steaming. The strongest changes were observed within the first hour of steaming, while steaming up to 14 h led only to a minor further decrease of the intensity of the OH groups.

The results of the temperature programmed desorption of NH_3 from the BEA samples are shown in Figure 2.6; a comparison of the acid site concentration determined by TPD and IR spectroscopy is shown in Table 2.5. In agreement with the decrease in the intensity of the OH groups, the concentrations of acid sites determined by TPD of NH_3 and adsorption of pyridine (see next paragraph) decreased. TPD of NH_3 results in a concentration of all acid sites of HBEA35-parent of 548 µmol/g. During the first 14 h of

steaming, the concentration of acid sites decreased and remained constant at 228 µmol/g after steaming for 24 h.

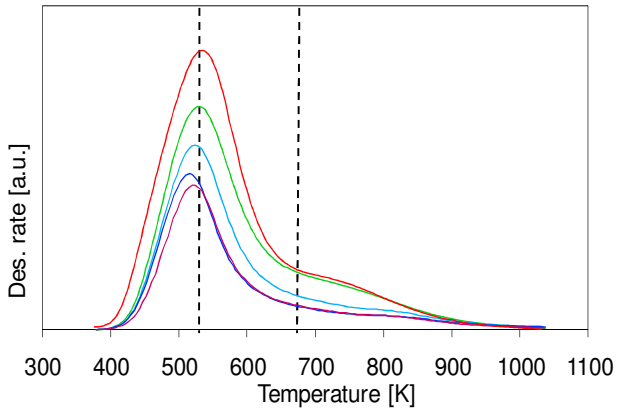

Figure 2.6: TPD of NH_3 for HBEA35-parent (red), HBEA35-s1 (green), HBEA35-s5 (light blue), HBEA35-s14 (dark blue), HBEA35-s24 (purple).

The desorption rates of NH_3 can be divided into contributions from weak (desorption maximum at 528 K) and strong acid sites (desorption maximum at 677 K). The low temperature peak is assigned to desorption of NH_3 from Brønsted acid sites, which can be shown by desorption of pyridine at different temperatures. The strong acid sites are attributed to ammonia bound to Lewis acid sites. The Brønsted acid sites were primarily affected by the steaming within the first hours, while the Lewis acid sites were stable during the first hour of steaming and started to decrease at steaming times exceeding 1 h. After 14 h of steaming significant changes in the acid site concentration were not observed (see Table 2.5).

The adsorption of pyridine on the samples led to the coverage of all Brønsted acidic SiOHAl groups and to a decrease of the vibrations assigned to SiOH groups and to hydroxyl groups on extraframework Al species. The typical IR bands for pyridine adsorbed on Lewis and Brønsted acid sites, which are presented in Figure 2.7, were observed at 1454 and 1545 cm^{-1}, respectively.[42] Outgassing of the sample at 723 K led to desorption of pyridine adsorbed on the weak acid sites, while it remained adsorbed on the strong acid sites. The concentration of Lewis acid sites stayed almost constant after outgassing at 723 K, while the concentration of pyridine adsorbed on Brønsted acid sites decreased significantly. This allows the assignment of the weak acid sites to Brønsted acid sites and of the low temperature desorption maximum in TPD of NH_3.

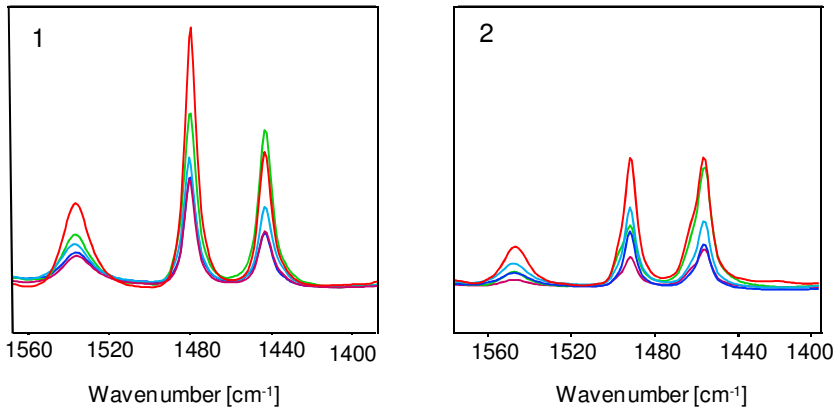

Figure 2.7: Difference IR spectra of pyridine adsorbed on HBEA35-parent (red), HBEA35-s1 (green), HBEA35-s5 (light blue), HBEA35 s14 (dark blue), HBEA35-s24 (purple). after out-gassing at 423 K (1) and 723 K (2).

The total concentration of acid sites determined by IR spectroscopy of adsorbed pyridine was 642 µmol/g for the parent material and decreased to 249 µmol/g for the sample HBEA35-s24. Sorption of pyridine allows differentiating between Brønsted acid sites and Lewis acid sites; the concentrations of the acid sites are summarized in Table 2.5. The concentrations of Brønsted acid sites determined by IR spectroscopy of adsorbed pyridine and ^{1}H MAS NMR spectroscopy are identical (within the experimental errors), indicating that all Brønsted acid sites were accessible for the pyridine molecules.

Table 2.5: Concentrations of Brønsted acid sites and Lewis acid sites in µmol/g determined by NH_3-TPD (a), IR spectroscopy of adsorbed pyridine (b) and ^{1}H MAS NMR spectroscopy (c).

sample	total acid sites[a]	weak acid sites[a]	strong acid sites[a]	total acid sites[b]	Brønsted acid sites[b]	Lewis acid sites[b]	Brønsted acid sites[c]
HBEA35-parent	548	377	179	642	310	332	341
HBEA35-s1	435	262	179	496	176	331	167
HBEA35-s5	310	207	114	320	145	175	143
HBEA35-s14	240	161	90	232	115	117	118
HBEA35-s24	228	151	84	239	124	124	125

2.4. Discussion

The characterization of zeolite BEA after steaming allowed identifying the different processes occurring during steaming. The crystallinity and particle size of the samples were not affected by steaming, as both XRD and SEM analysis did not show any significant differences between the parent and the steamed samples. While the particle morphology was not affected, the micropore volume decreased about 20 % as a result of blocking of the pores by extraframework Al. The chemical analysis of the parent material resulted in a Si/Al ratio of 18, while ^{29}Si MAS NMR revealed a Si/Al ratio of 22 for the atoms in the framework, indicating that about 30 % of the Al present in the sample is present as extraframework Al species.[43] It should be noted that this zeolite sample was already calcined (in large batch operation after synthesis) to remove the template, which appears to be the reason for the high concentration of extraframework Al species. About half of these extraframework species are present in octahedral coordination, while the remaining half is present as tetrahedral extraframework Al species. After steaming for 24 h, the ratio of Si/Al in the framework increased to 30, which indicates that steaming led to an increase of the extraframework species to 40 % (see Table 2.6), while the micropore volume decreased from 206 mm³/g to 167 mm³/g. The formation, migration and condensation of the newly formed as well as the already existing extraframework species is contended to block a portion of the pore system resulting in the decrease of the micropore volume.[26,27,33]

A better understanding of the reactions occurring during the steaming treatment could be reached by further MAS NMR spectroscopy, where the typical resonances for zeolite BEA were observed for the parent sample.[18,37] The high concentration of silanol sites present in the parent material and resulting from the two structure polymorphs is reflected by the resonance at -103 ppm in the ^{29}Si MAS NMR spectra as well as the resonances at 1.7 ppm and 1.9 ppm in the ^{1}H MAS NMR spectra and the bands at 3724 cm^{-1} and 3740 cm^{-1} in the IR spectra. About 16 % of the total Si atoms were found to be associated to silanol sites in the parent BEA sample. Steaming led to a decrease of the concentration of Q^3 sites to 9 % resulting from the condensation into Q^4 species. This process mainly occurs in the first five hours of steaming as 56 % of the Q^3 sites were removed, while in parallel the corresponding concentration of Q^4

species increased. The IR and ^{1}H NMR spectra revealed that the loss of Q^3 sites is due to the healing of defect sites (band at 3724 cm^{-1}, resp. 1.9 ppm), while naturally the concentration of terminal SiOH groups (band at 3740 cm^{-1}, resp. 1.7 ppm) stays nearly constant. Further steaming did not change the population of the Q^3 and Q^4 species, which indicates that the stacking disorder of zeolite BEA requires a certain fraction of silanol sites, which cannot be converted into Q^4 sites by the here applied steaming treatment. The condensation of the defect sites during steaming leads to less strain in the T-O-T bonds and consequently to a higher stability of the lattice.[40]

It is well known that steaming of zeolites leads to the hydrolysis of framework O-Al-O bonds resulting eventually in the detachment of the hydrolyzed alumina from the zeolite framework. For zeolite BEA it was proposed that dealumination of the framework proceeds via octahedral intermediates.[22,44,45] Our results from ^{27}Al MAS NMR spectroscopy indicate that the dealumination takes place only in T3 – T9 lattice positions, while the T1 and T2 sites are unaffected from this treatment. The results clearly show that the dealumination of the T3 – T9 sites occurs during the first 5 h of steaming, while their concentration stays nearly constant afterwards. Over the whole steaming procedure only 32 % of these Al species were removed from their positions. This indicates on the one hand that Al in the T1 and T2 positions is highly stable in the framework and cannot be dealuminated even after 24 h of steaming treatment. On the other hand, steaming leads to a stabilization of Al remaining at the T3 – T9 positions. The stability of the T1 and T2 sites observed is in good agreement with the work of van Bokhoven et al., who reported a high thermal stability for the T1 and T2 sites,[16,38] but is in contrast to the work of Müller et al., who argue that the T1 and T2 sites should theoretically dealuminate first as they are located in the four membered rings of the zeolites which are the most stressed T atoms.[40] As our results indicate the T1 and T2 sites are the most stable substitution sites for Al, we propose an additional stabilization by extraframework Al species in the pores. Structurally the T1 and T2 sites are located at the 1.2 nm cavities at the channel intersections, allowing a high concentration of extraframework Al species to be locally present close to these positions and contribute some stabilization effect (see Figure 2.8).

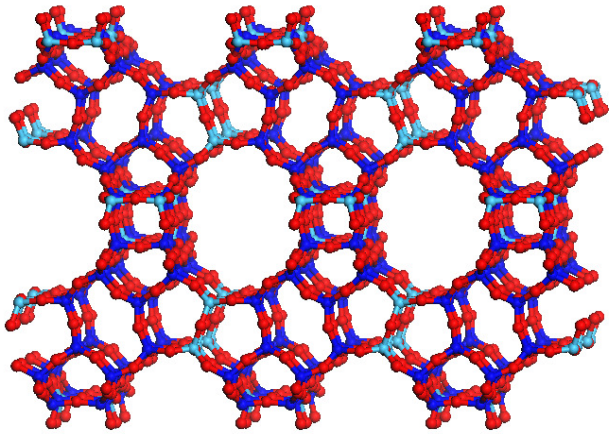

Figure 2.8: Location of the T-sites in the lattice of zeolite BEA. The T1 and T2 sites are marked with light blue, the T3 – T9 sites with dark blue and the oxygen atoms with red spheres.

Steaming does not only lead to dealumination of the framework, but also has a high influence on the coordination of the already existing extraframework Al species. Two different coordination sites for octahedral Al species were found in all samples. The sharp peak at 0 ppm in the ^{27}Al MAS NMR spectra was assigned to Al species in a perfect octahedral coordination, while the broad peak around -10 ppm (indicating a high quadrupolar coupling constant) is assigned to octahedral Al in a more distorted environment.[38]

In our studies we observed a decrease of the sharp peak, due to a gradual loss of well-ordered arrangement during steaming for 24 h. The removal of Al from the framework sites does not lead to the formation of additional octahedral extraframework species as only a marginal increase (i.e., from 16 % to 18 %) of octahedral Al species was observed by ^{27}Al MAS NMR spectroscopy. This strongly suggests that the formation of octahedral species during dealumination, which was proposed in literature for this material may be incorrect.[16]

Nevertheless, we also detected changes in the tetrahedrally coordinated extra-framework Al species. In the ^{27}Al MAS NMR spectra two types of extraframework Al species with resonances at 40 and 63 ppm were observed. The species observed at 40 ppm are highly distorted tetrahedrally coordinated Al species, which explains the large broadening and the large quadrupolar coupling constant related to this peak. The

second peak at 63 ppm is assigned to tetrahedral Al species in another electronic and magnetic surrounding. The detailed structure of these species is not clear yet.[23-25]

Before the steaming, only the band at 40 ppm was observed, whereas the tetrahedral extraframework Al species at 63 ppm were formed only during steaming. As pre-calcined samples were used for this study, we expect that the extraframework Al species resulting in the band at 40 ppm were formed during the initial template removal. Note that for zeolite BEA the formation of extraframework Al during template removal was already shown by Capek et al.[44] The appearance of the band at 63 ppm and the simultaneous decrease of the band at 40 ppm (see Figure 2.5), suggests that steaming not only leads to the dealumination of the framework, but also to the conversion of extraframework species. This is also illustrated by the changes in intensity observed for the two Al-OH groups on the external Al species with resonances at 0.6 ppm and 2.7 ppm in the ^{1}H NMR spectra. At the same time, the formation of Al species, which cannot be detected in ^{27}Al MAS NMR (i.e., “NMR-invisible Al species”) was observed from the Al mass balance. These species are proposed to be small extraframework clusters with Al in a highly distorted environment, which results in a high quadrupolar coupling constant and consequently in a severe line broadening.[22, 39]

The extraframework Al species formed during the removal of the template as well as during the steaming play an important role in stabilizing the zeolite framework. If positively charged, the extraframework Al species can act as counter ions for the negative charge of the zeolite framework resulting from the isomorphous substitution of Si by Al.[23-25] In general, cations at ion exchange positions can prevent further dealumination and, thus, stabilize the zeolite.[44,46] This effect appears to be related to the stabilization of USY by extraframework species.[47] On this basis we would like to propose that the extraframework species, present in the parent sample as well as the ones generated by steaming are occupying the ion exchange positions and, thus, stabilize the framework and preventing further dealumination.[44,48] The extremely stable T1 and T2 sites are located close to the intersections between the pores and therefore we suggest that they are already occupied with extraframework Al species, before the steaming treatment and being so the hydrothermally most stable positions for the Al atoms in the lattice.

This hypothesis is also supported by conclusions drawn from the determination of the acid site concentration by IR spectroscopy, the sorption of basic probe molecules (NH_3 and pyridine) and ^{1}H MAS NMR spectroscopy. ^{1}H MAS NMR as well as adsorption of pyridine showed a loss of 63 % and 59 % of the initially present Brønsted acid sites after steaming for 24 h.

The decrease of the concentration of the Brønsted acid sites should be directly related to the removal of Al atoms from framework positions. It is generally accepted that one framework Al atom leads to one Brønsted acid site, therefore, it should be possible to calculate the concentration of Brønsted acid sites from the relative integral area of the framework Al atoms determined by ^{27}Al MAS NMR spectroscopy and the total Al concentration determined by AAS. In contrast, we found that the concentrations of Brønsted acid sites determined by ^{1}H MAS NMR spectroscopy and IR spectroscopy of adsorbed pyridine are much lower than the concentrations of framework Al calculated from ^{27}Al MAS NMR. A comparison between the calculated Al framework concentration and the Brønsted acid site concentration measured by ^{1}H MAS NMR spectroscopy is shown in Table 2.6. For the parent sample only about half the concentration of the 601 µmol/g Brønsted acid sites calculated from ^{27}Al MAS NMR spectroscopy was actually detected with the other techniques. For the sample after 24 h of steaming the difference was even larger, as only 125 µmol/g of the expected 518 µmol/g Brønsted acid sites were observed by ^{1}H MAS NMR spectroscopy and IR spectroscopy of adsorbed pyridine. This indicates that the zeolite contains a significant fraction of Al tetrahedrally coordinated atoms in the framework, which do not contribute to the Brønsted acidity.

Table 2.6: Concentrations of Al T atoms, extraframework Al species and Brønsted acid sites as determined from ^{27}Al and ^{1}H MAS NMR spectroscopy.

sample	framework Al [µmol/g]	extraframework Al [µmol/g]	Brønsted acid sites [µmol/g]
HBEA35-parent	601	275	341
HBEA35-s1	556	320	167
HBEA35-s5	531	345	143
HBEA35-s14	519	357	118
HBEA35-s24	518	358	125

This discrepancy between the concentration of Al T atoms and the concentration of Brønsted acid sites can be explained, when taking into account the role of the extra-framework (probably cationic) Al species.[23-25]

In zeolite systems, cations usually act as counter ions for Al T atoms, compensating the negative charge in the zeolites and thus blocking one potential Brønsted acid site. The total concentration of extraframework Al species for the sample HBEA35-parent was calculated to be 275 µmol/g from the relative integral area in the ^{27}Al MAS NMR spectra and the total concentration of Al determined by AAS. Assuming that each mol of extraframework Al is blocking one mol of framework Al T atom, the discrepancy between the concentration of Brønsted acid sites calculated from ^{27}Al MAS NMR spectroscopy and the measured concentration of Brønsted acid sites can be explained (see Table 2.6).

The same holds true for the steamed samples. The concentration of all extraframework Al species equals the difference between the concentration of Brønsted acid sites calculated from ^{27}Al MAS NMR spectroscopy and the actually measured concentration of Brønsted acid sites. As a consequence of this, each dealuminated Al atom leads to the loss of two Brønsted acid sites - one by the dealumination itself and one by the blockage of a second T atom. This is clarified in Figure 2.9 where the concentration of Brønsted acid sites calculated from the concentration of framework T atoms is plotted against the actually measured concentration of Brønsted acid sites. The resulting linear

correlation has a slope of two related to the loss of two Brønsted acid sites per dealuminated framework Al atom.

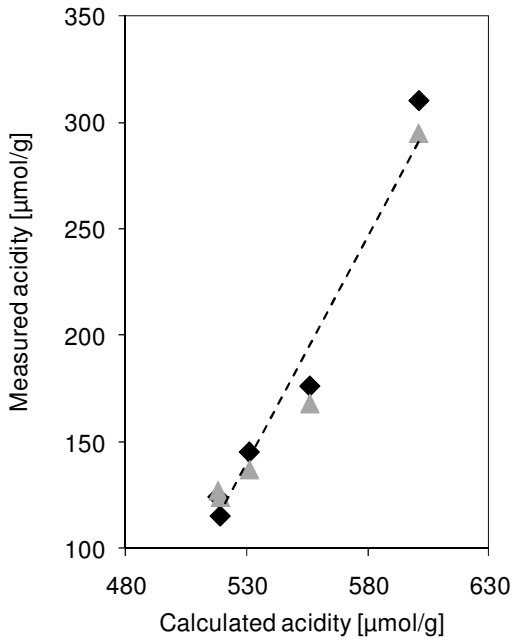

Figure 2.9: Comparison of the acid site concentrations calculated from the results of ^{27}Al MAS NMR and measured by ^{1}H MAS NMR spectroscopy (grey) and IR spectroscopy of adsorbed pyridine (black).

2.5. Conclusions

Zeolite HBEA35 was treated at 753 K in 100 % steam and characterized in respect to its stability against steaming treatment and the effect this treatment has on the acidity. It was found that several processes must be taken into account and that the treatment leads to a stable coordination after 14 h of steaming. The first effect observed is the condensation of silanol groups occupying defect sites in the zeolite lattice. The condensation leads to the formation of Q^4 sites, which reduces the strain in the zeolite matrix and, thus, stabilizes the lattice. However, 9 % of the Si atoms present in the zeolite lattice remain at silanol sites even after 24 h of steaming indicating that the special stacking disorder in zeolite BEA induces a minimum concentration of defect sites.

The main effect of steaming is the dealumination of the framework T3 – T9 sites, while the T1 and T2 sites are stable against dealumination. 14 % of all Al T atoms were removed from the framework and transformed into extraframework species. At the same time an extensive transformation and migration of extraframework Al species was observed. The dealumination of the framework Al atoms should be in agreement with the decrease of the concentration of Brønsted acid sites in the zeolite matrix. In contrast to this, we found that the unsteamed sample HBEA35-parent holds only 341 µmol/g Brønsted acid sites, while it was expected to hold 601 µmol/g Brønsted acid sites as calculated from the concentration of framework Al atoms. For the steamed samples we also observed a too low concentration of Brønsted acid sites compared with the expected concentration. In addition, we find that the further decrease of Brønsted acid sites induced by steaming doubles the concentration of dealuminated framework Al atoms.

We explain these apparent discrepancies with the role of extraframework Al species present in the zeolite. We conclude that the cationic extraframework Al species are located at the ion exchange positions and, thus, exchange the Brønsted acid sites. Note, that one dealuminated Al atom leads to the loss of two Brønsted acid sites; one by the dealumination itself and one by the blockage of another framework Al atom as extraframework Al species.

Extraframework Al species in ion exchange positions stabilize the lattice and protect the remaining Al framework atoms from further dealumination. As consequence, they are crucial to obtain a hydrothermally stable zeolite.

2.6. Acknowledgements

The authors would like to thank Martin Neukamm for SEM imaging and AAS measurements as well as Xaver Hecht for N_2-sorption experiments. Discussions in the framework of IDECAT are gratefully acknowledged. The project was funded by the Bayerisches Staatsministerium für Wissenschaft, Forschung und Kunst.

2.7. References

(1) Newsam, J. M.; Treacy, M. M. J.; Koetsier, W. T.; Gruyter, C. B. D. *Proc. R. Soc. London. A,* **1988**, *420*, 375.

(2) Higgins, J. B.; LaPierre, R. B.; Schlenker, J. L.; Rohrman, A. C.; Wood, J. D.; Kerr, G. T.; Rohrbaugh, W. J. *Zeolites* **1988**, *8*, 446.

(3) Dartt, C. B.; Davis, M. E. *Catal. Today* **1994**, *19*, 151.

(4) Tanabe, K.; Hölderich, W. F. *Appl. Catal., A* **1999**, *181*, 399.

(5) Nivarthy, G. S.; He, Y. J.; Seshan, K.; Lercher, J. A. *J. Catal.* **1998**, *176*, 192.

(6) Feller, A.; Guzman, A.; Zuazo, I.; Lercher, J. A. *Stud. Surf. Sci. Catal.* **2003**, *145*, 67.

(7) Bellussi, G.; Pazzuconi, G.; Perego, C.; Girotti, G.; Terzoni, G. *J. Catal.* **1995**, *157*, 227.

(8) Degnan, T. F.; Smith, C. M.; Venkat, C. R. *Appl. Catal., A* **2001**, *221*, 283.

(9) Jansen, J. C.; Creyghton, E. J.; Njo, S. L.; van Koningsveld, H.; van Bekkum, H. *Catal. Today* **1997**, *38*, 205.

(10) Creyghton, E. J.; Ganeshie, S. D.; Downing, R. S.; van Bekkum, H. *J. Mol. Catal. A: Chem.* **1997**, *115*, 457.

(11) Katada, N.; Kageyama, Y.; Takahara, K.; Kanai, T.; Begum, H. A.; Niwa, M. *J. Mol. Catal. A: Chem.* **2004**, *211*, 119.

(12) Botella, P.; Corma, A.; Rey, F.; Valencia, S. *Stud. Surf. Sci. Catal.* **2002**, *142*, 651.

(13) Beyerlein, R. A.; McVicker, G. B.; Yacullo, L. N.; Ziemiak, J. J. *J. Phys. Chem.* **1988**, *92*, 1967.

(14) Beyerlein, R. A.; Choi-Feng, C.; Hall, J. B.; Huggins, B. J.; Ray, G. J. *Fluid Catalytic Cracking III*, **1994**.

(15) Munoz, J. J. L.; Canos, A. C.; Delgado, J. M. F. *US Patent US5057471* **1991**.

(16) van Bokhoven, J. A.; Koningsberger, D. C.; Kunkeler, P.; van Bekkum, H.; Kentgens, A. P. M. *J. Am. Chem. Soc.* **2000**, *122*, 12842.

(17) Treacy, M. M. J.; Newsam, J. M. *Nature* **1988**, *332*, 249.

(18) Fyfe, C. A.; Feng, Y.; Grondey, H.; Kokotailo, G. T.; Gies, H. *Chem. Rev.* **1991**, *91*, 1525.

(19) Stelzer, J.; Paulus, M.; Hunger, M.; Weitkamp, J. *Microporous Mesoporous Mater.* **1998**, *22*, 1.

(20) Kuehl, G. H.; Timken, H. K. C.; *Microporous Mesoporous Mater.* **2000**, *35-36*, 521.

(21) Kentgens, A. P. M. *Geoderma* **1997**, *80*, 271.

(22) Bourgeat-Lami, E.; Massiani, P.; Di Renzo, F.; Espiau, P.; Fajula, F. *Appl. Catal., A* **1991**, *72*, 139.

(23) Lisboa, O.; Sánchez, M.; Ruette, F. *J. Mol. Catal. A: Chem.* **2008**, *294*, 93.

(24) Benco, L.; Demuth, T.; Hafner, J.; Hutschka, F.; Toulhoat, H. *J. Catal.* **2002**, *209*, 480.

(25) Bhering, D. L.; Ramirez-Solis, A.; Mota, C. J. A. *J. Phys. Chem. B* **2003**, *107*, 4342.

(26) Marques, J. P.; Gener, I.; Ayrault, P.; Lopes, J. M.; Ribeiro, F. R.; Guisnet, M. *Chem. Commun.* **2004**, 2290.

(27) Ribeiro Carrott, M. M. L.; Russo, P. A.; Carvalhal, C.; Carrott, P. J. M.; Marques, J. P.; Lopes, J. M.; Gener, I.; Guisnet, M.; Ramôa Ribeiro, F. *Microporous Mesoporous Mater.* **2005**, *81*, 259.

(28) Aloi, D.; Testa, F.; Pasqua, L.; Aiello, R.; Nagy, J. B. *Impact Of Zeolites And Other Porous Materials On The New Technologies At The Beginning Of The New Millennium, Pts A And B, Vol. 142*, Elsevier Science Bv, Amsterdam, **2002**, pp. 469.

(29) Guisnet, M.; Ayrault, P.; Coutanceau, C.; Alvarez, M. F.; Datkac, J. *J. Chem. Soc., Faraday Trans.* **1997**, *93*, 1661.

(30) Bisio, C.; Martra, G.; Coluccia, S.; Massiani, P. *J. Phys. Chem. C* **2008**, *112*, 10520.

(31) Su, B.-L.; Norberg, V. *Zeolites* **1997**, *19*, 65.

(32) Trombetta, M.; Busca, G.; Storaro, L.; Lenarda, M.; Casagrande, M.; Zambon, A. *Phys. Chem. Chem. Phys.* **2000**, *2*, 3529.

(33) Marques, J. P.; Gener, I.; Ayrault, P.; Bordado, J. C.; Lopes, J. M.; Ramôa Ribeiro, F.; Guisnet, M. *Microporous Mesoporous Mater.* **2003**, *60*, 251.

(34) Batonneau-gener, I.; Yonli, A.; Hazael-pascal, S.; Pedro Marques, J.; Madeira Lopes, J.; Guisnet, M.; Ramôa Ribeiro, F.; Mignard, S. *Microporous Mesoporous Mater.* **2008**, *110*, 480.

(35) Lippens, B. C.; Linsen, B. G.; d. Boer, J. H. *J. Catal.* **1964**, *3*, 32.

(36) Harkins, W. D.; Jura, G. *J. Am. Chem. Soc.* **1944**, *66*, 1366.

(37) Pérez-Pariente, J.; Sanz, J.; Fornés, V.; Corma, A. *J. Catal.* **1990**, *124*, 217.

(38) Beers, A. E. W.; van Bokhoven, J. A.; de Lathouder, K. M.; Kapteijn, F.; Moulijn, J. A. *J. Catal.* **2003**, *218*, 239.

(39) Alexander, S. M.; Bibby, D. M.; Howe, R. F.; Meinhold, R. H. *Zeolites*, **1993**, *13*, 441.

(40) Müller, M.; Harvey, G.; Prins, R. *Microporous Mesoporous Mater.* **2000**, *34*, 135.

(41) Jentys, A.; Warecka, G.; Lercher, J. A. *J. Mol. Catal.* **1989**, *51*, 309.

(42) Parry, E. P. *J. Catal.* **1963**, *2*, 371.

(43) Lippmaa, E.; Samoson, A.; Magi, M. *J. Am. Chem. Soc.* **1986**, *108*, 1730.

(44) Capek, L.; Dedecek, J.; Wichterlová, B. *J. Catal.* **2004**, *227*, 352.

(45) Omegna, A.; Vasic, M.; van Bokhoven, J. A.; Pirngruber, G.; Prins, R. *Phys. Chem. Chem. Phys.* **2004**, *6*, 447.

(46) Sievers, C.; Liebert, J. S.; Stratmann, M. M.; Olindo, R.; Lercher, J. A. *Appl. Catal., A* **2008**, *336*, 89.

(47) van Bokhoven, J. A.; Roest, A. L.; Koningsberger, D. C.; Miller, J. T.; Nachtegaal, G. H.; Kentgens, A. P. M. *J. Phys. Chem. B* **2000**, *104*, 6743.

(48) Bortnovsky, O.; Sobalík, Z.; Wichterlová, B. *Microporous Mesoporous Mater.* **2001**, *46*, 265.

This chapter is based on:

Maier, S.M.; Jentys, A.; Lercher,J.A.; *J. Phys. Chem. C* **2011**, *115*, 8005-8013.

Chapter 3

Determination of the Redox Processes in FeBEA catalysts in NH_3-SCR Reaction by Mößbauer and X-Ray Absorption Spectroscopy

The nature and oxidation state of iron species in Fe-exchanged BEA zeolites treated in synthetic air or nitrogen were determined by a combination of Mößbauer and X-ray absorption spectroscopy. The linear correlation between the edge energy of the XANES and the oxidation state determined by Mößbauer spectroscopy allowed determining the fraction of Fe^{2+} in situ. The distribution of Fe^{2+} and Fe^{3+} in the catalysts depends on the Fe concentration and the conditions of the thermal treatment. It is possible to stabilize isolated Fe^{2+} cations under ambient atmosphere in the zeolite pores, while FeBEA catalysts show a temperature dependent oxidation and reduction of the active Fe species during the selective catalytic reduction of nitrogen oxides by NH_3 (NH_3-SCR), reflecting the equilibrium for NO oxidation.

3.1. Introduction

Fe-exchanged zeolites have the potential to replace the conventionally used WO_3/V_2O_5-TiO_2 catalysts in the selective catalytic reduction of nitrogen oxides with ammonia (NH_3-SCR) in exhaust gas treatment of diesel engines.[1-4]

$$4\ NO + 4\ NH_3 + O_2 \rightarrow 4\ N_2 + 6\ H_2O \qquad (2)$$

The key challenge to reproducibly prepare the catalysts and to understand their activity stems from the fact that regardless of the preparation method a variety of Fe species including isolated cations, oxygen bridged cation pairs, Fe_xO_y and Fe_2O_3 clusters in di - and trivalent oxidation states are formed.[5-7] UV/Vis, EPR, XAS and IR spectroscopy of adsorbed NO and CO are for example used to characterize these materials, but a reliable characterization method for the active Fe species is still missing.[8-13] The co-existence of Fe in different oxidation states in the various species makes it difficult to identify the active Fe cations, as most of the techniques are only sensitive to one oxidation state of Fe, making it very difficult to close a mass balance of all cations.[14]

Mößbauer spectroscopy is a well-established technique to quantitatively differentiate between Fe species in different oxidation states, but it requires recoil free emission and adsorption of γ-quanta.[15-17] The intensity of the Mößbauer signal is, therefore, strongly temperature dependent and, thus, the quantitative determination of the oxidation state is not possible *in situ* during reactions at elevated temperatures.[17] On the other hand, the X-ray absorption near edge structure (XANES) can be measured *in situ* under reaction conditions allowing to determine the concentration of Fe^{2+} and Fe^{3+} cations during the catalytic reaction. While the edge position of the XANES provides qualitative information on the electron density of the (absorber) metal in the catalyst, a direct quantitative correlation to the oxidation state is not possible, as the coordination of the Fe atoms strongly influences the edge shape and energy.[18-20] Therefore, the XANES of a catalyst with unknown oxidation state of Fe cations cannot be quantified by the XANES of reference materials of known oxidation state and structure such as $FePO_4$ or Mohr's salt. As consequence, the extended X-ray absorption fine structure (EXAFS) is mostly used to determine the coordination state and the nuclearity of the Fe species and only few studies have been reported that use *in situ* XANES for the qualitative,[21-23] but not the quantitative [24-26] determination of the redox properties of Fe-zeolites.

In this study, a series of FeBEA catalysts synthesized by wet-ion exchange and heat treated in air (a) or nitrogen (n) with Fe concentrations between 0.79 and 7.02 wt. % were characterized with respect to their oxidation state. The wet-ion exchange leads to the exchange of one Fe atom per Brønsted acid site in the zeolite and thus to the presence of Fe-OH groups compensating the excess charge of the Fe cations. We combined XANES and Mößbauer spectroscopy to obtain a correlation between the edge energy observed in XANES and the oxidation state determined by Mößbauer spectroscopy. This in turn allows for the first time determining the relative concentrations of Fe^{2+} and Fe^{3+} species under reaction conditions and relating the concentration and oxidation state to the catalytic activity of the Fe containing zeolites.

3.2. Experimental

3.2.1. Materials

The Fe containing zeolite samples were synthesized by single wet-ion exchange of zeolite HBEA (Si/Al = 18, provided by Süd-Chemie AG) with an acidic solution (pH = 2) of $FeSO_4$*$7H_2O$ (Flucka) for 20 h under nitrogen atmosphere. The nitrogen atmosphere was necessary to prevent the oxidation of Fe^{2+} to Fe^{3+} and the subsequent formation of $Fe(OH)_3$ and Fe_2O_3 in the zeolite samples. The concentration of the $FeSO_4$ solution was varied from 0.04 to 0.1 mol/l to control the Fe loadings on the zeolite. After ion-exchange the FeBEA samples were washed five times with H_2O dest. and subsequently freeze dried. The dried samples were heat treated in N_2 or synthetic air at 753 K for 2 h and stored under atmospheric conditions in air. Non porous SiO_2 (Aerosil 200) was used as parent material for the sample $FeSiO_2$ 7.02. In order to obtain a sample with a high concentration of Fe^{3+} species, the synthesis of this sample was carried out under air. The Fe contents of all samples were determined by atomic absorption spectroscopy (AAS) using a Solaar M5 Dual Flame graphite furnace AAS from *Thermo Fisher*. The synthesis conditions as well as the resulting Fe contents are summarized in Table 3.1.

Table 3.1: Synthesis conditions of FeBEA samples.

sample	c ($FeSO_4$) [mol/l]	heat treatment	Fe concentration [wt. %]
FeBEA 0.79a	0.04	air	0.79
FeBEA 0.81n	0.04	nitrogen	0.81
FeBEA 0.92n	0.04	nitrogen	0.92
FeBEA 0.99n	0.1	nitrogen	0.99
FeBEA 1.38n	0.1	nitrogen	1.38
$FeSiO_2$ 7.02a	0.1	air	7.02

3.2.2. Diffuse reflectance UV/Vis measurements

UV/Vis measurements of the FeBEA samples were performed with an avantes avaspec2048 spectrometer in diffuse reflectance (DR) mode. The samples were measured as powders at ambient conditions in a sample cup of 10 mm diameter and 3 mm depth. The DR UV/Vis spectra are presented in form of the Kubelka-Munk function being defined as $F(R) = (1 - R)^2/(2 \cdot R)$ with $R = R_s/R_r$, where R_s is the reflectance of the sample and R_r is the reflectance of HBEA.

3.2.3. X-ray absorption spectroscopy

X-ray absorption spectra were measured at HASYLAB, DESY, Hamburg, Germany on beam line X1 using the Si (111) monochromator with an energy resolution of $\Delta E/E = 1.33*10^{-4}$, corresponding to 0.9 eV at 7 keV. The theta goniometer is equipped with a Heidenhain ROD 800 angle encoder within a tolerance of 10^{-5} degree. The storage ring was operated at 4.5 GeV and an average current of 100 mA. The intensity of higher order reflections was minimized by detuning the second crystal of the monochromator to 60 % of the maximum intensity. The samples were prepared as self-supporting wafers having a total absorption of 2.0 (sample weight 30 mg/cm^2 – 70 mg/cm^2, depending on the Fe content) to optimize the signal to noise ratio. X-ray absorption spectra were recorded at the Fe K edge (7112 eV) and analyzed with XANES dactyloscope software.

In situ NH_3-SCR experiments were carried out in a stainless steel reaction cell while measuring XAS at temperature intervals of 100 K. The samples were prepared as self-supporting wafers, activated in a He flow of 100 ml/min at 723 K for 1 h (heating ramp 10 K/min) and afterwards cooled to 423 K. The NH_3-SCR reaction was carried out in a gas mixture of 1000 ppm NO, 1000 ppm NH_3 and 5 vol. % oxygen balanced in He with a total flow of 60 ml/min. The temperature dependence of the NH_3-SCR reaction was determined under steady-state conditions at 423 K, 523 K, 623 K and 723 K. Afterwards the temperature was reduced to 623 K, 523 K and 423 K in order to verify the reversibility of the oxidation/reduction of the Fe species in the catalyst.

3.2.4. Mößbauer spectroscopy

The Mössbauer spectra were measured with a spectrometer utilizing a gas proportional detector and a ^{57}Co source embedded in a rhodium matrix. The spectra were collected at 4.2 K while both source and sample were kept in liquid helium in a bath cryostat. The isomer shifts δ were calibrated with respect to the $^{57}Co/Rh$ source. The peaks of all Mössbauer spectra were fitted with Lorentzian line shapes to match the absorption envelope, while the individual Lorentzian duplets were not initially assigned to specific iron sites. This approach allows obtaining reliable average hyperfine parameters and relative amounts of Fe^{2+} and Fe^{3+} ions.[27,28]

3.2.5. Catalytic activity tests

The catalytic activity was studied in a fixed-bed flow reactor made from quartz glass, at a gas-hourly space velocity (GHSV) of 74050 h^{-1} in a temperature range between 423 K and 873 K in steps of 50 K. The gas flow was composed of 1000 ppm NO, 1000 ppm NH_3 and 5 vol. % O_2 balanced with N_2. The conversion at each temperature was measured after 0.5 h of steady-state reaction. The NO and NH_3 concentrations were continuously monitored by IR spectroscopy (Thermo Nicolet). Prior to the activity tests, the catalysts were activated in N_2 for 1 h at 723 K with a ramp of 10 K/min and subsequently cooled to 423 K.

3.3. Results and Discussion

3.3.1. UV/VIS measurements

DR UV/Vis spectroscopy indicated that the samples FeBEA0.79a, FeBEA0.81n, FeBEA0.92n and FeBEA0.99n contain mainly isolated Fe species, which is also reflected in the white color of these samples. The samples FeBEA1.38n and $FeSiO_2$7.02a are characterized by a pinkish to dark red color arising from the higher Fe_2O_3 content of these samples. The UV/Vis spectra of the samples FeBEA0.79a, FeBEA0.81n, FeBEA0.92n and FeBEA0.99n show only peaks at 214 nm and 270 nm, which are assigned to isolated Fe ions in tetrahedral and octahedral coordination.[29] According to Pérez-Ramirez et al., oligomeric Fe_xO_y species show peaks between 300 nm and 400 nm, while transitions of hematite like Fe_2O_3 particles can be detected at wavelengths above 400 nm.[30] Thus, the sample FeBEA1.38n contains fractions of Fe_xO_y and Fe_2O_3 particles, while the sample $FeSiO_2$7.02a consists mainly of Fe_2O_3 with a small fraction of isolated Fe ions. To illustrate the contributions of the respective Fe species to the UV/Vis spectra, the spectra were fitted with Gaussian functions (see Figure 3.1)

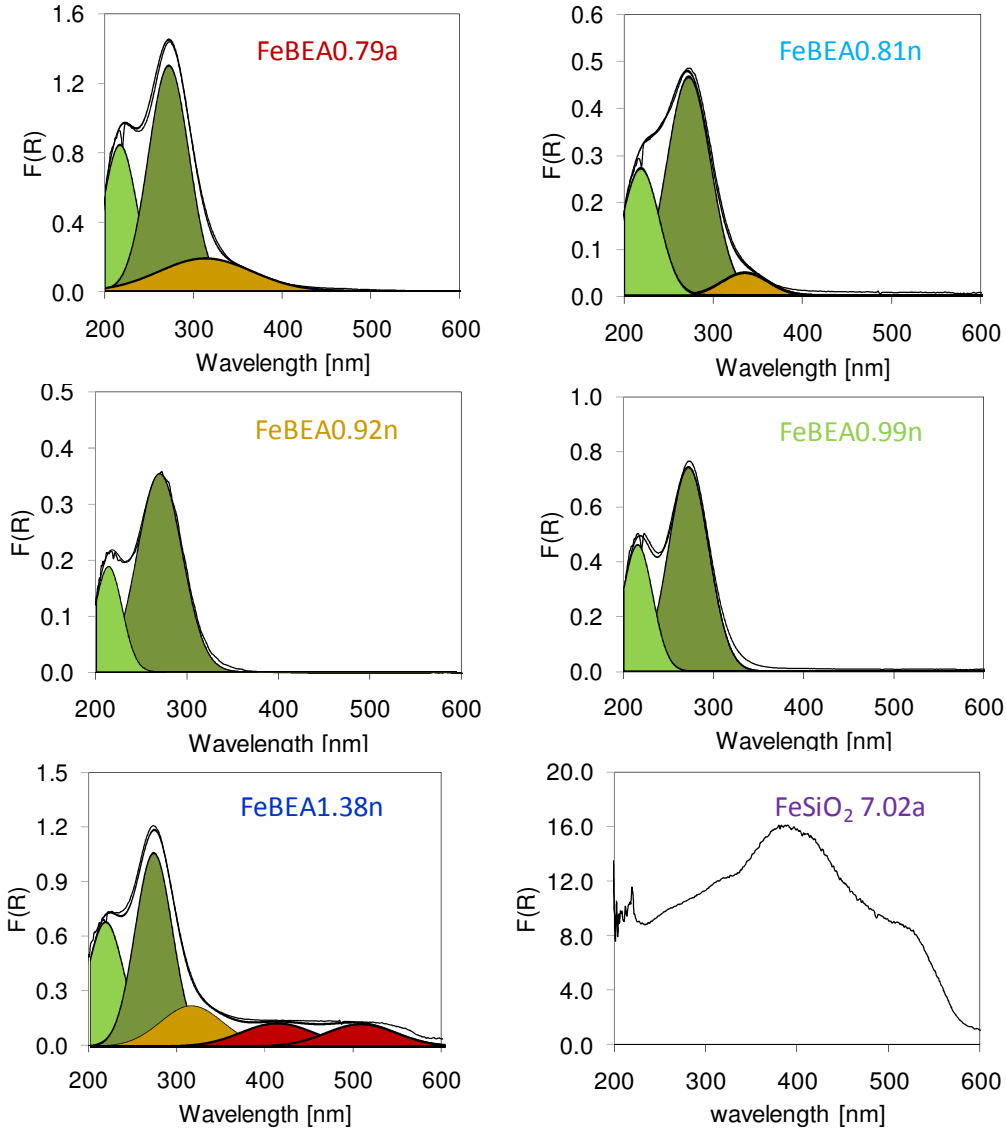

Figure 3.1: DR UV/Vis spectra of the samples FeBEA0.79a, FeBEA0.81n, FeBEA0.92n, FeBEA0.99n, FeBEA1.38n and $FeSiO_2$7.02a. The contributions of isolated Fe species are marked in green, the contributions of Fe_xO_y clusters in gold and the ones from Fe_2O_3 clusters in red.

3.3.2. Catalytic activity

The activity of the FeBEA catalysts in the reduction of NO by NH_3 is shown in Figure 3.2. The conversion levels of NO and NH_3 were around 10 % at 423 K for all FeBEA catalysts and increased up to 85 % at 723 K. The NO conversion levels

decreased at temperatures above 673 K, while the NH_3 conversion level further increased to nearly 100 % because of the direct oxidation of NH_3 to N_2. All FeBEA samples showed similar activities, although they contain varying concentrations of Fe and Fe species with different oxidation states and nuclearity (see XANES and Mößbauer results). Only $FeSiO_2$7.02, which was prepared on an amorphous SiO_2 as support, was not active in the reduction of NO below 573 K, which is attributed to the fact that only Fe_2O_3 is present in this catalyst.

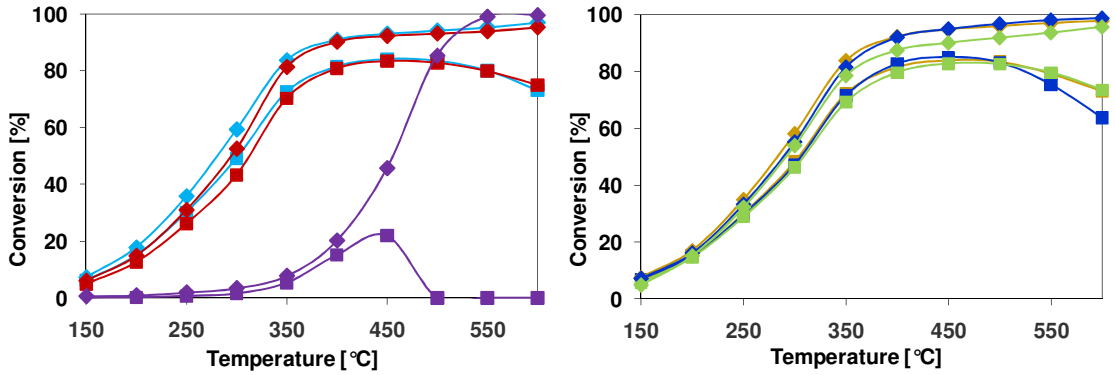

Figure 3.2: Conversions of NO (□) and NH_3 (◇) in the NH_3-SCR reaction for the samples FeBEA0.79a (red), FeBEA0.81n (light blue), FeBEA0.92n (gold), FeBEA0.99n (green), FeBEA1.38n (dark blue) and $FeSiO_2$7.02a (purple).

3.3.3. XANES

The Fe K edge spectra of the series of Fe containing zeolite samples are shown in Figure 3.3. The XANES of the FeBEA samples show a pre-edge peak due to 1s → 3d transitions in Fe^{3+} at around 7113 eV. Although this transition is spin-forbidden for an ideal octahedral coordination, it usually appears for distorted or tetrahedral coordination spheres without an inversion centre.[31, 32] The pre-edge peak was found at 7113.7 eV for Fe^{3+} species and at 7112.3 eV for Fe^{2+} species.[33-35] In several cases the deconvolution of the pre-edge peak allowed a quantitative differentiation of the two oxidation states, which could be verified with the help of Moessbauer spectroscopy.[36-40] However, in the present case the Fe concentration is very low (< 1 wt. % Fe) and Fe is located in an octahedral coordination due to saturation of the coordination sphere with H_2O ligands in the hydrated zeolite samples, which results in weak pre-edge peaks that do not permit a quantitative differentiation between Fe^{2+} and Fe^{3+} species. It should be

emphasized at this point that the low Fe content in the FeBEA samples is favorable for the formation of isolated Fe cations and Fe_xO_y clusters of low nuclearity and prevents the formation of inactive Fe_2O_3 particles.

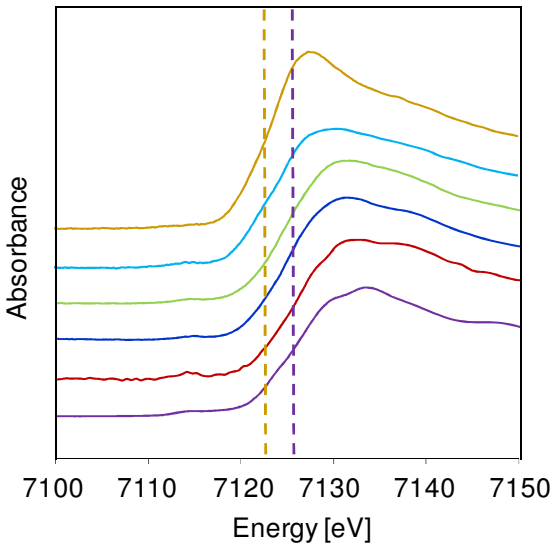

Figure 3.3: XANES spectra of the FeBEA samples FeBEA0.79a (red), FeBEA0.81n (light blue), FeBEA0.92n (gold), FeBEA0.99n (green), FeBEA1.38n (dark blue) and $FeSiO_2$7.02a (purple).

Therefore, the position of the absorption edge is used instead of the pre-edge peak to identify the oxidation state of the Fe species in the catalysts. Depending on the synthesis conditions, the edge energies (defined here as the energy of the inflection point) for the different samples vary between 7121.7 eV and 7125.7 eV. This energy range is typical for Fe^{2+} and Fe^{3+} and indicates that different fractions of Fe^{2+} and Fe^{3+} species are present in the samples. The edge energies of all samples are compiled in Table 3.2.

3.3.4. Mößbauer spectroscopy

The Mößbauer absorption spectra of all Fe containing samples measured at 4.2 K are shown in Figure 3.4. The isomer shift and the quadrupole splitting in the Mößbauer spectrum reflect the valence and coordination of the Fe cations in the samples. The sample $FeSiO_2$7.02a is characterized by a sextet with an isomeric shift δ of 0.2 mm/s, a quadrupole splitting Δ of -0.2 mm/s and relative line areas close to 3:2:1:1:2:3. These features indicate that the Fe cations in this sample form large Fe_2O_3 domains

with hematite structure. The Mößbauer spectra of all other Fe containing BEA samples show a superposition of three groups of signals. In addition to the sextet arising from hematite, doublets of Fe^{2+} and isolated Fe^{3+} cations were observed with varying intensities depending on the nature of iron cations exchanged into the zeolite. Note that it is not possible to differentiate between monomeric, bimeric and trimeric Fe-hydroxyl-species with Mößbauer spectroscopy only. Therefore, the term isolated Fe ions is used for all Fe-hydroxyl-species not giving a magnetic hyperfine splitting throughout this manuscript. The valence states of the Fe cations were derived from the isomeric shifts of the respective signals. Divalent and trivalent Fe cations are characterized by an isomeric shift of about 1.2 mm/s and 0.2 mm/s, respectively. The quadrupole splitting of the Fe^{2+} doublet is 3.4 mm/s, while the quadrupolar splitting of the isolated Fe^{3+} ions is 1.0 mm/s.[38] As the peak areas in Mößbauer spectroscopy at 4.2 K are directly proportional to the concentration of the respective species, the integrated areas under the peaks assigned to Fe^{2+} and Fe^{3+} species were used to determine the atomic fraction of Fe^{2+}. The quantification of the different Fe species is summarized in Table 3.2. The concentration of Fe_xO_y clusters and Fe_2O_3 particles (for both a magnetic hyperfine splitting was observed) increases with increasing Fe loading of the FeBEA catalysts. Isomeric shifts and the quadrupole splitting constants of the respective species are compiled in the appendix (see B.4).

Table 3.2: Quantification of different Fe species by Mößbauer spectroscopy.

sample	edge energy [eV]	Fe^{2+} (doublet) [%]	Fe^{3+} (doublet) [%]	Fe_2O_3 (sextet) [%]
FeBEA 0.92n	7121.7	72.1	11.5	16.4
FeBEA 0.81n	7122.3	67.5	14.5	18.0
FeBEA 0.99n	7122.9	51.3	24.5	24.2
FeBEA 1.38n	7123.9	35.7	17.5	46.8
FeBEA 0.79a	7125.1	13.9	62.4	23.7
$FeSiO_2$ 7.02a	7125.7	0.0	0.0	100.0

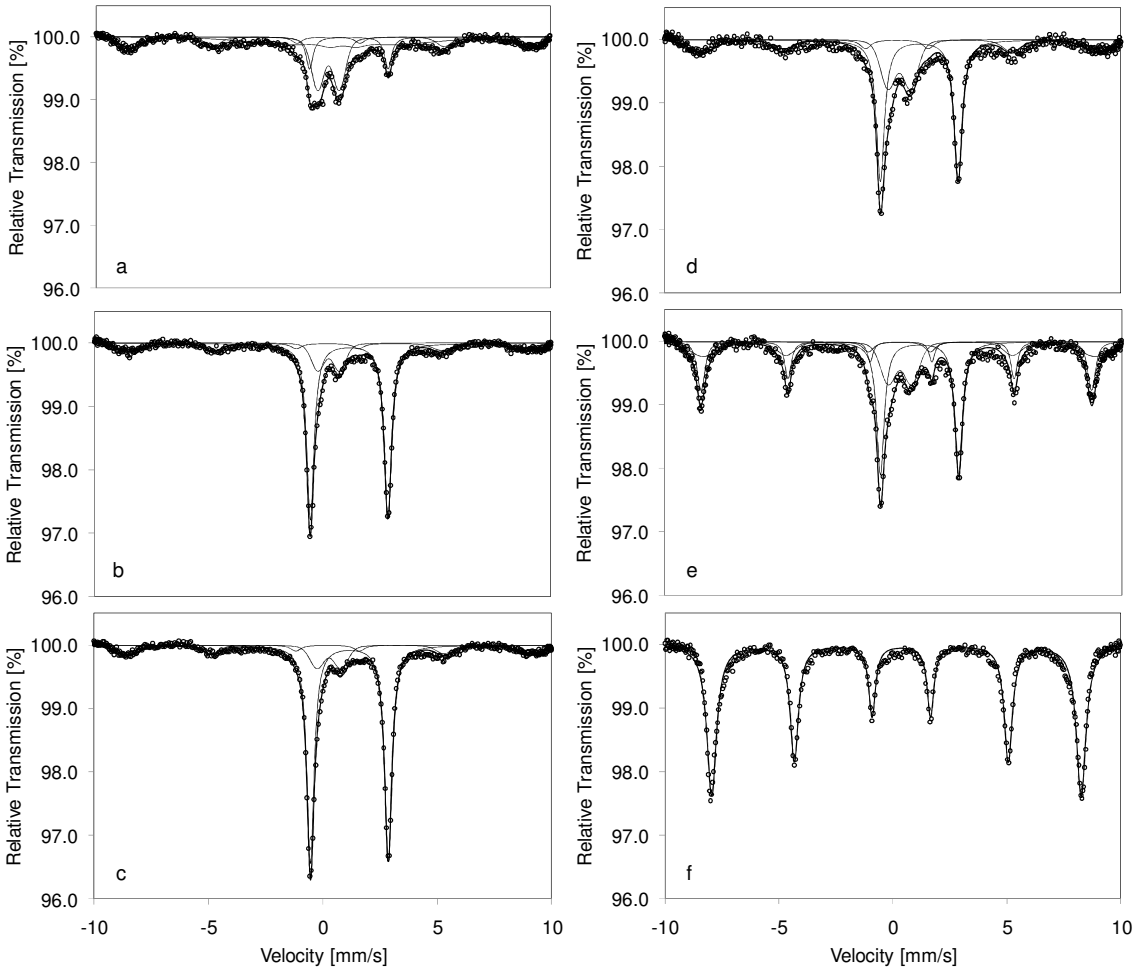

Figure 3.4: Mößbauer spectra with corresponding fits of the FeBEA samples FeBEA0.79a (a), FeBEA0.81n (b), FeBEA0.92n (c), FeBEA0.99n (d), FeBEA1.38n (e) and $FeSiO_2$7.02a (f).

The samples heat treated in N_2, showed high concentrations of Fe^{2+} even though they were stored in air after synthesis and Fe^{2+} has a high tendency towards oxidation to Fe^{3+} under such conditions. This indicates that the particular environment at the ion exchange positions in the zeolite make the lower oxidation state more favorable, probably due to the acid environment and/or the acid strength of the zeolite hydroxyl groups. It should be noted at this point that Fe^{2+} hydroxyl species can be stabilized in an acidic environment, due to the acid-dependence of the O_2/H_2O redox reaction. A high concentration of H^+ ions prevents the precipitation of $Fe(OH)_3$ and thus hinders the oxidation of Fe^{2+} hydroxyl species.[41,42] In addition, samples, which were heat treated in N_2, contain a high fraction of isolated Fe cations and only low concentrations of Fe_2O_3.

The increase of the Fe concentration (e.g., sample FeBEA 1.38n) leads to the extensive formation of Fe_2O_3 (47 %) indicating that isolated species can only be stabilized in the zeolite structure up to a Fe/Al ratio of 0.3.

From the quantitative determination of the Fe_2O_3 phase from Mößbauer spectroscopy, the atomic fraction of Fe^{2+} in the isolated Fe species were calculated (see Table 3.3). Assuming that the Fe_2O_3 phase is not active in the NH_3-SCR reaction and only taking into account the isolated Fe species, the turnover frequency (TOF) of the NO conversion at 573 K, being a typical temperature for the application of FeBEA catalysts for the automotive NH_3-SCR applications, was calculated.[8] Although the atomic fraction of Fe^{2+} varies between 0.18 and 0.86, the TOF of all five FeBEA samples were identical within experimental errors, leading to the conclusion that all five catalysts hold the same fraction of active Fe species. This also indicates that the activity of the catalysts does not depend on the primary oxidation state of the Fe species after synthesis, as isolated Fe cations rapidly assume their equilibrium oxidation state under reaction conditions.

Table 3.3: Atomic fraction of Fe^{2+} based on the fraction of isolated Fe species and corresponding TOF at 573 K.

sample	$Fe^{2+}/\Sigma Fe_{exch}$	TOF(NO) [s^{-1}]
FeBEA 0.79a	0.18	0.044
FeBEA 0.81n	0.82	0.043
FeBEA 0.92n	0.86	0.039
FeBEA 0.99n	0.68	0.041
FeBEA 1.38n	0.67	0.040

In order to obtain a reliable method for the quantification of the oxidation state under reaction conditions, we correlated the edge energy of the XANES against the atomic fraction of Fe^{2+} from Mößbauer spectroscopy as shown in Figure 3.5.

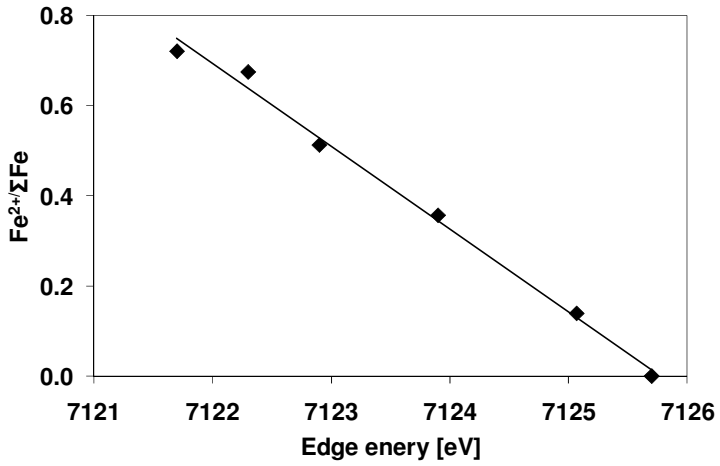

Figure 3.5: Linear correlation between the XANES edge energy and the $Fe^{2+}/\sum Fe$ ratio obtained from Mößbauer spectroscopy.

The edge energy of the Fe K edge can so be directly related to the atomic fraction of Fe^{2+} measured by Mößbauer spectroscopy, as long as a high structural similarity is maintained among the samples, such as for the FeBEA catalysts. Berry et al. published a similar comparison between Mößbauer spectroscopy and XANES on Fe species in minerals but as they could not obtain a structural similarity throughout their samples, they did not find a linear trend.[43] Our correlation allows in turn determining quantitatively the atomic fractions of Fe^{2+} and Fe^{3+} species in Fe containing zeolites in complex oxidation/reduction processes (e.g., during the NH_3-SCR reaction) also at elevated temperatures.

3.3.5. In situ characterization of working catalyst

In situ X-ray absorption spectra were measured for the catalyst FeBEA0.99n after activation in He at 723 K and during the NH_3-SCR reaction at temperatures between 423 K and 723 K (see Figure 3.6). The activation in He and the addition of the reaction gases led to a shift of the edge position of the sample FeBEA0.99n in the range between 7123.0 eV and 7124.5 eV.

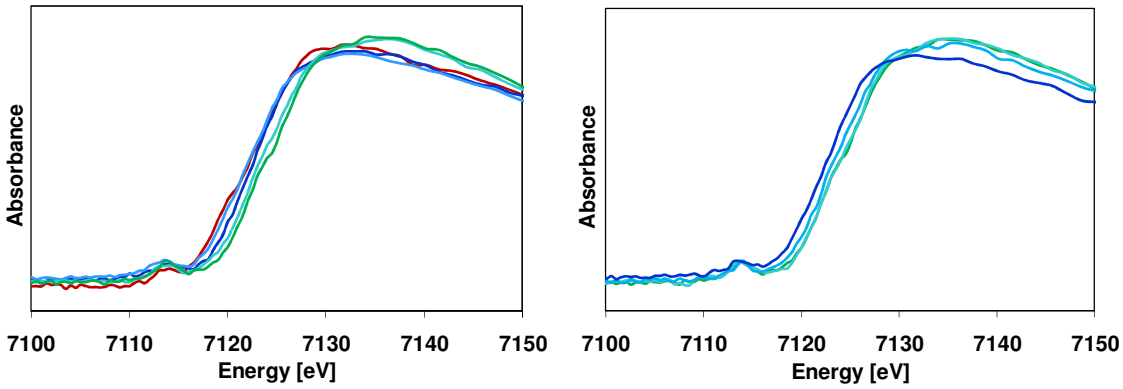

Figure 3.6: *In situ* XANES spectroscopy of the sample FeBEA0.99n after activation (red), during heating (left) and cooling (right) in 1000 ppm NO, 1000 ppm NH_3 and 5 % O_2at 423 K (dark blue), 523 K (light blue), 623 K (cyan) and 723 K (green).

The application of the above found correlation allowed the quantitative determination of the oxidation state at the respective reaction temperatures. Mößbauer spectroscopy indicated that the sample FeBEA0.99n contains 24 % inactive and difficult to reduce Fe_2O_3 phase, which will not be further considered. Before activation, 68 % of the isolated Fe species was present as Fe^{2+}. During activation in He, the sample was reduced resulting in a fraction of 83 % Fe^{2+} cations.

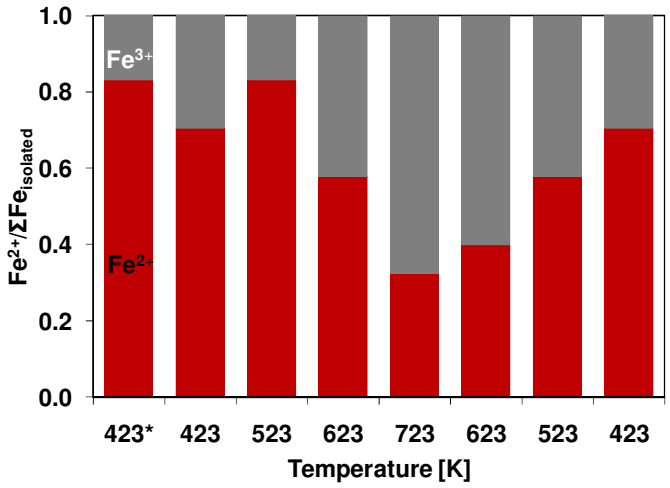

Figure 3.7: Determination of the atomic fraction of Fe^{2+} species based on isolated Fe species for the sample FeBEA0.99n from *in situ* XANES measurements during NH_3-SCR in 1000 ppm NO, 1000 ppm NH_3 and 5 vol. % O_2.*label the sample after activation in inert gas.

The addition of the reaction gas at 423 K led to a partial oxidation of Fe^{2+} species, resulting in an atomic fraction of Fe^{2+} species of 0.70. With increasing reaction temperature the Fe^{2+} species were partially oxidized, leading finally to an atomic fraction of Fe^{2+} of 0.32 at 723 K. The subsequent decrease of the reaction temperature under reaction conditions to 423 K led to the reduction of the catalyst until an atomic fraction of Fe^{2+} of 0.70 was reached again, indicating that the oxidation is fully reversible. Based on these results we conclude that the ion exchanged Fe^{2+}/Fe^{3+} species are reversibly oxidized and reduced under reaction conditions up to 723 K, thus, allowing a broad operational window of the catalyst for the NH_3-SCR reaction. Furthermore, we showed experimentally that the isolated Fe species act as active sites in the NH_3-SCR reaction and take part in a redox cycle, making the determination of the exact ratio between Fe^{2+}/Fe^{3+} species mandatory for further studies on the understanding of the reaction mechanism.

3.4. Conclusions

The oxidation states of Fe-exchanged zeolite BEA were examind *ex situ* and *in situ* by means of Mössbauer and X-ray absorption spectroscopy. It was found that Fe^{2+} ions can be stabilized when exchanged into the zeolite matrix in atmospheric conditions without oxidation of Fe^{2+} to Fe^{3+}. This is due to the high acid strength of the zeolite, as strong acids are able to change the redox potential of Fe^{2+}/Fe^{3+}.

In our studies we could show that the energy of the absorption edge is directly proportional to the $Fe^{2+}/\sum Fe$ ratio which can be determined by Mössbauer spectroscopy carried out at 4.2 K. With the help of this linear correlation it is for the first time possible to directly determine the $Fe^{2+}/\sum Fe$ ratio from the edge position in XANES. This is of significant importance on the understanding of *in situ* redox processes as they take place in many catalized reactions, e.g. in the reduction of NO by NH_3 over Fe-exchanged zeolites in the widely applied NH_3-SCR reaction.

The activation of FeBEA in He flow at 723 K leads to the reduction of Fe^{2+}, while the subsequent addition of the reaction gas at 423 K leads to an oxidation of the catalyst. The increase of the temperature under reaction conditions up to 723 K leads to a further oxidation of the catalyst, which is reversible when the reaction temperature is again decreased to 423 K. This behaviour shows that the oxidation of NO over the catalyst is controlling the NH_3-SCR reaction as the oxidation state of the Fe species is in line with the chemical equilibrium of the oxidation of NO. The following desorption of NO_2 can be then regarded as the rate determining step of the overall NH_3-SCR reaction.

In addition we could conclude that the oxidation of the catalyst at high temperatures under reaction conditions is not due to the formation of hematite, which would not be reducable again by a decrease of the reaction temperature.

3.5. Acknowledgements

Portions of this research were carried out at the light source facility DORIS III at DESY, Hamburg, Germany. DESY is a member of the Helmholtz Association (HGF). We thank Adam Webb in assistance in using Beamline X1. The authors thank Martin Neukamm for AAS measurements and Prof. Dr. Friedrich Wagner for the fruitful discussion and his help with the Mößbauer measurements. Discussions in the framework of ERIC are gratefully acknowledged. The project was funded by the Bayerisches Staatsministerium für Wissenschaft, Forschung und Kunst.

3.6. References

(1) Joyner, R.; Stockenhuber, M. *J. Phys. Chem. B* **1999**, *103*, 5963.

(2) Long, R. Q.; Yang, R. T. *J. Am. Chem. Soc.* **1999**, *121*, 5595.

(3) Busca, G.; Lietti, L.; Ramis, G.; Berti, F. *Appl. Catal., B* **1998**, *18*, 1.

(4) Janssen, F. J. Handbook of Heterogeneous Catalysis; Ertl, G., Knözinger, H., Weitkamp, J., Eds., 1997; Vol. 4; pp 1633.

(5) Heinrich, F.; Schmidt, C.; Löffler, E.; Menzel, M.; Grünert, W. *J. Catal.* **2002**, *212*, 157.

(6) Kumar, M. S.; Schwidder, M.; Grünert, W.; Brückner, A. *J. Catal.* **2004**, *227*, 384.

(7) Xia, H.; Sun, K.; Liu, Z.; Feng, Z.; Ying, P.; Li, C. *J. Catal.* **2010**, *270*, 103.

(8) Brandenberger, S.; Krocher, O.; Tissler, A.; Althoff, R. *Appl. Catal., B* **2010**, *95*, 348.

(9) Hadjiivanov, K. I. *Catal. Rev.-Sci. Eng.* **2000**, *42*, 71.

(10) Iwasaki, M.; Yamazaki, K.; Banno, K.; Shinjoh, H. *J. Catal.* **2008**, *260*, 205.

(11) Kumar, M. S.; Schwidder, M.; Grünert, W.; Bentrup, U.; Brückner, A. *J. Catal.* **2006**, *239*, 173.

(12) Schwidder, M.; Kumar, M. S.; Brückner, A.; Grünert, W. *Chem. Commun* **2005**, 805.

(13) Sun, Q.; Gao, Z.-X.; Chen, H.-Y.; Sachtler, W. M. H. *J. Catal.* **2001**, *201*, 88.

(14) Schmidt, R.; Amiridis, M. D.; Dumesic, J. A.; Zelewski, L. M.; Millman, W. S. *J. Phys. Chem. B* **1992**, *96*, 8142.

(15) Dubkov, K. A.; Ovanesyan, N. S.; Shteinman, A. A.; Starokon, E. V.; Panov, G. I. *J. Catal.* **2002**, *207*, 341.

(16) Mauvezin, M.; Delahay, G.; Coq, B.; Kieger, S.; Jumas, J. C.; Olivier-Fourcade, J. *J. Phys. Chem. B* **2001**, *105*, 928.

(17) Overweg, A. R.; Crajé, M. W. J.; van der Kraan, A. M.; Arends, I. W. C. E.; Ribera, A.; Sheldon, R. A. *J. Catal.* **2004**, *223*, 262.

(18) Lazar, K.; Pozdnyakova, O.; Wootsch, A.; Fejes, P. *Hyperfine Interactions* **2006**, *167*, 779.

(19) Prietzel, J.; Thieme, J.; Eusterhues, K.; Eichert, D. *Eur. J. Soil Sci.* **2007**, *58*, 1027.

(20) Choi, S. H.; Wood, B. R.; Ryder, J. A.; Bell, A. T. *J. Phys. Chem. B* **2003**, *107*, 11843.

(21) Marturano, P.; Drozdova, L.; Kogelbauer, A.; Prins, R. *J. Catal.* **2000**, *192*, 236.
(22) Klukowski, D.; Balle, P.; Geiger, B.; Wagloehner, S.; Kureti, S.; Kimmerle, B.; Baiker, A.; Grunwaldt, J. D. *Appl. Catal., B* **2009**, *93*, 185.
(23) Xia, H.; Fleischman, S. D.; Li, C.; Scott, S. L. *J. Phys. Chem. Lett.* **2011**, *2*, 190.
(24) Battiston, A. A.; Bitter, J. H.; Koningsberger, D. C. *J. Catal.* **2003**, *218*, 163.
(25) Jia, J.; Sun, Q.; Wen, B.; Chen, L. X.; Sachtler, W. M. H. *Catal. Lett.* **2002**, *82*, 2.
(26) Pirngruber, G. D.; Roy, P. K.; Weiher, N. *J. Phys. Chem. B* **2004**, *108*, 13746.
(27) Karabulut, M.; Metwalli, E.; Day, D. E.; Brow, R. K. *J. Non-Cryst. Solids* **2003**, *328*, 199.
(28) Diar, M. D. *Am. Mineral.* **1985**, *70*, 304.
(29) Bordiga, S.; Buzzoni, R.; Geobaldo, F.; Lamberti, C.; Giamello, E.; Zecchina, A.; Leofanti, G.; Petrini, G.; Tozzola, G.; Vlaic, G. *J. Catal.* **1996**, *158*, 486.
(30) Pérez-Ramírez, J.; Kapteijn, F.; Brückner, A. *J. Catal.* **2003**, *218*, 234.
(31) Calas, G.; Petiau, J. *Solid State Commun.* **1983**, *48*, 625.
(32) Requejo, F. G.; Ramallo-López, J. M.; Beltramone, A. R.; Pierella, L. B.; Anunziata, O. A. *Appl. Catal., A* **2004**, *266*, 147.
(33) Berlier, G.; Spoto, G.; Bordiga, S.; Ricchiardi, G.; Fisicaro, P.; Zecchina, A.; Rossetti, I.; Selli, E.; Forni, L.; Giamello, E.; Lamberti, C. *J. Catal.* **2002**, *208*, 64.
(34) Farges, F.; Lefrère, Y.; Rossano, S.; Berthereau, A.; Calas, G.; Brown, J. G. E. *J. Non-Cryst. Solids* **2004**, *344*, 176.
(35) Petit, P.-E.; Farges, F.; Wilke, M.; Sole, V. A. *J. Synchrotron Radiat.* **2001**, *8*, 952.
(36) Bajt, S.; Sutton, S. R.; Delaney, J. S. *Geochimica et Cosmochimica Acta* **1994**, *58*, 5209.
(37) Cottrell, E.; Kelley, K. A.; Lanzirotti, A.; Fisher, R. A. *Chemical Geology* **2009**, *268*, 167.
(38) Heijboer, W. M.; Glatzel, P.; Sawant, K. R.; Lobo, R. F.; Bergmann, U.; Barrea, R. A.; Koningsberger, D. C.; Weckhuysen, B. M.; de Groot, F. M. F. *J. Phys. Chem. B* **2004**, *108*, 10002.
(39) Wilke, M.; Partzsch, G. M.; Bernhardt, R.; Lattard, D. *Chemical Geology* **2005**, *220*, 143.
(40) De Guire, M. R.; O'Handley, R. C.; Kalonji, G.; Darby Dyar, M. *J. Non-Cryst. Solids* **1986**, *81*, 351.

(41) Wiberg, N. *Lehrbuch der anorganischen Chemie* Berlin, 2007.

(42) Weidenthaler, C.; Zibrowius, B.; Schimanke, J.; Mao, Y.; Mienert, B.; Bill, E.; Schmidt, W. *Microporous Mesoporous Mater.* **2005**, *84*, 302.

(43) Berry, A. J.; O'Neill, H. S.; Jayasuriya, K. D.; Campbell, S. J.; Foran, G. J. *Am. Miner.* **2003**, *88*, 967.

This chapter is based on:

Maier, S.M.; Jentys, A.; Metwalli, E.; Müller-Buschbaum, P.; Lercher, J.A.; *J. Phys. Chem. Lett.* **2011,** *2,* 950.

Chapter 4

Unique Dynamic Changes of Fe Cationic Species under NH_3-SCR Conditions

Fe containing zeolites are important catalysts for the selective catalytic reduction of NO_x with NH_3. To better understand their active sites, the type and location of Fe cations and their structural changes under NH_3-SCR conditions are explored. Adsorption of basic probe molecules such as NH_3 and pyridine show that in operando additional Brønsted acid sites are formed on the expense of Lewis acidic octahedrally coordinated Fe cations. The formation of new tetrahedrally coordinated Fe species suggests that Fe cations are incorporated into the zeolite framework at tetrahedral positions. UV/Vis, XAFS and IR spectra indicate that these species are formed only during cooling under NH_3-SCR conditions. In situ EXAFS shows Fe cations forming bridging Fe-O-Fe species at cation-exchange sites above 573 K under reaction conditions. This indicates that the Fe cations undergo a unique reversible transformation during temperature cycles under NH_3-SCR conditions.

4.1. Introduction

Fe-exchanged zeolites have found numerous applications in industrial catalysis, such as the oxidation of benzene to phenols by N_2O, the reduction/decomposition of N_2O, as well as the selective catalytic reduction of nitrogen oxides using ammonia (NH_3-SCR) or hydrocarbons as reducing agents.[1-7] The latter approach is widely applied in the exhaust gas treatment of diesel engines.[8]

Although the first studies of Fe-exchanged zeolites date back to the late 1960s, a general agreement with regard to the structural properties of the active Fe species present does not exist.[9,10] All synthesis procedures lead to a variety of cationic Fe species, ranging from isolated Fe ions, binuclear Fe-O-Fe cations, and Fe_xO_y-clusters of varying nuclearity to larger particles of Fe_2O_3 at the external zeolite surface.[11-16] While different active species have been claimed to exist (binuclear Fe-O-Fe cationic species are the most frequently suggested), the reported activities are surprisingly nearly identical.

This complex and unclear attribution of active species is also mirrored in other applications. Based on various characterization techniques including Mössbauer spectroscopy, H_2-TPR, EXAFS, UV Vis and EPR spectroscopy, binuclear Fe-species with a structure similar to the Fe cluster in methane monooxygenase are proposed to be active in the selective oxidation of methane to methanol, providing oxygen.[9,17-21] Dubkov et al. proposed a similar binuclear Fe structure to be active in the reduction of N_2O by aromatic molecules and reported the uptake of one oxygen atom per site.[1] It is important to note that these sites are selectively generated by the oxidation of Fe^{2+} with N_2O. This is in line with the results of Xia et al. who observed the generation of NO_2 from NO in the presence of N_2O over Fe-exchanged zeolites. This can be seen as an indication that the binuclear Fe-O-Fe sites, formed in the presence of N_2O, can act as oxygen source for the oxidation of NO to NO_2.[22]

Fe cations can be synthetically inserted into framework T-atom positions during the hydrothermal synthesis by addition of Fe cation containing precursors to the synthesis gel, which leads to the formation of Brønsted acidic bridging SiOHFe hydroxyl groups. These SiOHFe sites are characterized by an OH stretching vibration at 3627 cm^{-1}.[23,24] In contrast to Al at framework positions, the Fe atoms are less stable and it was found

that they can be easily extracted from the T atom positions at higher temperatures during calcination, leading to the formation of extra-framework Fe oxide species.[25-27] In this context it was reported that Fe-containing zeolites can be prepared by extraction of Fe from the tetrahedral positions by calcination leading to highly dispersed Fe cations, which are active in the SCR reaction. In contrast, Fe cations present in zeolite T atom positions cannot be reduced and are, therefore, not active in the NH_3-SCR reaction requiring oxidation and reduction of iron cations.[27-29]

Understanding the stability and the *in situ* transformation of Fe-exchanged zeolites is of great importance for the optimal application and further development of these materials in exhaust gas treatment. Under NH_3-SCR conditions Fe-zeolites are exposed to steam, ammonia and nitrogen oxides, among which at least the first two are expected to have a marked influence on the coordination of the iron species.

Several studies suggest a moderate dealumination and formation of extra-framework Al species upon the exposure of zeolite BEA to steam. In a recent study, we showed that steaming of zeolite BEA leads to the extraction of only 15 % of the framework Al atoms during 14 h of steaming at 753 K, while the system stabilizes itself during longer steaming, limiting the concentration of Al extracted from the framework.[30] Van Bokhoven et al. reported that Al^{3+}, which was extracted from the framework by steam, can be reinserted by exposing the zeolite to NH_3 at 373 K. They emphasized, however, that extra-framework Al can only be reinserted into the framework, as long as it is connected to it.[31] In analogy, Bordiga et al. observed the extraction of Fe cations from framework T positions of Fe-silicalite and a restoration of the tetrahedral geometry of the Fe cations after treatment with NH_3.[32]

We decided, therefore, to explore the structural properties of Fe species in ion exchanged zeolite BEA under NH_3-SCR conditions in order to better understand the specific role of iron cationic species for the activity of the catalyst.

4.2. Experimental

4.2.1. Materials

The Fe containing zeolite samples were synthesized by single wet-ion exchange of zeolite HBEA (Si/Al = 18, Süd-Chemie AG) at pH=2 with a 0.04 molar solution of $FeSO_4 \cdot 7H_2O$ (Fluka) for 20 h under N_2. The FeBEA samples were washed with H_2O for five times, freeze dried and heated in N_2 at 753 K for 2 h. Additional steaming was carried out in a fixed-bed plug-flow reactor made from quartz glass at temperatures between 723 K and 873 K for 12 h in a reaction gas mixture typical for NH_3-SCR conditions consisting of 1000 ppm NO, 1000 ppm NH_3, 5 vol. % O_2 and 5 vol. % H_2O balanced in N_2. The Fe and Al contents of all samples were determined by atomic absorption spectroscopy (AAS) using a Solaar M5 Dual Flame graphite furnace AAS from Thermo Fisher. The synthesis conditions are summarized in Table 4.1.

Table 4.1: Synthesis and steaming conditions of FeBEA samples.

sample	treatment
FeBEA	None
FeBEA 723	NO, NH_3, O_2 at 723 K
FeBEA 723st	NO, NH_3, O_2, H_2O at 723 K
FeBEA 773st	NO, NH_3, O_2, H_2O at 773 K
FeBEA 823st	NO, NH_3, O_2, H_2O at 823 K
FeBEA 873st	NO, NH_3, O_2, H_2O at 873 K

4.2.2. X-ray diffraction

The crystal structure of all samples was analyzed by X-ray powder diffraction. Measurements were done using a “Philips X’Pert Pro System” using Cu-Kα-radiation of 0.154056 nm (45 kV and 40 mA). The experiments were carried out on a rotating powder sample holder in a 2θ range of 5° to 70° with a step size of 0.019 °/s.

4.2.3. IR spectroscopy

The infrared spectra were measured on a Perkin-Elmer 2000 spectrometer with a resolution of 4 cm^{-1}. The samples were prepared as self-supporting wafers (~ 10 mg/cm^{-2}) and activated in vacuum (p = 10^{-6} mbar) with a heating rate of 10 K/min to 723 K maintaining that temperature for 1 h. After cooling to 423 K the samples were exposed to pyridine (p = 10^{-1} mbar) for 1 h and then outgassed (p = 10^{-6} mbar) at 423 K for 1 h. All spectra were collected at 423 K. To directly compare the surface coverage of the adsorbed species all spectra were normalized using the overtone and combination vibrations of zeolite BEA between 2095 and 1755 cm^{-1} after activation. For quantification, molar integral extinction coefficients of 0.73 cm/µmol and 0.96 cm/µmol were used for pyridine adsorbed on Brønsted (1545 cm^{-1}) and Lewis acid sites (1455 cm^{-1}), respectively. These were determined from a reference material (H-ZSM-5, Si/Al = 45 from Süd-Chemie AG) using a combination of IR spectroscopy of adsorbed pyridine and micrograviметric measurements of the thermal stability of adsorbed ammonia.

4.2.4. Temperature programmed desorption of ammonia

For temperature programmed desorption of ammonia about 50 mg of the samples were granulated to a particle size between 500 and 710 µm and activated in vacuum (p = 10^{-3} mbar) at 723 K (heating rate = 10 K/min) for 1 h. After cooling to 373 K, 1 mbar of NH_3 was adsorbed for 1 h, followed by outgassing the samples for 2 h. The temperature was increased to 1043 K at a rate of 10 K/min, while desorption of NH_3 was monitored by mass spectroscopy using the $m/z^+ = 16$ signal. The acid site concentration was determined by comparing the integral area of the desorption peaks to a standard zeolite material with known acid site concentration (H-ZSM-5, Si/Al = 45 from Süd-Chemie AG, total acid site concentration = 0.360 mmol acid sites g^{-1}).

4.2.5. Diffuse reflectance UV/Vis spectroscopy

Diffuse reflectance UV/Vis measurements of the FeBEA samples were performed with an Avantes avaspec2048 spectrometer in diffuse reflectance mode. The samples were measured as powder at ambient conditions in a sample cup of 10 mm diameter and 3 mm depth. Prior to the measurements the steamed FeBEA samples were washed

with distilled water in order to remove NH_4NO_3 formed during the steaming treatment. The DR UV/Vis spectra are presented in form of the Kubelka Munk function being defined as $F(R) = (1-R)^2/(2 \cdot R)$ with $R = R_s/R_r$, where R_s is the reflectance of the sample and R_r is the reflectance of HBEA.

4.2.6. X-ray absorption spectroscopy (Fe K edge)

X-ray absorption spectra were measured at HASYLAB, DESY, Hamburg, Germany on beamline X1 using the Si (111) monochromator. The storage ring was operated at 4.5 GeV and an average current of 100 mA. The intensity of higher order reflections was minimized by detuning the second crystal of the monochromator to 60 % of the maximum intensity. The samples were prepared as self-supporting wafers having a total absorption of 2.0 (sample weight ~50 mg/cm^2) to optimize the signal to noise ratio. XANES were recorded at the Fe K edge (7112 eV) and analyzed with XANES dactyloscope software, while the analysis of the EXAFS region was done with the VIPER software. The oscillations of the EXAFS region were extracted from the background using a combination of a first and third order polynomial function. The oscillations were weighted with k^2 and Fourier transformed within the limit k = 2.5-10 Å^{-1}. The local environment of the Fe atoms was determined from the EXAFS in k-space using the phase shift and amplitude function for Fe-Fe and Fe–O including multiple scattering processes (FEFF version 8.4).[33,34]

In situ NH_3-SCR experiments were carried out in a stainless steel reaction cell. The samples were prepared as self-supporting wafers, activated in a He flow of 100 ml/min at 723 K for 1 h (heating ramp = 10 K/min) and afterwards cooled to 77 K. The NH_3-SCR reaction was carried out in a gas mixture of 1000 ppm NO, 1000 ppm NH_3 and 5 vol. % oxygen balanced in He with a total flow of 60 ml/min. The temperature dependence of the NH_3-SCR reaction was determined under steady-state conditions at 423 K, 523 K, 623 K and 723 K. After each temperature step, the catalyst was quenched to 77 K to minimize lattice vibrations while measuring the EXAFS. Afterwards the sample was heated to the next temperature step with an increment of 10 K/min.

4.2.7. X-ray absorption spectroscopy (Al K edge)

X-ray absorption spectra of were measured at Swiss Light Source, Paul Scherrer Institute, Villigen, Switzerland on the Phoenix beam line using the Si (111) monochromator. The storage ring was operated at 2.4 GeV and an average current of 400 mA. The intensity of higher order reflections was minimized by detuning the second crystal of the monochromator to 60 % of the maximum intensity. The samples were prepared as self-supporting wafers and measured in the fluorescence mode. X-ray absorption spectra were recorded at the Al K edge (1559 eV) and analyzed with XANES dactyloscope software.

4.2.8. Catalytic activity

The catalytic activity tests were carried out in a fixed-bed flow reactor made from quartz glass, at a gas-hourly space velocity (GHSV) of 74050 h^{-1} in a temperature range between 423 K and 873 K in steps of 50 K. The gas flow for the NH_3-SCR reaction was composed of 1000 ppm NO, 1000 ppm NH_3 and 5 vol. % O_2 balanced with N_2. The conversion at each temperature was measured after 0.5 h of steady-state reaction. The NO and NH_3 concentrations were continuously monitored by IR spectroscopy (Thermo Nicolet). Prior to the activity tests, the catalysts were activated in N_2 for 1 h at 723 K with a ramp of 10 K/min and subsequently cooled to 423 K.

4.3. Results

The single-step wet-ion exchange of zeolite HBEA resulted in a FeBEA sample with a Fe content of 1.0 wt. %, corresponding to a molar Fe/Al ratio of 0.3. The steaming treatment under NH_3-SCR conditions in a plug-flow reactor did not change the overall Fe and Al content as well as the crystal structure of all FeBEA samples (for the diffraction patterns see C.1).

4.3.1. Characterization of the acidity of the FeBEA samples

The concentration of Brønsted and Lewis acid sites of the FeBEA samples after activation at 723 K was determined by IR spectroscopy of adsorbed pyridine (see Figure 4.1). Two characteristic bands at 1452 cm^{-1} and 1545 cm^{-1} emerge upon adsorption of pyridine, which are attributed to adsorption on Lewis acid sites and the formation of pyridinium ions (adsorption on Brønsted acid sites), respectively.[35]

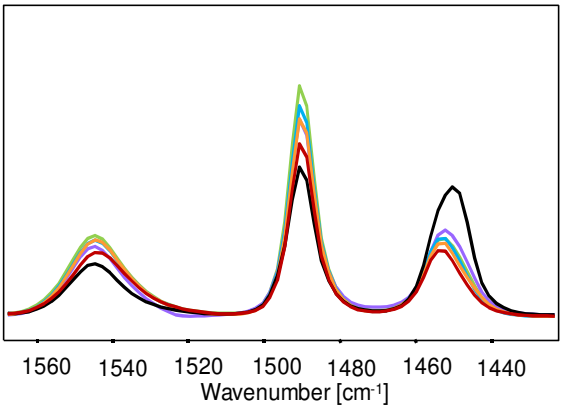

Figure 4.1: IR spectra of adsorbed pyridine on the samples FeBEA (black), FeBEA 723 (purple), FeBEA 723st (blue), FeBEA 773st (green), FeBEA 823st (orange), FeBEA 873st (red).

The band characteristic of Lewis acid bound pyridine can be further divided into two contributions with maxima at 1454 cm^{-1} and 1448 cm^{-1}, assigned to the adsorption of pyridine on Lewis acidic (extra framework) Al species (1454 cm^{-1}) and Lewis acidic Fe species (1448 cm^{-1}). The unsteamed sample FeBEA is characterized by a concentration of Brønsted acid sites of 284 µmol/g and a concentration of Lewis acid sites of 380 µmol/g (see Table 4.2). The deconvolution of the band assigned to pyridine adsorbed on Lewis acid sites showed that 54 % of these sites can be related to Fe

cations at ion exchange positions. The treatment of this sample with NO, NH_3 and O_2 at 723 K increased the concentration of Brønsted acid sites to 410 µmol/g and decreased the concentration of Lewis acid sites to 265 µmol/g. The samples FeBEA 723st to FeBEA 873st show a further decrease of the concentration of Lewis acidic Fe species (about 50 µmol/g) and a further increase of the concentration of Brønsted acid sites. For the sample treated at 873 K a slight decrease of the concentration of Brønsted acid sites was detected. It should be noted that the concentration of Lewis acidic Al sites remained constant within the experimental error for all FeBEA studied samples.

Table 4.2: Concentration of acid sites for FeBEA samples as determined by IR spectroscopy of adsorbed pyridine.

sample	Brønsted acid sites [µmol/g]	Lewis acidic Al sites [µmol/g]	Lewis acidic Fe sites [µmol/g]
FeBEA	284	175	205
FeBEA 723	410	192	73
FeBEA 723st	447	186	65
FeBEA 773st	431	191	49
FeBEA 823st	428	187	53
FeBEA 873st	394	172	46

The temperature programmed desorption of NH_3 from the FeBEA samples after activation at 723 K shows two desorption maxima at 565 K and at 790 K. For zeolite BEA, the desorption peak at lower temperature (565 K) is characteristic to the desorption of NH_3 from Brønsted acid sites, while the high temperature desorption peak (790 K) is assigned to desorption of NH_3 from Lewis acid sites.[30] The desorption peaks (diffusion broadening) were fitted with Gaussian functions in order to estimate the concentrations of weaker and stronger acid sites (see Table 4.3 and C.2).

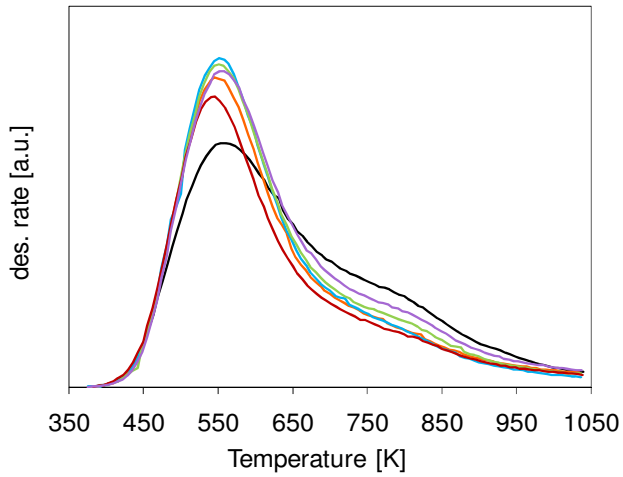

Figure 4.2: Results of NH_3-TPD of the samples FeBEA (black), FeBEA 723 (purple), FeBEA 723st (blue), FeBEA 773st (green), FeBEA 823st (orange), FeBEA 873st (red).

The treatment of the FeBEA catalysts under NH_3-SCR conditions and steam caused the concentration of weaker acid sites to increase and the concentration of stronger acid sites to decrease, suggesting a transformation of Lewis acid sites into Brønsted acid sites. The desorption maximum of NH_3 from the weaker acid sites shifted about 10 K to lower temperatures. The total concentration of acid sites increased throughout the steaming and NH_3 treatment for the samples FeBEA, FeBEA 723, FeBEA 723st and FeBEA 773st and decreased slightly for the samples FeBEA 823st and FeBEA 873st. This is in accordance to the concentration of acid sites determined by the adsorption of pyridine indicating a transformation of Lewis into Brønsted acid sites.

Table 4.3: Concentrations of weaker and stronger acid sites derived from deconvolution of the NH_3-TPD profiles**.**

sample	weaker acid sites [µmol/g]	stronger acid sites [µmol/g]
FeBEA	257	268
FeBEA 723	354	219
FeBEA 723st	385	180
FeBEA 773st	396	171
FeBEA 823st	334	184
FeBEA 873st	322	155

In order to further understand the increase of the Brønsted acidity during the NH_3-SCR treatment at elevated temperatures, the coordination of the Al atoms was characterized by Al XANES. The line-shape of the XANES shows characteristic features for octahedral and tetrahedral Al and allows monitoring dealumination of zeolites during steaming. The Al-XANES of the untreated sample FeBEA shows a sharp white line at 1566.5 eV and an edge energy (determined at the inflection point of the edge) of 1565 eV. In addition, the spectrum shows two small peaks 5 and 10 eV above the absorption edge and one at 1583 eV, reflecting the tetrahedral coordination of the Al in the framework positions of zeolite BEA.[36,37] Interestingly, the Al-XANES of the samples treated under NH_3-SCR conditions and steam show the identical features (see Figure 4.3), which indicates that the coordination of Al and, particularly, the concentration of octahedral and tetrahedral coordinated Al is not affected by the NH_3-SCR treatment in all FeBEA samples investigated.

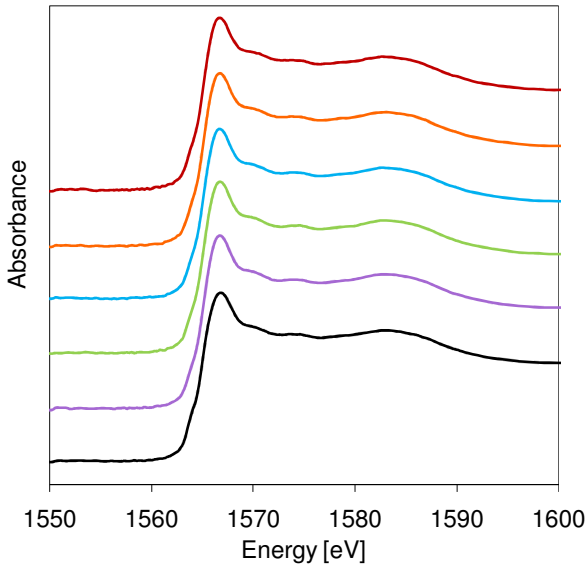

Figure 4.3: Al XANES of the samples FeBEA (black), FeBEA 723 (purple), FeBEA 723st (blue), FeBEA 773st (green), FeBEA 823st (orange), FeBEA 873st (red).

4.3.2. Characterization of the structural properties of Fe species in the FeBEA samples

The nature and distribution of Fe^{3+} species in the zeolite were studied using diffuse reflectance UV/Vis spectroscopy. Fe^{3+} species in the zeolite can be classified by UV/Vis spectroscopy into isolated Fe^{3+} ions (λ<300 nm), Fe in small oligomeric Fe_xO_y clusters inside the zeolite channels (300 nm<λ<400 nm) and Fe in hematite like Fe_2O_3 clusters (λ>400 nm).[38] For isolated Fe^{3+} ions, the d-d transitions are symmetry- and spin-forbidden and, therefore, only the $Fe^{3+} \leftarrow O$ charge transfer (CT) bands can be observed in the UV/Vis spectra.[39] For isolated Fe^{3+} ions usually two CT bands are expected in the range between 200 nm and 300 nm. The exact positions depend on the number of ligands, allowing a differentiation between octahedral and tetrahedral coordinated Fe^{3+} ions. For Fe cations in tetrahedral symmetry in framework T atom positions of zeolites, these transitions are observed at 215 nm and 241 nm, while they are observed in the ranges between 187 nm-234 nm and 244 nm-305 nm for Fe in octahedral matrices such as in extraframework ion exchange positions.[25,40]

The DR UV/Vis spectrum of the untreated sample FeBEA is characterized by two bands at 220 nm and 271 nm, indicating the octahedral coordination of isolated Fe^{3+} ions in this sample (see Figure 4.4). In addition, a small shoulder between 300 nm and 350 nm indicates the presence of a very small fraction of Fe_xO_y species in the zeolite channels. The existence of large Fe_2O_3 clusters can be ruled out by the absence of bands in the energy range above 400 nm.

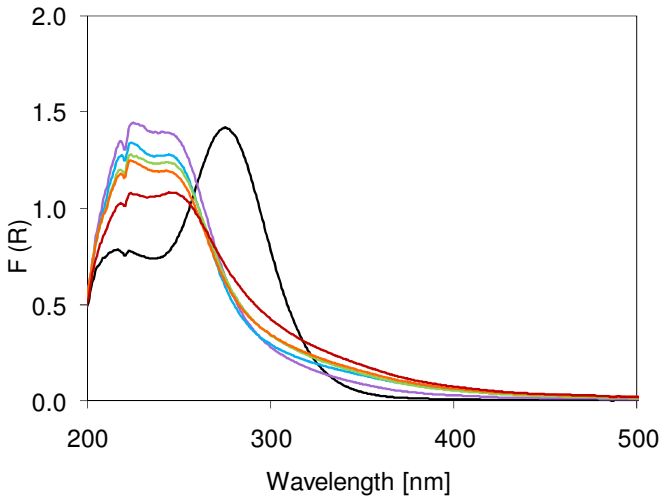

Figure 4.4: Diffuse reflectance UV/Vis spectra of FeBEA (black), FeBEA 723 (purple), FeBEA 723st (blue), FeBEA 773st (green), FeBEA 823st (orange), FeBEA 873st (red).

The treatment under NH_3-SCR conditions led to the appearance of two new bands at 214 nm and 241 nm, which are assigned to Fe^{3+} in a tetrahedral coordination. This indicates that the octahedral coordinated Fe^{3+} ions, initially present in extraframework ion exchange positions are incorporated into framework T atom positions of the zeolite during this treatment. The shoulder observed between 300 nm and 400 nm is attributed to a small concentration of Fe_xO_y species, which increased with increasing steaming temperature. However, even at a steaming temperature of 873 K bands above 400 nm were not observed, confirming that large Fe_2O_3 clusters were not formed during this treatment.

The XANES of the FeBEA samples were analyzed in order to further understand the coordination of the Fe species in the steamed and NH_3-treated samples. Several features in the XANES region can be related to the oxidation state and the coordination of the Fe species in the zeolite samples. A typical feature, which is sensitive to the coordination of Fe is the pre-edge peak being usually observed for Fe K edges between 7110 eV and 7115 eV.[41-43] In general, the pre-edge peak in the XANES of a K edge is related to 1s $\rightarrow$ 3d transitions, which are spin-forbidden for ideal octahedral coordination geometries. In distorted octahedral and especially in tetrahedral geometries, however, the mixing of p and d levels increases the intensity of this peak. Therefore, the occurrence of a pre-edge peak is a clear indication for Fe species in

tetrahedral coordination symmetry.[5,44,45] Furthermore, the energy of the edge can be directly related to the oxidation state of the iron species, as shown recently using Mössbauer spectroscopy.[28]

The XANES of the FeBEA samples are shown in Figure 4.5. The unsteamed sample showed only a weak pre-edge peak at 7113 eV, indicating the presence of Fe species in a distorted octahedral symmetry.

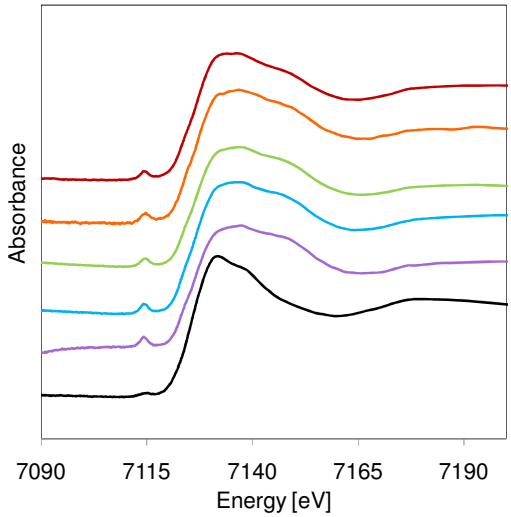

Figure 4.5: Fe-XANES of the samples FeBEA (black), FeBEA 723 (purple), FeBEA 723st (blue), FeBEA 773st (green), FeBEA 823st (orange), FeBEA 873st (red).

Steaming and NH_3-treatment led to an increase of the pre-edge peak, which is attributed to the transformation from octahedral to tetrahedral coordinated Fe cations. The intensity of the pre-edge peaks of the samples exposed to steam and NH_3 is about four to five times larger compared to unsteamed FeBEA. A further indication of the tetrahedral coordination of the Fe species is the general shape of the XANES, which is identical to that of Fe-silicalite having Fe tetrahedrally coordinated in T-atoms positions.[25] The energy of the edge (7124.5 eV) is identical for all six samples. According to our previously established correlation between the oxidation state of the Fe species and the edge energy the oxidation state of Fe is, therefore, +3.[28]

The coordination of the Fe species was further explored by the analysis of the EXAFS, which are shown in Figure 4.6. The Fourier transform of the EXAFS for the untreated FeBEA sample shows only one maximum at 2.15 Å, which is assigned to Fe-O

backscattering in the first shell and indicates isolated Fe ions in octahedral coordination, whose coordination sphere is completed with H_2O.

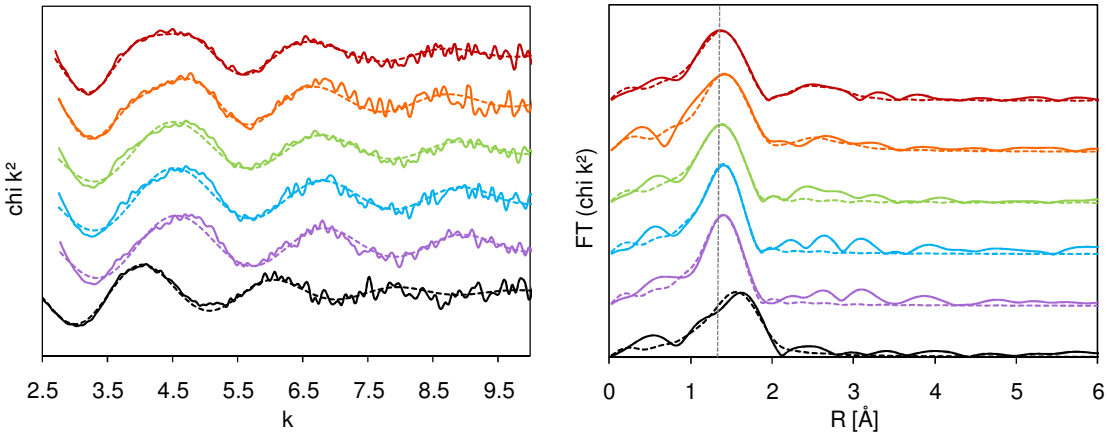

Figure 4.6: EXAFS of the samples FeBEA (black), FeBEA 723 (purple), FeBEA 723st (blue), FeBEA 773st (green), FeBEA 823st (orange), FeBEA 873st (red).

This is in line with the slightly distorted octahedral coordination of Fe in this sample as indicated by UV/Vis spectroscopy and XANES. The Fe-O distance of around 2.1 Å is typical for Fe cations in ion exchange positions.[15,32,46] The steaming and NH_3 treatment at 723 K and 773 K led to a decrease of this distance to 1.86 Å. Together with the Fe-O coordination number of four, this indicates that Fe is present in a tetrahedral coordination at the zeolite T atom positions. Steaming and NH_3-SCR treatment at higher temperatures led to an increase of the Fe-O coordination numbers and to the appearance of Fe-Fe backscattering pairs, which indicates that the isolated Fe can be stabilized in the presence of NH_3 up to 773 K, while at higher temperatures partial agglomeration into small Fe_xO_y clusters occurred.

Table 4.4: Coordination numbers and Fe-O respective Fe-Fe distances derived from the EXAFS of the samples FeBEA, FeBEA 723, FeBEA 723st, FeBEA 773st, FeBEA 823st and FeBEA 873st.

sample	n (Fe-O)	d (Fe-O) [Å]	n (Fe-Fe)	d (Fe-Fe) [Å]
FeBEA	6	2.15	0	0
FeBEA 723	4	1.86	0	0
FeBEA 723st	4	1.86	0	0
FeBEA 773st	4	1.86	0	0
FeBEA 823st	5	1.89	0	0
FeBEA 873st	5	1.89	2	2.78

The influence of the NH_3 and steaming treatment on the type and concentration of hydroxyl groups was further studied by IR spectroscopy of the activated FeBEA catalysts (see Figure 4.7).

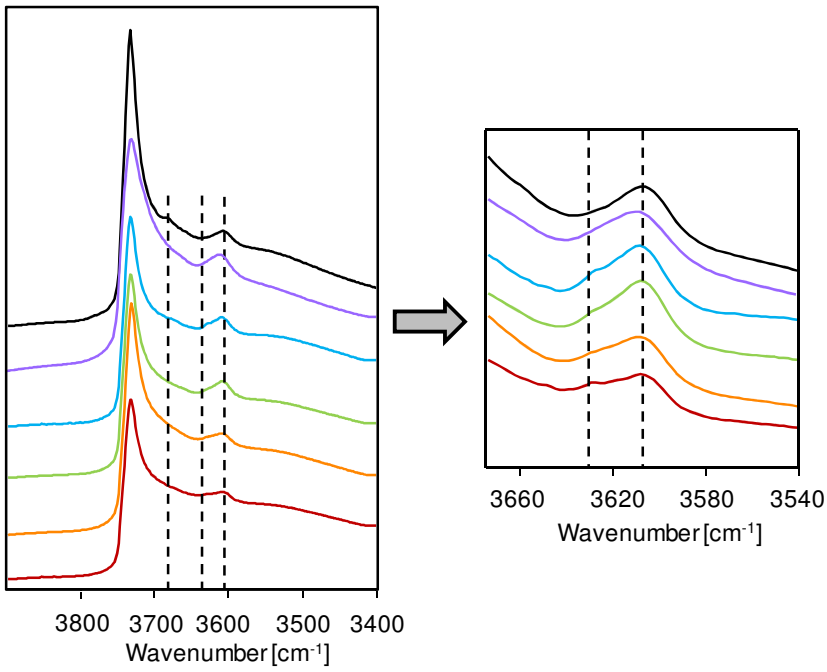

Figure 4.7: IR spectra of the hydroxyl vibration of the samples FeBEA (black), FeBEA 723 (purple), FeBEA 723st (blue), FeBEA 773st (green), FeBEA 823st (orange), FeBEA 873st (red).

The IR spectrum of the untreated sample shows the typical stretching vibrations of the OH groups for zeolite BEA, i.e., external and internal silanol groups at 3740 and 3725 cm^{-1}, respectively, bridged SiOHAl groups at 3606 cm^{-1} and hydrogen-bonded disturbed hydroxyl groups at 3200-3500 cm^{-1}.[24,47-49] As zeolite BEA has a high concentration of defect sites and stacking disorders, the concentration of silanol sites is very high for this zeolite type. In addition to the hydroxyl groups originating from the zeolite, a band at 3682 cm^{-1} was observed for the Fe loaded samples, which is assigned to hydroxyl groups on Fe species in ion exchange positions.[50] This band indicates that in the unsteamed sample Fe^{3+} species are present at ion exchange positions with some charge being compensated by OH groups. The ammonia and steam treatment led to the disappearance of the band at 3682 cm^{-1} and at the same time to the formation of a new OH band at 3627 cm^{-1} assigned to acidic bridging SiOHFe groups suggesting the insertion of Fe into T atom positions of the zeolite framework.[51] The treatment also led to a decrease of the concentration of silanol groups at 3725cm^{-1} due to the insertion of Fe^{3+} cations and the formation of Si-O-Fe bonds. The concentration of the SiOHAl groups (observed at 3606 cm^{-1}) stayed nearly constant. Only a minor decrease after the treatment at higher temperatures was observed, which is attributed to a slight dealumination of the zeolite. The concentration of SiOHFe and SiOHAl is the highest for the sample FeBEA 723st indicating a minor extraction of Al and Fe from the zeolite framework positions during steaming at higher temperatures.

4.3.3. Activity of steamed and NH_3-treated FeBEA samples in the NH_3-SCR reaction

The activity of the unsteamed FeBEA catalyst in the NH_3-SCR reaction is shown in Figure 4.8. The NO conversion of the FeBEA catalysts was around 3 % at 423 K and increased up to 70 % at 723 K to 873 K. As frequently reported, the NO conversion followed a S-shaped curve with a sharp increase of the conversion between 523 K and 623 K. The conversion of NH_3 tracks the conversion of NO for temperatures up to 673 K, but in contrast to the NO conversion the NH_3 conversion increases further at higher temperatures. Consequently, the reaction follows a 1:1 stoichiometry between

NO and NH_3 for temperatures below 673 K, while at higher temperatures the side-reaction of NH_3 to N_2 starts to play a role, which limits the further reduction of NO.

The conversions of NO of the FeBEA catalysts treated under NH_3-SCR conditions were identical to the untreated sample FeBEA at temperatures up to 623 K and slightly lower at higher reaction temperatures. The lower activity results most probably from the formation of Fe_xO_y clusters limiting the reaction at higher temperatures. The conversion of NH_3 of the samples FeBEA 723, FeBEA 723st, FeBEA 773st, FeBEA 823st and FeBEA 873st also follows the trend of the unsteamed sample. The activity decreases about 10 % for reaction temperatures between 550 K and 770 K and reaches the values of the unsteamed sample FeBEA for higher temperatures.

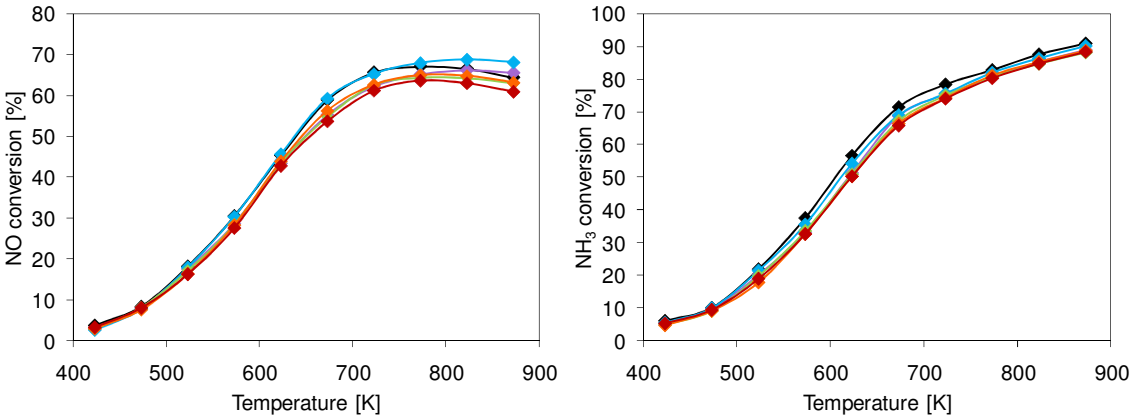

Figure 4.8: NO and NH_3 conversions of the catalysts FeBEA (black), FeBEA 723 (purple), FeBEA 723st (blue), FeBEA 773st (green), FeBEA 823st (orange), FeBEA 873st (red).

4.3.4. Determination of the coordination of the Fe species after activation and under reaction conditions

The results from the characterization of the Fe species in the hydrated state indicate that the insertion of Fe into T atom positions takes place quantitatively. The question arises now, whether or not this insertion is maintained during activation at 723 K and what structure the Fe species assume under NH_3-SCR conditions. The oxidation state of the Fe species before and after activation of the samples FeBEA 723 and FeBEA 823st was derived from the edge position (inflection point) of the XANES.[28] During activation, a shift of the edge energy to lower energies was observed for both samples, indicating a reduction of the Fe cations (see Figure 4.8). In addition, the

intensity of the pre-edge peak decreased during activation indicating a partial loss of the perfect tetrahedral coordination in the hydrated sample. For FeBEA 723, the edge energy shifted from 7125.0 eV to 71221.1 eV. The former energy corresponds to a $Fe^{2+}/\sum Fe$ ratio of 0.15, while the latter corresponds to a $Fe^{2+}/\sum Fe$ ratio of 0.68. The situation for FeBEA 823st is similar. The edge energy before activation was 7125.1 eV and shifted to 7122.7 eV during the activation, corresponding to a $Fe^{2+}/\sum Fe$ ratio of 0.13 before activation and 0.59 after activation.

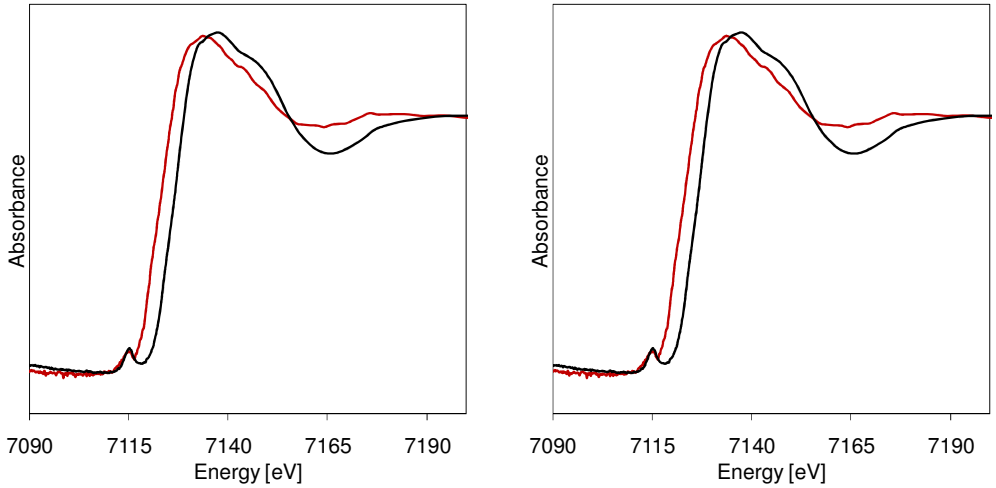

Figure 4.9: XANES of FeBEA723 and FeBEA823st before (black) and after activation (red).

As Fe has to be in the oxidation state +3 to be incorporated in T atom positions, the change in the oxidation states suggests that parts of the tetrahedrally coordinated Fe is eliminated from the lattice T atom positions during the activation and is present again in ion-exchange positions.

In order to further understand these structural changes, the coordination of the Fe cations was additionally examined by EXAFS analysis on the unsteamed FeBEA sample under reaction conditions at 423 K, 523 K, 623 K and 723 K. In addition, the Fe coordination after activation at 723 K in He was also measured. After activation in He, the formation of Fe-O-Fe bridges and a change in the symmetry of the Fe atoms from an octahedral to a tetrahedral coordination was observed. The average Fe-O distance after activation was 2.00 Å, which is shorter than in the hydrated sample. The Fe-Fe distance was determined to be 3.01 Å with an average coordination number of ~1, indicating that mainly dimers were formed during activation (see Figure 4.10 and

Table 4.5). The addition of the reaction gas mixture at 423 K led to a further decrease of the Fe-O distance to 1.86 Å. As Fe-Fe contributions were not observed in the EXAFS we conclude that Fe-O-Fe bonds were broken.

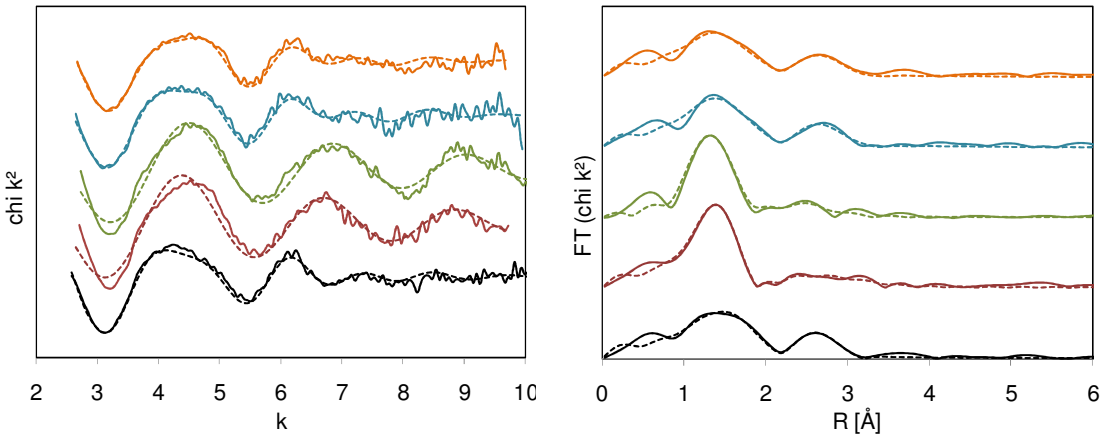

Figure 4.10: EXAFS of the sample FeBEA after activation (black), after reaction at 423 K (brown), 523 K (green), 623 K (blue) and 723 K (gold).

The increase of the reaction temperature to 523 K leads to a minor contribution of Fe-Fe backscattering revealing a Fe-Fe distance of 2.97 Å and a coordination number of 0.1. This low coordination number shows that only a small part of the Fe cations form Fe-O-Fe bridges at this temperature. For the EXAFS after reaction at 623 K and 723 K we observed an increase in the Fe-O bond length to 1.95 Å as well as significant contributions of Fe-Fe scattering. The Fe-Fe distance is 3.06 Å with a corresponding coordination number of ~1.

Table 4.5: Coordination numbers and Fe-O respective Fe-Fe distances derived from the EXAFS of the sample FeBEA after activation and reaction from 423 K to 723 K.

sample	n (Fe-O)	d (Fe-O) [Å]	n (Fe-Fe)	d (Fe-Fe) [Å]
after activation	4	2.00	1.3	3.01
reaction at 423 K	4	1.85	0.0	0
reaction at 523 K	4	1.87	0.1	2.97
reaction at 623 K	4	1.95	1.2	3.06
reaction at 723 K	4	1.95	1.2	3.05

4.4. Discussion

4.4.1. Structure of the Fe after ion exchange

Mainly isolated Fe ions in ion exchange positions exist in the untreated FeBEA, prepared by single-step wet-ion exchange. UV Vis and X-ray absorption spectroscopy show that Fe is present in an octahedral environment in this sample under ambient conditions, indicating the saturation of the Fe ions with hydroxyl groups and water ligands present in the zeolite pores (see Figure 4.11). The very small fraction of Fe_xO_y clusters present in the materials after ion exchange will be neglected in the following discussion.

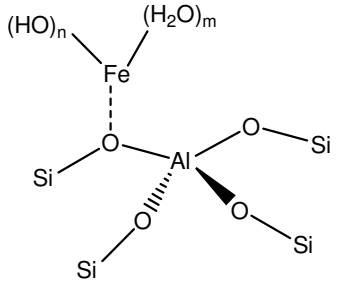

Figure 4.11: Scheme of octahedrally coordinated Fe in an ion exchange position.

To understand the activity of FeBEA in the NH_3-SCR reaction it is essential to identify whether the octahedral coordination is maintained under reaction conditions and to which extent changes in the coordination of Fe occur in the presence of NO, NH_3 and steam at reaction temperatures between 423 K and 873 K.

4.4.2. Insertion of Fe into zeolite T atom positions under NH_3-SCR conditions

After exposing this sample to reaction conditions the pre-edge peak in the XANES increased, bands appeared at 214 nm and 241 nm in the UV Vis spectra and the Fe-O distance was 1.86 Å, indicating that the octahedral coordination of Fe was converted to a tetrahedral one. This is concluded to be related to the insertion of Fe^{3+} cations, presumably silanol nests. This incorporation is also paralleled by the decrease of the stretching vibrations of hydroxyl groups of Fe cations at ion exchange positions

(3682 cm^{-1}) and the formation of a new band at 3627 cm^{-1} assigned to bridging SiOHFe groups.[51]

It is interesting to note that reports such as reinsertion of Al atoms are limited to Al^{3+} coordinated to some extent to the framework and have not been published for extra-framework oxide clusters.[36,37] The present results indicate that insertion can occur from ion exchange places. The mechanism behind the reinsertion is based on the basic properties of NH_3, polarizing the SiOH groups and favoring so the condensation with partially hydroxylated Fe^{3+} cationic species. The decrease of the vibration of the SiOH groups at defect sites (3725 cm^{-1}) complements this information. Please note that the high concentration of silanol nests present in zeolite BEA allows even the quantitative insertion of the Fe^{3+} cations into zeolite T positions.

NH_3-TPD and the IR spectra of adsorbed pyridine also complement the evidence for this transformation as strong Lewis acid sites are converted to (weaker) Brønsted acid sites leading to an increase of the concentration of Brønsted acid sites, which appear to be nearly as acidic as SiOHAl groups.[51] With the increase of the concentration of Brønsted acid sites by 163 µmol/g for the sample FeBEA 723st compared to the untreated FeBEA, a decrease of 130 µmol/g for the concentration of Lewis acid sites was observed. Even assuming that the Fe^{3+} cations only balance one aluminum containing tetrathedron, the insertion of Fe into T atom positions should lead to the formation of two Brønsted acid sites per inserted Fe cation. One Brønsted acidic OH group would be formed by the inserted Fe^{3+} cation and one by the aluminum containing tetrahedron, which is not compensated by the Fe cation.

Thus, the increase of the concentration of Brønsted acid sites by only 163 µmol/g in the presence of a total concentration of 180 µmol/g Fe is too small, especially as the UV/Vis and XANES data indicate a quantitative insertion of Fe^{3+} cations under ambient conditions. The reason for this discrepancy is attributed to the fact that the concentration of acid sites was measured with activated samples, in contrast to the UV/Vis spectra and XANES, which were done on hydrated samples. The XANES of the activated samples FeBEA 723 and FeBEA 823st showed the reduction of the Fe species and, thus, indirect the extraction of Fe^{3+} cations from T atom positions during the activation process. For the sample FeBEA 723, a molar fraction of Fe^{3+} of 0.32 after

activation was derived from the position of the edge energy. Assuming that all Fe^{3+} is present in T atom positions, this would mean that from the total 180 µmol/g Fe atoms, 51 µmol/g Fe atoms are present in T atom positions, generating then 102 µmol/g new Brønsted acid sites compared with the untreated FeBEA sample. This value agrees with the experimental estimation of the concentration of acid sites.

The same conclusion can be drawn from the results on the samples FeBEA 823st. The molar fraction of Fe^{3+} after activation is 0.41, indicating that 74 µmol/g Fe are present in T atom positions after the activation treatment. This would imply an increase in the concentration of Brønsted acid sites compared with the untreated FeBEA sample of 148 µmol/g. The results of the adsorption of pyridine showed an increase in the concentration of Brønsted acid sites of 147 µmol/g.

Steaming and NH_3 treatment, thus, led only to changes in the coordination of the Fe sites, while the coordination of the Al sites was not significantly changed. The concentration of Lewis acidic Al sites as well as the shape of the Al XANES stayed constant for most of the investigated samples, indicating that the Al coordination is not affected by steaming and NH_3 treatment. In agreement with the studies of van Bokhoven et al., who described that Al species connected to the framework can be reinserted by NH_3 treatment into the zeolite matrix, we can conclude that Al, which could have been removed from the lattice during steaming treatment, is reinserted into the lattice in the presence of NH_3 during the cooling. Only the severely steamed samples FeBEA 823st and FeBEA 873st showed a minor decrease in the intensity of the OH stretching vibration of the SiOHAl sites at 3606 cm^{-1}, which is probably due to a slight dealumination at these steaming temperatures.

4.4.3. Activity of FeBEA catalysts in the NH_3-SCR reaction

The characterization data indicate that Fe can only be stabilized in zeolite T atom positions under formation of Brønsted acid sites, when Fe is present as trivalent atom. However, in this coordination it is not possible that Fe is participating in a redox cycle during the NH_3-SCR reaction. It should be noted that the catalytic activities of all investigated FeBEA samples were similar and comparable to Fe-zeolite catalysts reported in the literature. If we assume that the insertion of Fe is quantitative for the steam and NH_3 treated samples, one would have expected a lower catalytic activity for

the steam and NH_3 treated sample. However, regardless of the steam and NH_3 treatment of the FeBEA catalysts, we observed the same conversion levels of NO and NH_3, which again leads to the conclusion that Fe^{3+}, cannot be present at zeolite T atom positions under reaction conditions. The extraction of Fe and the formation of the active Fe-O-Fe bridges takes place during the activation procedure, which was demonstrated by the XANES and is also reflected in the EXAFS. The EXAFS analyses of the untreated and hydrated sample FeBEA show an octahedral coordination of the Fe species in isolated positions. As Fe-Fe backscattering contributions were not found in the EXAFS, the existence of species with Fe-O-Fe bridges can be ruled out in the hydrated samples. The situation changes after the activation of the sample in He at 723 K, where EXAFS shows Fe-Fe contributions, indicating a condensation of two Fe-OH groups to Fe-O-Fe units under a reduction of Fe^{3+} to Fe^{2+}. This condensation is also reflected by a shortening of the average Fe-O distance to 2.00 Å (see Figure 4.12).

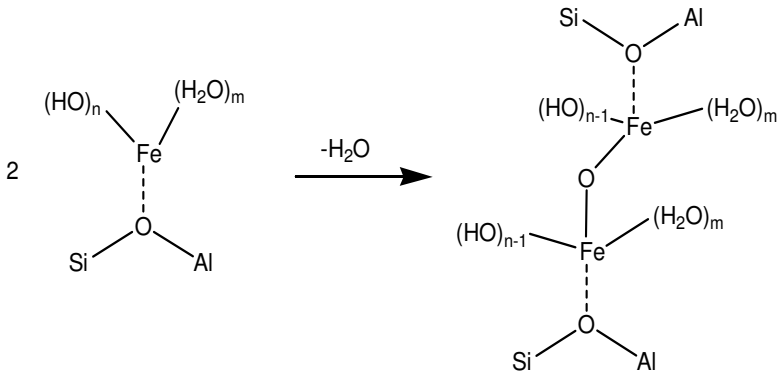

Figure 4.12: Formation of the Fe-O-Fe bridges under condensation of Fe-OH groups.

Another important question arising at this point is whether the binuclear Fe-O-Fe units are maintained under reaction conditions. For the sample quenched after addition of the reaction gases at 423 K we observed the loss of the Fe-Fe contributions and, therefore, propose a cleavage of the Fe-O-Fe bonds under NH_3-SCR conditions at 423 K. This means that isolated Fe cationic species at ion-exchange are formed under addition of the reaction gases. The increase of the reaction temperature to 523 K leads to a minor contribution of Fe-Fe backscattering, which can be seen as a first indication for the formation of Fe-O-Fe units resulting from the condensation of Fe-OH groups.

Assuming that only dimeric Fe-O-Fe units are formed, the Fe-Fe coordination number of 0.1 indicates that around 10 % of the Fe cations are present in these units, while the remaining 90 % are still present in isolated Fe cationic species. At reaction temperatures of 623 K and 723 K, the EXAFS are characterized by a further enhancement of contributions from Fe-Fe backscattering with a coordination number of around 1, indicating that all Fe cations are present in Fe-O-Fe units under the assumption that only isolated and dimeric species can be formed. Therefore, we can conclude that the formation of the active Fe-O-Fe units is highly dependent on the reaction temperature and the presence of the reaction gases. After activation in He, the Fe-O-Fe bridges are only cleaved at 423 K in the presence of the reaction gases and they are again formed in the presence of the reaction gases at temperatures between 623 K and 723 K.

The insertion of the Fe cations into framework T atom positions takes only place during cooling after the reaction in reaction gases to room temperature. But as this coordination is broken after activation in He at 723 K, all catalysts studied showed the same activity. The low concentrations of small Fe_xO_y clusters, formed during the steaming and NH_3 treatment at temperatures above 823 K, can lead to a minor loss of activity as it was observed for the catalysts FeBEA 823st and FeBEA 873st. In addition, the cooling under NH_3-SCR conditions probably prevents the dealumination of the zeolite matrix as well as the formation of an inactive Fe_2O_3 phase.

4.5. Conclusions

The wet-ion exchange of zeolite BEA with Fe cations leads to the formation of isolated Fe cations in ion-exchange positions which are characterized by an octahedral coordination in the hydrated state. Under reaction conditions, these Fe cationic species undergo temperature dependant changes ranging from the formation of dimeric Fe-O-Fe units to the insertion of Fe cations into T atom positions of the zeolite framework. The activation of the hydrated catalysts in inert gases at 723 K causes the formation of Fe-O-Fe units which can be seen as the main active species in the NH_3-SCR reaction. The addition of the reaction gases at 423 K leads to the cleavage of these units and the formation of isolated Fe species in ion-exchange positions, while an increase of the reaction temperature to 623 K again induces the formation of the active Fe-O-Fe units. A subsequent cooling in the presence of the reaction gases NH_3, NO and O_2 to room temperature leads to the quantitative insertion of Fe cations into zeolite T atom positions and a corresponding healing of silanol nests. This quantitative insertion of Fe is possible because the used HBEA sample posseses a high intrinsic concentration of silanol nests. We can conclude that the active Fe species in the NH_3-SCR reaction are formed *in situ* under reaction conditions and that the structure of the Fe species is depending on the reaction temperature. The catalytic activity is mostly maintained throughout the ageing treatment in the presence of steam, and only a minor decrease in activity at higher temperatures was observed due to the formation of a small fraction of Fe_xO_y species. Cooling of the FeBEA catalysts in the presence of NH_3 is beneficial to enhance the stability of the catalysts and prevents dealumination of the zeolite framework.

4.6. Acknowledgement

Portions of this research were carried out at the light source facility DORIS III at DESY, Hamburg, Germany. DESY is a member of the Helmholtz Association (HGF). We would like to thank Adam Webb and Michael Murphy for assistance in using beamline X1. The authors would like to thank Martin Neukamm for AAS measurements and Edith Ball for preparation of the FeBEA samples. The project was funded by the Bayerisches Staatsministerium für Wissenschaft, Forschung und Kunst.

4.7. References

(1) Dubkov, K. A.; Ovanesyan, N. S.; Shteinman, A. A.; Starokon, E. V.; Panov, G. I. *J. Catal.* **2002**, *207*, 341.

(2) El-Malki, E.-M.; van Santen, R. A.; Sachtler, W. M. H. *J. Catal.* **2000**, *196*, 212.

(3) Heinrich, F.; Schmidt, C.; Löffler, E.; Menzel, M.; Grünert, W. *J. Catal.* **2002**, *212*, 157.

(4) Joyner, R.; Stockenhuber, M. *J. Phys. Chem. B* **1999**, *103*, 5963.

(5) Kumar, M. S.; Schwidder, M.; Grünert, W.; Brückner, A. *J. Catal.* **2004**, *227*, 384.

(6) Long, R. Q.; Yang, R. T. *J. Am. Chem. Soc.* **1999**, *121*, 5595.

(7) Ribera, A.; Arends, I. W. C. E.; de Vries, S.; Pérez-Ramírez, J.; Sheldon, R. A. *J. Catal.* **2000**, *195*, 287.

(8) Busca, G.; Lietti, L.; Ramis, G.; Berti, F. *Appl. Catal., B* **1998**, *18*, 1.

(9) Garten, R. L.; Delgass, W. N.; Boudart, M. *J. Catal.* **1970**, *18*, 90.

(10) Morice, J. A.; Rees, L. V. C. *Transactions of the Faraday Society* **1968**, *64*, 1388.

(11) Brandenberger, S.; Kröcher, O.; Tissler, A.; Althoff, R. *Appl. Catal., B* **2010**, *95*, 348.

(12) Long, R. Q.; Yang, R. T. *Catal. Lett.* **2001**, *74*, 201.

(13) Santhosh Kumar, M.; Schwidder, M.; Grünert, W.; Bentrup, U.; Brückner, A. *J. Catal.* **2006**, *239*, 173.

(14) Schwidder, M.; Kumar, M. S.; Brückner, A.; Grünert, W. *Chem. Commun.* **2005**, 805.

(15) Sklenak, S.; Andrikopoulos, P. C.; Boekfa, B.; Jansang, B.; Nováková, J.; Benco, L.; Bucko, T.; Hafner, J.; Dedecek, J.; Sobalík, Z. *J. Catal.* **2010**, *272*, 262.

(16) Sobalik, Z.; Vondrová, A.; Tvaruzková, Z.; Wichterlová, B. *Catal. Today* **2002**, *75*, 347.

(17) Battiston, A. A.; Bitter, J. H.; de Groot, F. M. F.; Overweg, A. R.; Stephan, O.; van Bokhoven, J. A.; Kooyman, P. J.; van der Spek, C.; Vankó, G.; Koningsberger, D. C. *J. Catal.* **2003**, *213*, 251.

(18) Battiston, A. A.; Bitter, J. H.; Heijboer, W. M.; de Groot, F. M. F.; Koningsberger, D. C. *J. Catal.* **2003**, *215*, 279.

(19) Chen, H. Y.; El-Malki, E.-M.; Wang, X.; van Santen, R. A.; Sachtler, W. M. H. *J. Mol. Catal. A: Chem.* **2000**, *162*, 159.

(20) Chen, H. Y.; Sachtler, W. M. H. *Cataly. Today* **1998**, *42*, 73.
(21) Marturano, P.; Drozdová, L.; Kogelbauer, A.; Prins, R. *J. Catal.* **2000**, *192*, 236.
(22) Xia, H.; Sun, K.; Liu, Z.; Feng, Z.; Ying, P.; Li, C. *J. Catal.* **2010**, *270*, 103.
(23) Gorte, R. J. *Catal. Lett.* **1999**, *62*, 1.
(24) Guisnet, M.; Ayrault, P.; Coutanceau, C.; Alvarez, M. F.; Datkac, J. *J. Chem. Soc., Faraday Trans.* **1997**, *93*, 1661.
(25) Bordiga, S.; Buzzoni, R.; Geobaldo, F.; Lamberti, C.; Giamello, E.; Zecchina, A.; Leofanti, G.; Petrini, G.; Tozzola, G.; Vlaic, G. *J. Catal.* **1996**, *158*, 486.
(26) Meagher, A.; Nair, V.; Szostak, R. *Zeolites* **1988**, *8*, 3.
(27) Pérez-Ramírez, J.; Santhosh Kumar, M.; Brückner, A. *J. Catal.* **2004**, *223*, 13.
(28) Maier, S. M.; Jentys, A.; Metwalli, E.; Müller-Buschbaum, P.; Lercher, J. A. *J. Phys. Chem. Lett.* **2011**, *2*, 950.
(29) Schmidt, R.; Amiridis, M. D.; Dumesic, J. A.; Zelewski, L. M.; Millman, W. S. *J. Phys. Chem. B* **1992**, *96*, 8142.
(30) Maier, S. M.; Jentys, A.; Lercher, J. A. *J. Phys. Chem. C* **2011**, *115*, 8005.
(31) van Bokhoven, J. A.; Koningsberger, D. C.; Kunkeler, P.; van Bekkum, H.; Kentgens, A. P. M. *J. Am. Chem. Soc.* **2000**, *122*, 12842.
(32) Bordiga, S.; Scarano, D.; Lamberti, C.; Zecchina, A.; Geobaldo, F.; Vlaic, G.; Buzzoni, R.; Tozzola, G.; Petrini, G. *J. de Physique IV* **1997**, *7*, 907.
(33) Ankudinov, A. L.; Ravel, B.; Rehr, J. J.; Conradson, S. D. *Phys. Rev. B: Condens. Matter Mater. Phys.* **1998**, *58*, 7565.
(34) Ankudinov, A. L.; Rehr, J. J. *Phys. Rev. B: Condens. Matter Mater. Phys.* **2000**, *62*, 2437.
(35) Parry, E. P. *J. Catal.* **1963**, *2*, 371.
(36) van Bokhoven, J. A.; Koningsberger, D. C.; Kunkeler, P.; van Bekkum, H. *J. Catal.* **2002**, *211*, 540.
(37) van Bokhoven, J. A.; Sambe, H.; Ramaker, D. E.; Koningsberger, D. C. *J. Phys. Chem. B* **1999**, *103*, 7557.
(38) Pérez-Ramírez, J.; Kapteijn, F.; Brückner, A. *J. Catal.* **2003**, *218*, 234.
(39) Pérez-Ramírez, J.; Groen, J. C.; Brückner, A.; Kumar, M. S.; Bentrup, U.; Debbagh, M. N.; Villaescusa, L. A. *J. Catal.* **2005**, *232*, 318.
(40) Tippins, H. H. *Phys. Rev. B* **1970**, *1*, 126.

(41) Berlier, G.; Spoto, G.; Bordiga, S.; Ricchiardi, G.; Fisicaro, P.; Zecchina, A.; Rossetti, I.; Selli, E.; Forni, L.; Giamello, E.; Lamberti, C. *J. Catal.* **2002**, *208*, 64.

(42) Farges, F.; Lefrère, Y.; Rossano, S.; Berthereau, A.; Calas, G.; Brown, J. G. E. *J. Non-Cryst. Solids* **2004**, *344*, 176.

(43) Petit, P.-E.; Farges, F.; Wilke, M.; Sole, V. A. *J. Synchrotron Radiat.* **2001**, *8*, 952.

(44) Bordiga, S.; Coluccia, S.; Lamberti, C.; Marchese, L.; Zecchina, A.; Boscherini, F.; Buffa, F.; Genoni, F.; Leofanti, G. *J. Phys. Chem.* **1994**, *98*, 4125.

(45) Calas, G.; Petiau, J. *Solid State Commun.* **1983**, *48*, 625.

(46) Yan, G.; Long, J.; Wang, X.; Li, Z.; Wang, X.; Xu, Y.; Fu, X. *J. Phys. Chem. C* **2007**, *111*, 5195.

(47) Bisio, C.; Martra, G.; Coluccia, S.; Massiani, P. *J. Phys. Chem. C* **2008**, *112*, 10520.

(48) Marques, J. P.; Gener, I.; Ayrault, P.; Bordado, J. C.; Lopes, J. M.; Ramôa Ribeiro, F.; Guisnet, M. *Microporous Mesoporous Mater.* **2003**, *60*, 251.

(49) Trombetta, M.; Busca, G.; Storaro, L.; Lenarda, M.; Casagrande, M.; Zambon, A. *Phys. Chem. Chem. Phys.* **2000**, *2*, 3529.

(50) Kefirov, R.; Ivanova, E.; Hadjiivanov, K.; Dzwigaj, S.; Che, M. *Catal. Lett.* **2008**, *125*, 209.

(51) Chu, C. T. W.; Chang, C. D. *J. Phys. Chem.* **1985**, *89*, 1569.

This chapter is based on:

Maier, S.M.; Jentys, A.; Janousch, M.; van Bokhoven, J.A.; Lercher, J.A.; *paper ready for submission*

Chapter 5

Summary / Zusammenfassung

5.1. Summary

In order to improve the air quality and reduce the greenhouse effect, nitrogen oxide emissions from mobile diesel engines have to be reduced by the selective catalytic reduction process with ammonia as reducing agent. Fe-exchanged zeolites are promising catalysts to replace the conventional V_2O_5/WO_3 catalysts, which are toxic, volatile and potentially cancerogenic. Understanding of the ageing properties and the hydrothermal stability as well as the structure of the catalytically active species is essential for further improvement of the new catalytic system. Therefore, the ageing properties and the structure of the active Fe species were examined using a series of Fe-exchanged BEA zeolite type samples.

Steaming of the parent HBEA zeolite sample at 753 K causes a fast dealumination in the first hours, but after 14 h of steaming a stable coordination of Al and Si could be reached. The simultaneous condensation of SiOH groups and subsequent formation of Q^4 sites reduces the strain in the zeolite lattice and, thus, stabilizes the lattice. The coexistence of two polymorphs (A and B) in zeolite BEA induces a minimum concentration of defect sites, which cannot be healed even at longer steaming times.

The dealumination takes place only in the T3 – T9 sites, while the T1 and T2 sites are stable against dealumination. During the whole steaming process only 14 % of all Al atoms in tetrahedral positions are removed from the framework and transformed into extraframework species, while the double amount of Brønsted acid sites is lost. This apparent discrepancy can be explained with the role of the extraframework Al species in the zeolite. These cationic extraframework Al species generated by dealumination are located at the ion exchange positions and, thus, block further Brønsted acid sites, stabilize the lattice and protect the remaining Al framework atoms from further dealumination. As consequence, they are crucial to obtain a hydrothermally stable zeolite.

Ion-exchange of the parent material with $Fe^{2+/3+}$ leads to the formation of isolated Fe cations, Fe_xO_y moieties and Fe_2O_3 clusters at the external crystal surface, depending on the synthesis conditions and the Fe loading. Due to the high acid strength of zeolites, it is possible to stabilize Fe^{2+} ions in the zeolite pores under atmospheric conditions without further oxidation to Fe^{3+}. The *in situ* characterization of the Fe

oxidation state was achieved by a newly found linear correlation between the edge energy in XANES and the $Fe^{2+}/\sum Fe$ ratio, which can be determined *ex situ* by Mössbauer spectroscopy. Therefore, it was for the first time possible to directly determine the $Fe^{2+}/\sum Fe$ ratio under reaction condtions from the edge position in *in situ* XANES experiments. The Fe cations undergo a temperature dependant, reversible oxidation/reduction process, which reflects the chemical equilibrium of the oxidation of NO. The following desorption of NO_2 can then be regarded as the rate determining step of the overall NH_3-SCR reaction. The formation of an inactive Fe_2O_3 phase could not be observed under these conditions, emphasizing the thermal stability of FeBEA catalysts and demonstrating their potential for diesel exhaust gas aftertreatment systems.

The catalytic activity could also be maintained during ageing experiments in the presence of the reaction gases and steam, where additional inactive Fe_xO_y clusters were only formed at temperatures above 823 K. *In situ* XAFS revealed that the active Fe-O-Fe bridges are formed during activation in inert gas by the condensation of Fe-OH groups, explaining why the synthesis method is only of marginal importance to the later catalytic activity. The octahedral coordinated Fe cations located at ion exchange positions in the hydrated state are transferred into the catalytically active binuclear Fe species. In the presence of NH_3, this coordination is influenced and Fe cations can be inserted into zeolite tetrahedral framework positions, especially at low temperatures (<400 K). At higher temperatures, the Fe cations are extracted from the framework and the highly active Fe-O-Fe bridges are formed again. Comparison of the stability of the parent zeolite HBEA with ion exchanged FeBEA steamed in the presence of NH_3 reveals the stabilizing properties of NH_3 not only on the Fe species but also on the Al T atoms as dealumination is suppressed under these conditions. Therefore, it can be concluded that cooling of the FeBEA catalysts from reaction temperature to room temperature in the presence of NH_3 is beneficial to enhance the stability of the catalysts.

On the basis of these observations, it is proposed to further optimize the conditions preventing the dealumination of the zeolite framework and the agglomeration of Fe species and to confer these results to industrially applied catalytic systems. This understanding will lead to a further optimization of the exhaust gas treatment and towards an environmentally friendly global mobility.

5.2. Zusammenfassung

Die Verbesserung der Luftqualität und die Verringerung des Treibhauseffektes gehören zu den Herausforderungen der heutigen Gesellschaft. Der Ausstoß von Stickoxiden durch dieselbetriebene Fahrzeuge kann mit Hilfe der selektiven katalytischen Reduktion unter Zuhilfenahme von Ammoniak als Reduktionsmittel vermindert werden. Die zur Zeit verwendeten, aber als giftig, umweltschädigend und potentiell kanzerogen eingestuften V_2O_5/WO_3 Katalysatoren können durch physiologisch unbedenkliche Fe-getauschte Zeolithsysteme ersetzt werden. Um diese neuen katalytischen Systeme zu optimieren, ist das Verständnis der Alterungsprozesse, der hydrothermalen Stabilität sowie der katalytisch aktiven Spezies von entscheidendem Interesse. Im Rahmen dieser Arbeit wurden diese Aspekte an Hand einer Reihe von Fe-getauschten Zeolith BEA Katalysatoren untersucht.

Die Alterung des Ausgangsmaterials HBEA durch Steamen führte in den ersten Stunden zu einer Dealuminierung des Zeolithgitters, während nach einer Steamingzeit von 14 h eine stabile Modifikation gebildet wurde. Die gleichzeitige Kondensation von SiOH Gruppen führte durch die Entspannung des Kristallgitters zu einer zusätzlichen Stabilisierung des Materials. Das Vorhandensein der beiden Modifikationen Polymorph A und B induziert allerdings eine Mindestkonzentrationen an Defektstellen im Kristallgitter und ist somit für eine hohe Konzentration an SiOH Gruppen zuständig. Diese SiOH Gruppen können auch bei längeren Steamingzeiten nicht kondensiert werden.

Die Dealuminierung findet ausschließlich an T3-T9 Positionen statt, während Al Atome in T1 und T2 Positionen nicht aus dem Zeolithgitter entfernt werden. Während des gesamten Steamingprozesses wurden insgesamt 14 % der im Zeolithgitter vorhandenen Al Atome in extraframework Al Spezies überführt. Gleichzeitig wurde die Konzentration an Brønstedsäurezentren um den doppelten Wert verringert. Diese Diskrepanz kann nur dadurch erklärt werden, dass durch die Dealuminierung kationische extraframework Al Spezies gebildet werden, welche ein zusätzliches Brønstedsäurezentrum blockieren und somit pro aus dem Gitter entfernten Al Atom zwei Brønstedsäurezentren verloren gehen. Dadurch wird das Zeolithgitter zusätzlich stabilisiert und eine weitere Dealuminierung verhindert. Dies unterstreicht die wichtige

Funktion der extraframework Al Spezies in Bezug zur hydrothermalen Stabilität des untersuchten Zeolithsystems.

In Abhängigkeit der Synthesebedingungen und der Eisenbeladung werden durch den wässrigen Ionentausch isolierte Eisenionen in Ionentauschpositionen, Fe_xO_y Cluster oder Fe_2O_3 Aggregate an der äußeren Oberfläche der Zeolithkristalle gebildet. Auf Grund der hohen Säurestärke der Zeolithe, können auch Fe^{2+} Kationen in den Zeolithporen stabilisiert werden ohne weiter zu Fe^{3+} oxidiert zu werden. Mit Hilfe einer Korrelation zwischen der Kantenposition der XANES und des durch *ex situ* Mößbauerspektroskopie bestimmten $Fe^{2+}/\sum Fe$ Verhältnisses, wurde zum ersten Mal die Möglichkeit entwickelt das $Fe^{2+}/\sum Fe$ Verhältnis direkt aus der Kantenposition von *in situ* durchgeführten XANES Experimenten zu bestimmen. Die isoliert vorliegenden Eisenkationen durchlaufen im Rahmen der NH_3-SCR Reaktion einen temperaturabhängigen Redoxzyklus, welcher das Gleichgewicht der NO Oxidation wiederspiegelt. Die nachfolgende Desorption des entstandenen NO_2 kann somit als geschwindigkeitsbestimmender Schritt der NH_3-SCR Reaktion gesehen werden. Zudem konnte unter den Bedingungen der NH_3-SCR Reaktion keine Bildung der inaktiven Fe_2O_3 Phase beobachtet werden. Dies unterstreicht die hohe thermische Stabilität und das Potential dieser Fe-haltigen Katalysatoren für den Einsatz in der Dieselabgasaufbereitung.

Die weitere Untersuchung des Alterungsverhalten zeigte, dass die katalytische Aktivität der FeBEA Katalysatoren auch während einer Alterung in Anwesenheit der Reaktionsgase und Wasserdampf erhalten bleibt. Erst ab einer Temperatur von 873 K werden inaktive Fe_xO_y Cluster gebildet. Mit Hilfe von *in situ* XAFS Experimenten konnte weiterhin gezeigt werden, dass sich die katalytisch aktive Fe Spezies erst bei der Aktivierung in Inertgasen bildet und die katalytische Aktivität somit teilweise unabhängig von der verwendeten Synthesemethode ist. Durch die Aktivierung in Inertgasen wird die Struktur der im hydratisierten Zustand oktaedrisch vorliegendem Fe Spezies verändert und durch die Kondensation von Fe-OH Gruppen Fe-O-Fe verbrückte Spezies gebildet. In Anwesenheit des Reaktionsgases Ammoniak, wird diese Koordination weiter beeinflusst und Eisen in tetreadrisch koordinierte Positionen im Zeolithgitter eingebaut. Dieser Einbau findet vor allem bei niedrigen Temperaturen (<400 K) statt, während höhere Temperaturen wieder zu einem Ausbau des Eisens aus den

tetreadrisch koordinierten Gitterplätzen, einer Belegung von Ionentauschpositionen und zur Bildung der aktiven Fe-O-Fe verbrückten Spezies führen. Die Stabilität der Katalysatoren unter den Bedingungen der NH_3-SCR Reaktion ist im Vergleich zu den an den ungetauschten HBEA Materialen durchgeführten Steamingversuchen verbessert, da die Dealuminierung und Bildung von Fe_2O_3 Aggregaten in Anwesenheit von Ammoniak unterdrückt wird.

Auf Grund dieser Beobachtungen wird für weiterführende Arbeiten vorgeschlagen, die Bedingungen welche die Dealmunierung der Zeolithe sowie die Bildung von Fe_2O_3 Aggregaten verhindern, weiter zu untersuchen und vor allem auf industriell angewandte Systeme zu übertragen. Diese Erkenntnisse können zu einer weiteren Optimierung der Abgasnachbehandlung im Sinne einer umweltfreundlichen globalen Mobilität führen.

Appendix

A. Appendix for Chapter 2

A.1. X-ray diffraction patterns

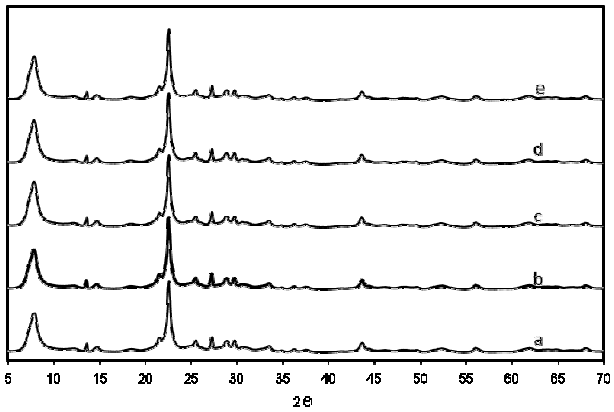

X-ray diffraction patterns of the samples HBEA35-parent (a), HBEA35-s1 (b), HBEA35-s5 (c), HBEA35-s14 (d), HBEA35-s24 (e).

A.2. Deconvolution of ^{29}Si MAS NMR spectra

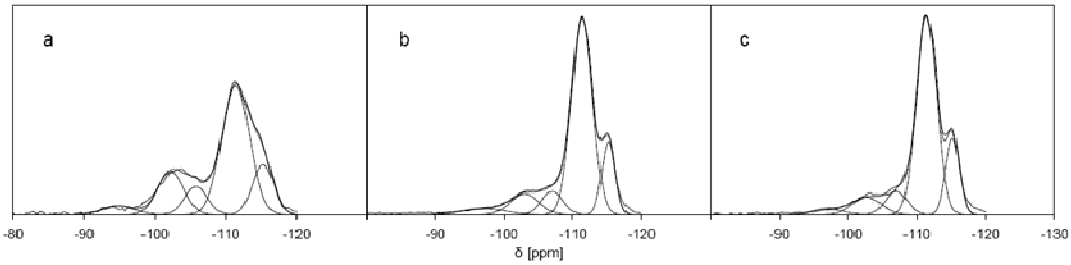

Deconvolution of the ^{29}Si MAS NMR spectra of the samples HBEA35-parent (a), HBEA35-s5 (b), HBEA35-s24 (c).

A.3. Deconvolution of ^{27}Al MAS NMR spectra

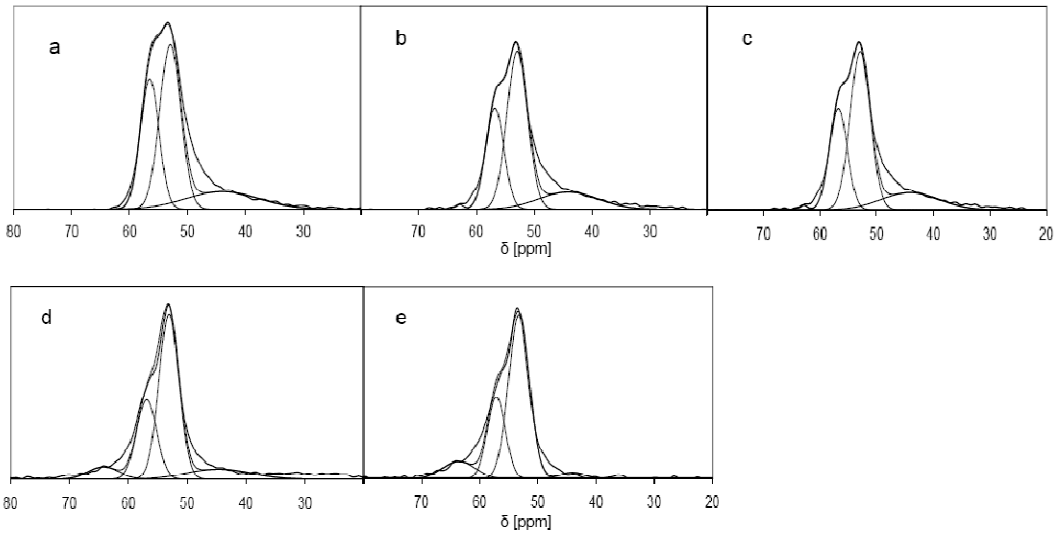

Deconvolution of the ^{27}Al MAS NMR spectra of the samples HBEA35-parent (a), HBEA35-s1 (b), HBEA35-s5 (c), HBEA35-s14 (d), HBEA35-s24 (e).

A.4. Deconvoultion of ^{1}H MAS NMR spectra

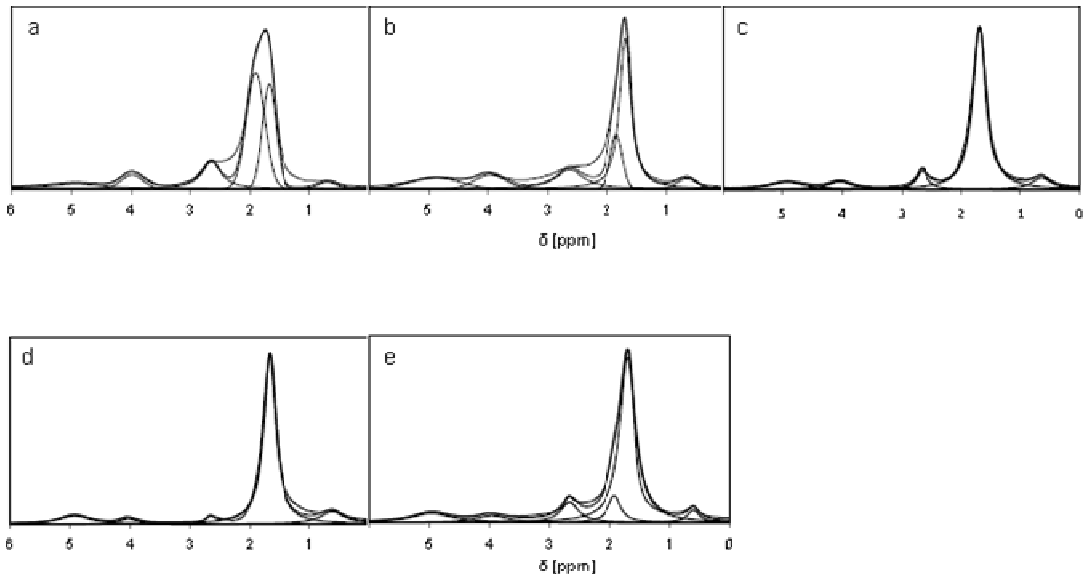

Deconvolution of the ^{1}H MAS NMR spectra of the samples HBEA35-parent (a), HBEA35-s1 (b), HBEA35-s5 (c), HBEA35-s14 (d), HBEA35-s24 (e).

B. Appendix for Chapter 3

B.1. Isomeric shifts and quadrupole splitting constants from Mössbauer results

sample	Fe^{2+} (doublet)			Fe^{3+} (doublet)			Fe_2O_3 (sextet)		
	%	δ [mm/s]	Δ [mm/s]	%	δ [mm/s]	Δ [mm/s]	%	δ [mm/s]	Δ [mm/s]
FeBEA 0.92n	72.1	1.2	3.4	11.5	0.3	1.0	16.4	0.2	0.1
FeBEA 0.81n	67.5	1.2	3.4	14.5	0.3	0.9	18.0	0.2	0.1
FeBEA 0.99n	51.3	1.2	3.4	24.5	0.3	1.0	24.2	0.2	0.1
FeBEA 1.38n	35.7	1.2	3.4	17.5	0.3	1.0	46.8	0.3	-0.2
FeBEA 0.79a	13.9	1.1	3.4	62.4	0.2	0.9	23.7	0.3	0.0
$FeSiO_2$ 7.02a	0.0	-	-	0.0	-	-	100.0	0.3	-0.2

C. Appendix for Chapter 4

C.1. X-ray diffraction patterns

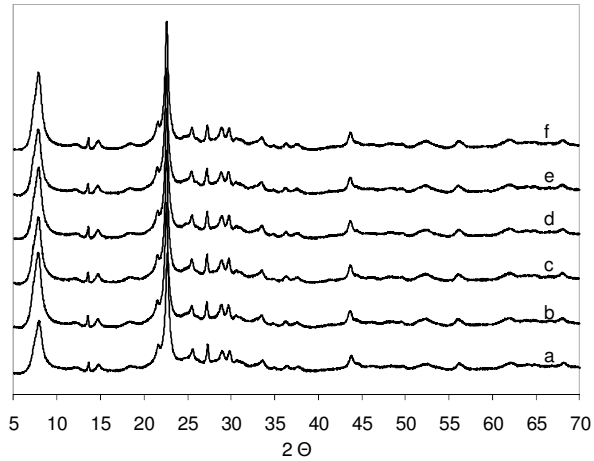

X-ray diffraction pattern of the samples FeBEA (a), FeBEA 723 (b), FeBEA 723st (c), FeBEA 773st (d), FeBEA 823st (e), FeBEA 873st (f)

C.2. Deconvolution of NH_3-TPD Profiles

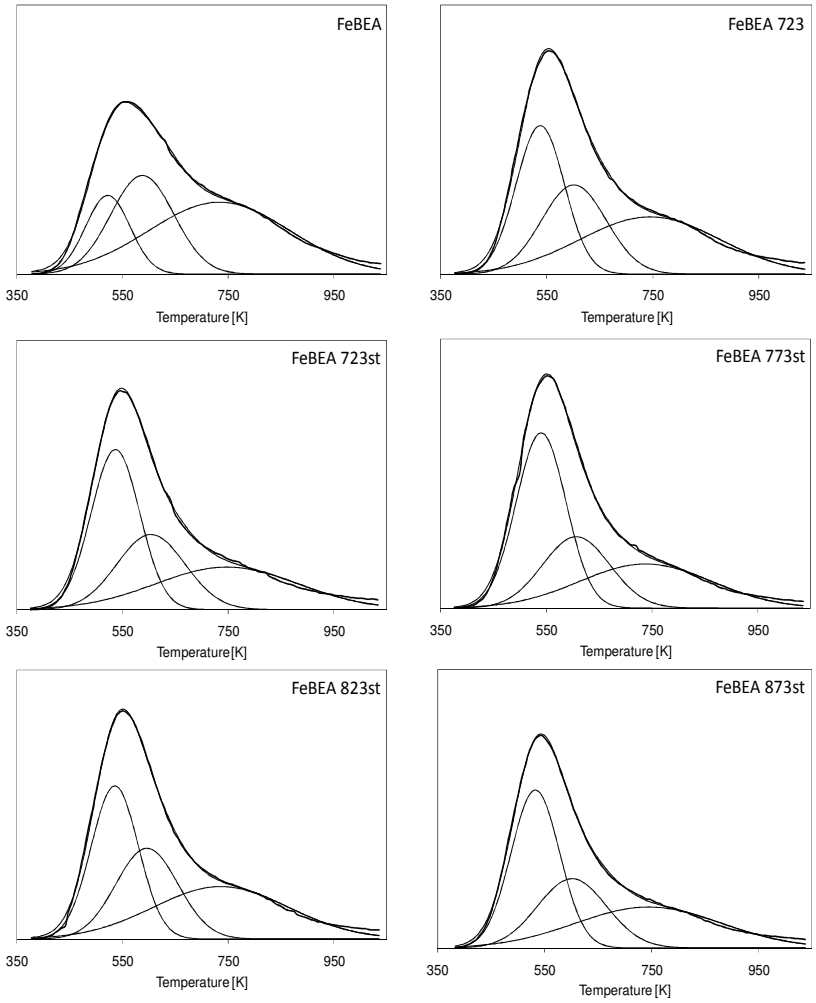

Deconvolution of the NH_3-TPD desorption profiles with Gaussian functions.

List of Publications

S.M. Maier, A. Jentys, J.A. Lercher, Steaming of Zeolite BEA and its Effect on Acidity: A comparative NMR and IR Spectroscopic Study. *J. Phys. Chem. C* **2011**, *115*, 8005-8013.

S.M. Maier, A. Jentys, E. Metwalli, P. Müller-Buschbaum, J.A. Lercher, Determination of the Redox Processes in FeBEA Catalysts in NH_3-SCR Reaction by Mössbauer and X-Ray Absorption Spectroscopy. *J. Phys. Chem. Lett.* **2011**, *2*, 950-955.

S.M. Maier, A. Jentys, M. Janousch, J.A. van Bokhoven, J.A. Lercher, Unique Dynamic Changes of Fe Cationic Species under NH_3-SCR Conditions, *paper ready for submission*.

Conference Contributions

03/2010 22. Deutsche Zeolithtagung, München
Hydrothermal treatment of zeolite BEA and its effect on acidity – a comparative NMR and IR spectroscopic study

03/2010 43. Jahrestreffen Deutscher Katalytiker, Weimar
Characterization of FeBEA and its activity in the NH_3-SCR reaction

06/2010 TU München/TU Eindhoven Nanoworkshop, Eindhoven
On the Characterization of Fe nano species in FeBEA zeolites

07/2010 16th International Zeolite Conference, Sorrento
On the nature of FeBEA active sites in NO_x reduction with NH_3

03/2011 23. Deutsche Zeolithtagung, Erlangen
Characterization of structural changes of FeBEA catalysts during NH_3-SCR reaction

03/2011 44. Jahrestreffen Deutscher Katalytiker, Weimar
Characterization of redox properties of FeBEA catalysts during NH_3-SCR reaction

05/2011 Joint Workshop Northwestern University/TU München, Garching
Characterization of FeBEA for the application in the NH_3-SCR reaction

07/2011 5th International FEZA conference, Valencia
Insertion of extraframework Fe species into zeolite T positions under NH_3-SCR conditions